INFORMATION TO USERS

This manuscript has been reproduced from the microfilm master. UMI films the text directly from the original or copy submitted. Thus, some thesis and dissertation copies are in typewriter face, while others may be from any type of computer printer.

The quality of this reproduction is dependent upon the quality of the copy submitted. Broken or indistinct print, colored or poor quality illustrations and photographs, print bleedthrough, substandard margins, and improper alignment can adversely affect reproduction.

In the unlikely event that the author did not send UMI a complete manuscript and there are missing pages, these will be noted. Also, if unauthorized copyright material had to be removed, a note will indicate the deletion.

Oversize materials (e.g., maps, drawings, charts) are reproduced by sectioning the original, beginning at the upper left-hand corner and continuing from left to right in equal sections with small overlaps. Each original is also photographed in one exposure and is included in reduced form at the back of the book.

Photographs included in the original manuscript have been reproduced xerographically in this copy. Higher quality 6" x 9" black and white photographic prints are available for any photographs or illustrations appearing in this copy for an additional charge. Contact UMI directly to order.

UMI®

Bell & Howell Information and Learning
300 North Zeeb Road, Ann Arbor, MI 48106-1346 USA
800-521-0600

Spectroscopy of Mass-Selected Transition Metal Clusters in Argon Matrices

by

Yifei Liu

A dissertation submitted to the Graduate Faculty in Chemistry in partial fulfillment of the requirements for the degree of Doctor of Philosophy, The City University of New York

1999

This manuscript has been read and accepted for the Graduate Faculty in Chemistry in satisfaction of the dissertation requirement for the degree of Doctor of Philosophy.

9-20-99
Date

Chair of Examining Committee

9/22/99
Date

Executive Officer

Supervisory Committee

THE CITY UNIVERSITY OF NEW YORK

ABSTRACT

SPECTROSCOPY OF MASS-SELECTED TRANSITION METAL CLUSTERS IN ARGON MATRICES

by

Yifei Liu

Advisors: Professor J. R. Lombardi and Professor D. M. Lindsay

Metal clusters have been studied in numerous experiments and theoretical investigations. Well understanding the properties of metal clusters needs to know further about the molecular chemistry and solid state physics. New experimental techniques as well as constantly improved theoretical calculations have been employed to determine the bonding energies, vibrational structures, dissociation energies, etc. Matrix isolation (MI) technique combined with mass-select system enables metal clusters to be a good spectral carrier which contains a monodispersed single-sized clusters. Using "Wien Filter", a velocity selector, metal cluster cations are mass-selected and then co-deposited with excess rare gas on a cold window in the presence of low energy electrons. Neutralized cluster samples are interrogated by absorption,

excitation, fluorescence and Raman spectroscopy. Vibrational frequency determined by Raman spectra provide an relatively accurate result of molecular information. Raman spectra of Hafnium trimer, yttrium dimer and lanthanum dimer, luminescence spectra of platinum dimer have been discussed.

ACKNOWLEDGMENT

First of all, I am very grateful to have two great mentors: Dr. Derek M. Lindsay and Dr. John R. Lombardi. During my graduate studies, Dr. Lindsay gave me beneficial, enrich advice and guidance. Unfortunately, Dr. Lindsay passed away this summer. Godspeed, Dr. Lindsay! Dr. Lombardi is my mentor not only in studies, but also in life. He teaches me how to be a great person with honesty, integrity and braveness which is also an excellent scientist's requirement.

I would also thank Dr. Ronald L. Birke, Dr. William Grossman, Dr. Gerald Keoppl for their help in studies and researches. I also appreciate the help of my fellow coworkers, Dr. Huaiming Wang, Dr. Robert Craig, Dr. Hanae Haouari, Dr. Li Fang, Dr. Wuming Wang, Mr. Xiaoyu Chen, and Mr. Xiaole Shen. I also must thank CASI director Dr. Daniel L. Akins, and the faculty of CCNY chemistry. Ms. O. Diane Adebowale, Ms. Vivian Mason in CUNY graduate school gave me generous help and encouragement. Thanks!

I could not have done it without my family's support. I dedicated this thesis to my father Yunchong Liu and my mother Xiuyu Chen.

Table of Contents

Lists of Tables

Lists of Illustrations

Chapter 1 Introduction

1.1 Why do we want to study metal clusters

Between the free atom and the bulk metal, there is a transition region called "clusters": aggregates of atoms or molecules. Clusters are not quite well understood compared with atoms and bulk metals. However, the nature, importance and potential applications of metal clusters are issues attracting wide attention by a large number of investigators working in quite diverse areas of research. This is especially evident from the number of specialized symposia [1-6] and review articles [7-13], where contributions have ranged from solid state physics through industrial synthesis.

Much of the early interest in cluster chemistry was driven by the realization that catalytic behavior is related largely or in part to the properties of small metal particles [7, 8, 14-22]. This is true for both homogeneous catalysis and heterogeneous catalysis, the two subdivisions into which this discipline has traditionally been subdivided. Interest in homogeneous catalysis has been stimulated by the discovery

and characterization of a large range of organometallic cluster compounds, species whose cluster core may contain as many as 44 metal atoms [22-26]. In the liquid phase, certain metal cluster compounds catalyze a wide variety of reactions often with a high degree of specificity [23, 24].

The majority of present day industrial catalysts are heterogeneous in nature. Often these consist of small particles supported on an inert substrate [20, 21, 27]. In many cases the active site may be a molecular sized cluster of "raft". For certain "demanding" reactions, catalytic activity is markedly improved as the degree of dispersion (ratio of atoms present in the surface to the total number of atoms) is increased [14, 16, 28, 29]. This effect arises not just from an increase in surface area, but also because small metal particles (< 50 Å) show a much greater activity than do larger particles. Certain bimetallic catalysts have a dispersion approaching unity, with particle sizes as small as 5 – 10 Å [16, 30]. Small Ag and Au clusters are essential to the photographic process. These latter species are formed photolytically and subsequently act as catalysts in the development of photograhpic materials. It has been demonstrated

[31, 32] that approximately four atoms of silver and two atoms of gold constitute the minimum cluster size for effective catalytic behavior.

A related effect is the observation [15, 29, 33, 34] that smooth, perfectly grown Pt surfaces are relatively inactive as catalysts. However, Pt surfaces prepared with a large number of kinks, terraces and other irregularities show enhanced activity. It is not, therefore, the structure of the bulk solid or whole crystalline plane which is important to study. Rather, it is the nature of the imperfections on the surface, which are related to metal cluster features appear as a common theme to surface science, and to heterogeneous catalysis. A current lack of experimental data on metal clusters makes it difficult to expand this concept beyond an intuitive level.

The potential application contributions have ranged from nuclear and solid state physics through material science and chemical synthesis. In the latter, clusters could provide a template for the design of new materials. Cluster beams could be a means of manufacturing macroscopic components or materials, for example as sources for epitaxial growth. Or, nanophase materials and quantum dot devices might be assembled using clusters or even on an atom-by-atom basis. A

good understanding of role of the clusters in the mechanism of catalytic reaction is quite helpful in design of powerful catalysts.

Stimulated by these new approaches, cluster science has now entered a new age. An overwhelming array of techniques has now been brought to bear in this area. Experimental studies focusing an absoption spectra at all frequencies, ionization phenomena, photoemission spectra, chemisorption reactions, surface scattering, and deposition have been described. Cluster assembled semiconductors and superclusters serves as benchmarks for new theoretical methods. Cluster science now encompasses parts of inorganic, organic, physical and theoretical chemistry, solid state, and atomic and molecular physics, as well as the interdisciplinary areas of surface science and materials science.

In order to study the various chemistry or physical properties of clusters, we first need to concentrate on basic, however, very important information on clusters, such as the structure, symmetry, bonding information, as well as dissociation energies. In the follow section, we will discuss the details of previous studies on metal clusters.

1.2 Previous studies on metal clusters

It is difficult to determine the beginnings of the study of metal and semiconductor clusters. Very early experiments producing metal atoms in heat pipes or electrical discharges perhaps first noted the possible presence of metal dimers, and it only took a small increment in thinking to conceive of trimers, tetramers, and beyond. In the earliest spectroscopic studies, furnaces were used to generate high vapor pressures of the coinage metals (Cu, Ag, and Au). Under these conditions some diatomic species were present, and ultraviolet and visible spectra of the dimers were obtained. Although these methods provided the first spectroscopic data on the transition-metal molecules, they were not readily extended to more refractory metals, and for many years little was learned of the more refractory transition-metal molecules. The field gained new life with the development of matrix isolation spectroscopy in which larger clusters could be prepared and studied. Another surge of interest came in the early 1980's when molecular beam techniques were applied. In 1981, Smalley and co-workers [35, 36] reported the first laser vaporization source with the cluster

distribution sampled with photoionization mass spectrometry. Soon thereafter, laser spectroscopy was applied to a variety of metal dimers and trimers in these beam environments, In 1984, Knight and co-workers [37] noted the evidence for shell closings in sodium clusters, again probed with molecular beam mass spectrometry. The most recent wave of "clustermania" came with the first macroscopic isolation of a cluster (C_{60} and the fullerenes) in 1990. [38]

Instead of listing the complete cluster types which had been explored such as silver-organic clusters, metal-carbon clusters, transition metal clusters are mainly discussed here. In earlier years, many researchers involved in studying clusters in the gas phase made considerable effort toward examining the dependence of well-defined electronic properties as a function of number of atoms in the cluster. Different experimental techniques such as laser induced fluorescence (LIF), [39] resonant two-photon ionization (R2PI), [40,41] collision induced dissociation (CID), [42] photodissociation, [43-47] gas-phase reaction followed by mass spectrometric detection, [48] etc. have been used to study alkali metal (Na_n), transition metal (Ni, Cu, Ag, Pt, Pd, Au), and semiconductor clusters(Al). However, in spite of considerable effort,

little experimental information is available on the structures and physical properties of small clusters. Most of our knowledge about cluster structure came from theoretical calculations. Other physical properties such as ionization potentials, electron affinities, and dissociation energies can be obtained experimentally and used to test the accuracy of the theoretical calculations. In the recent past, dramatic improvements in cluster generation and laser mass spectrometric techniques have enabled experimentalists to measure ionization potentials [49] and electron affinities [50] of larger alkali and transition metal clusters. Spectroscopic studies are of interest because they can provide information about the excited electronic states and the potential energy surface where dissociation occurs. Phtotodissociation of isolated gas-phase clusters can provide information on their spectroscopy, dissociation dynamics, and dissociation energies. With the exception of dimers, detailed spectroscopic studies have been performed for Na_3, [51] Cu_3, [52] Al_3, [53] Ni_3, [54] and Ag_3. [55]

LIF and R2PI techniques have had limited success with clusters larger than dimers and trimers. These spectral techniques are based on exciting the parent cluster to an excited electronic state, which then has

to survive long enough to be detected either by its fluorescence or its lowered ionization threshold, which prohibits observation of extremely rapid radiationless transitions. In 1990 Ray and Jarrold developed two different aspect of photodissociation: the first one concerns the process of photoabsorption (for small aluminum and copper clusters), and the second aspect deals with the process of dissociation and the measurement of dissociation energies, where a simple RRKM model was used for larger clusters (Fe_n^+ n= 2-10 and Nb_n^+ n= 2-6.) [56]

Besides these classical spectrosocopic methods, photoelectron spectroscopy (PES) has also been carried out to study more clusters with the development of intense ion, anion sources and mass selected isolation techniques. The laser vaporization (LVS) and the pulsed Arc Cluster Ion Source (PACIS) techniques combined with TOF (time-of-flight, first described by Mamyrin et al. [57]) were used to study Al_n^-, Sn_n^-, Cu_n^+, and W_n^+ by Meiwes-Broer [58]. The value of n in Na_n mass spectra could be up to 1500 atoms. Since the limits of the intriguing shell idea has not been explored, a further wide field in measurements of the electronic band structure is still under investigation. In CCNY, Dr.

Lindsay and Dr. Lombardi built a similar system. Some results on Zr_n^+, Nb_n^+ etc. have been accomplished.

Based on the matrix isolation technique, well-established methods are used where-by low temperature environments to stabilize high-temperature or reactive species. In the past three decades, matrix absorption Electron Spin Resonance (ESR) and Raman spectroscopy has been extensively utilized to investigate transition metal dimers, trimer, and larger clusters.

By trapping the clusters in rare gas matrices at low temperatures, a high enough concentration of reactive molecules is gained to meet Raman and ESR spectroscopic requirements. The spectra are then those of rigidly-held, randomly-oriented molecules isolated from each other by a relatively nonperturbing medium. The matrix ESR spectra can establish the multiplicity and symmetry of the ground electronic state, g tensor components, zero-field splittings, hyper-fine interaction constants and approximate spin densities, nuclear quadrupole coupling constants, and spin-rotation constants. [59]

One distinguishing advantage of ESR spectra is that they can be used to identify the ground state of the diatomoic cluster, say, Sc_2.

Theory has predicted several possible ground states. However, the ESR spectrum was unambiguous, since natural Sc is 100% ^{45}Sc, and it definitely established a $^{5}\Sigma$ ground state. [60] While in our experiment, a non-observation of the ESR of yttrium and lanthanum dimers could also provide converse information in determining the ground states. ESR spectra have been obtained for Cr_2, [61] Ni_2, [62] Cu_2, [63] ScNi, TiCo, [64] $CuAg_4$, Cu_2Ag_3 [65] and Y_3, [66] etc.

Raman spectroscopy is another sensitive probe for matrix containing cluster samples. Vibrational constants can be directly calculated from the vibration frequency of dimers, trimers and tetramers. By analyzing the spectrum, we may also obtain dissociation energies, ground state, and bonding configuration information.

Since the CCNY cluster laboratory was built with a mass-select cluster deposition system combined with laser Raman and SDS absorption spectroscopy, we successfully investigated in the last nine years V_2, Co_2, Zr_2, Nb_2, Hf_2, Ta_2, W_2, Re_2, Ni_2, Rh_2, Ru_2, Pt_2, Y_2, La_2, Zr_3, Nb_3, Hf_3, and Ta_4. In chapter 4, details in Y_2, La_2, Hf_3, Pt_2 will be discussed.

These two spectroscopic methods applied successfully in determining cluster structures and spectroscopic constants helped considerably to explain the tendency from *d-d* bonding to *s-s* bonding when going from the early transition metals to the late transition metals in the periodic table. Recent experiment on lanthanum dimer and yttrium dimer even gave exciting information about the effect of *f* electrons in dimer bonding.

Research in chemical science has always involved two parallel directions. One is experimental, while the other is theoretical. These two sides are complementary and mutual promoting. In the field of transition metal clusters, numerous theoretical calculations have been performed. Some fair results were obtained even before proper experimental techniques. An earlier treatment was carried on by third-law method, which is based on the statistical thermodynamics of dimerization. This method uses the statistical thermodynamic expression for the equilibrium constant of the reaction:

$$nM(g) \rightarrow M_n(g) \qquad (1.1)$$

to directly calculate D_0^0 (M_n). The third-law expression, therefore, is applicable to measurements made at only a single tempreature but

requires estimates of molecular parameters such as the bond length, vibrational frequency, ground-state electronic degeneracy, and the parameters of low-lying, thermally populated excited electronic states. Although the method gives results which are potentially more accurate than the second-law method, the necessity of estimating the molecular parameters of the relatively poorly understood transition-metal molecules limits its usefulness. In Chapter 4, we will compare the earlier theoretical results with our measurements on selected clusters. This shows that the earlier method is not accurate due to improper estimates. Accompanied by the development of the theoretical models and computation techniques, more and more complicated and feasible work was accomplished.

Small transition metal clusters are ideal candidates for high-level *ab initio* theoretical calculations because such studies could provide significant new insight into the nature of the metal-metal bonding and the role of the d orbitals in these bonds. Typically for these cluster several closely spaced electronic states have completely different geometries. Theoretical investigations could provide important and useful information on the low-lying electronic states of clusters, their

equilibrium geometries, bonding energies, and electron affinities. The computation models usually employed by cluster chemists are configuration interaction (CI) [67], complete-active-space self-consistent-field configuration interaction (CASSCF/CI), [68] complete-active-space-multiconfiguration self-consistent-field (CAS-MCSCF) [69] followed by multireference singles + doubles configuration interaction (MRSDCI), [70] et al. An interesting example was on the studies of Sc_2. In 1993, Walch and Bauschlicher [71] studied the $^3\Sigma_g^+$, $^1\Sigma_g^+$, $^3\Sigma_u^+$, $^5\Delta_u$ states of Sc_2 using CASSCF CI (SD) wavefunctions in a large gaussian basis set, and found only weakly bound states arising out of the $4s^23d^1 + 4s^23d^1$ asymptote in contrast to mass spectrometric experiments which indicated strong bonding. However at about the same time, Knight, Van Zee and Weltner [72] obtained the ESR spectrum of Sc_2, leading to the ground state of Sc_2 of $^5\Sigma$. This arose from $4s^23d^1 + 4s^13d^2$ atomic asymptote which has not been studied in detail theoretically. After reexamination, Walch et al. found $^5\Sigma$ has been missed due to its much shorter r_e. [73] This example reveals the relationship between the theoretical and experimental studies.

Some software and online databases have been established for commercial use or public use. The COLUMBUS Program System (made by MSU Chemistry), used extensively by other group members and visitors, is distributed publicly using the anonymous file transfer protocol (FTP) facility of the Internet. [74] This project includes development of multiconfiguration Self-Consistent-Field (MCSCF) and multireference single- and double-excitation configuration interaction (MRSDCI) methodology. The DALTON program system [75] created by T. Helgaker et al. is designed to allow convenient, automated determination of a large number of molecular properties based on an SCF, MP2 or MCSCF reference wave function. It could compute vibration frequencies, potential energies, and even Raman intensities.

Although theoretical computation on clusters has been improved rapidly recently, the theoretical interpretation still lags behind the experimental successes. The nature of cluster bonding is still an incompletely understood area. Both experimental and theoretical efforts are needed for a better understanding.

Chapter 2 Experiment system design and technique

2.1 Overview of system: the cluster beam

A detailed understanding of the structures of small metal clusters involves a symbiosis between molecular structure calculations, less sophisticated (though perhaps as far-reaching) theoretical models, and diverse experimental (particularly spectroscopic) measurements. Information about cluster excited states may be inferred from photoelectron studies and photodepletion spectra, which in a few cases also show vibrational fine structure. In general, however, well-resolved gas-phase spectra have been limited to metal dimers and a small number of trimer species like Cu_3, Na_3, Al_3, Ni_3, Ag_3, and Li_3. [1]

As is well known, the matrix isolation (MI) technique permits the preparation of stable samples containing large numbers of clusters at low temperature. Also vibrational spectra using the MI technique [2] are similar to gaseous phase spectra, in which neither intermolecular interactions are present nor lattice modes are observed. While the absorption spectra are different from those of the gas phase, MI spectra

have a most important aspect in that it tends to be simpler than gas-phase spectra because of a lack of rotational transitions.

The majority of reported spectroscopic measurements have employed matrix isolation methods which have the significant advantage that large numbers of (inherently cold) clusters may be accumulated for subsequent interrogation by absorption, fluorescence, Raman, ESR, etc., techniques. Since matrix samples are usually grown by aggregation from the atomic vapor, cluster formation is dependent upon the deposition conditions, [3, 4] although some control may be effected by subsequent annealing. As a consequence, matrix samples contain a complex, unknown distribution of cluster sizes and any measurements are severely hampered by ambiguities in assigning the spectral carrier. [5]

The assignment problem can be overcome by preparing matrices that contain single sized clusters. For example, a particular ion cluster could be mass selected in the gas phase and then neutralized during deposition in order to circumvent Coulomb repulsion effects in the matrix. For this approach to be successful requires: (1) an intense source of cluster ions, typically several nA mass selected, (2) an effective

means for collecting and neutralizing these ions, and (3) that the clusters be efficiently "soft landed" (i.e. decelerated with minimum fragmentation) before being frozen into the matrix.

Accordingly, the CCNY mass-selected cluster beam deposition system has been designed for depositing an intense beam of neutral clusters (soft landing) in rare gas matrices on a solid surface, such as CaF_2, silver, titanium sapphire or aluminum. Mainly it consists of three major components: the ion source, the mass select (Wien Filter) and the deposition chamber (see fig 2.1).

The ion source is a sputtering chamber where the metal target is located. An intense (typically 15 mA at 25 KeV) argon ion beam from a "CORDIS" ion source sputters metal clusters from a water cooled metal target maintained at about 300 V. The 50° inclination between the primary and secondary beam lines correspond closely to the optimum ejection angle for material sputtered from a metal surface.

Cluster cations sputtered from the target were extracted with a modified Colutron model 200-B lens system (L2 in Fig. 2.1). The secondary ions were mass selected by a Wien filter (Colutron 600-B) in conjunction with an approximately 175 mm long drift space and a 6.5

mm diameter aperture (A3). For the deposition experiments described here, the Wien filter was operated at a magnetic field of about 2000 G which gave a resolution ($M/\Delta M$) of approximately 6-7, i.e., sufficient to separate the dimer from the atom and trimer and to ensure that oxides are not present. Mass selection is meant to be the most important part of the beam because it enables us to study a monodispersed metal cluster. The secondary beam which includes extraction lens, Wien filter, drift space, etc. is floated at about –1.5 KV.

After mass separation, the dimer ion beam was bent by 10° (using deflector plates D2, mounted in a short bellows section) and then guided to the deposition region by two einzel-like lenses L3 and L4. The 10° bend separates dimer ions from the neutral sputtered products, whose flux may be comparable to or greater than that of the ions.

The deposition region consists of a substrate, usually CaF_2, where the matrices are embedded, a closed cycle cryostat to obtain and maintain cryogenic temperature, a Faraday cage to define potential for the arriving ions by applying a retarding potential to the Faraday plate, an electron source to neutralize the ions, because the deposition was designed to be of neutral clusters in argon matrices. Usually the desired

cluster ions were codeposited with Ar and electrons on a CaF_2 plate. The cryostat temperature was measured by a Si diode in conjunction with a Scientific Instruments model 5500 temperature controller. Deposition temperatures were typically about 20 K.

Matrices were grown at around 5-10 *u*/h with an Ar:metal dilution ratio of approximately 10^4:1, i.e., sufficient to ensure that the dimers remain well isolated both from each other and (more difficult to achieve) from any impurity species, which also ensures the spectra not only will reflect the molecule properties but also will be easier to interpret.

Matrix samples were interrogated *in situ* using both absorption and Raman spectroscopy. The absorption measurements were made by collecting the light at 90° to that incident, a technique we term "Scattering Depletion Spectroscopy" (SDS). Raman spectra were recorded using Argon ion lasers, dye lasers or Ti-Sapphire lasers. Scattered light was collected at 90° into a Spex 1877E Triplemate Spectrometer (0.6 m) and detected by a liquid nitrogen cooled CCD detector (Spex model "Spectrum One") with DM3000R software.

Almost any metal can be used as a target in this apparatus. However after a large number of depositions, we conclude following characteristics of good cluster candidates for Raman spectroscopy.

1. The material should have a large sputtering yield.
2. Secondary currents should not fall off too rapidly with cluster size.
3. The cluster ionization potential should be relatively low.
4. The cluster bond strength should be relatively large.
5. There should be visible absorption bands which overlap with Argon laser lines or a dye laser or Ti-sapphire laser.
6. Raman spectra should not be too obscured by fluorescence otherwise it will hinder the weak Raman signals and make the assignment a bit difficult.

2.2 "CORDIS": ion source

Ion order to undertake spectral analysis, it is essential to first identify the spectral carrier. An essential feature of mass-selected cluster

experiments involves the deposition of a sputtered (secondary ion), mass-selected metal cluster. These must be produced in sufficient number to be detectable and this in turn requires a very high brightness sputtering source (the primary source). Heavy gas (argon, krypton, etc.) primary ion beams operating at energies of up to 30 KeV are known to be efficient secondary ion producers. The secondary ions must be deposited at low energies in order to have minimum fragmentation (soft landing conditions), which requires a very large available secondary ion flux. To achieve these objectives, the CORDIS plasma ion source produces an intense, high energy and well collimated beam of gaseous (argon, krypton, etc.) ions. Specifically, a 25 KeV argon ion beam can routinely produce currents in excess of 15 mA with a 10 mm beam diameter 0.5 m from the source.The cluster ion source is shown schematically in figure 2.2. A similar ion source was used in another system and described by Harbich, Lindsay et al. [6]

The "CORDIS" ion source (Cold Reflex Discharge Ion Source) was designed by Rokion Ionenstrahl-Technologie, Darmstadt, Germany. CORDIS relies on the principle of a magnetic multipole/reflex discharge. The ion beam is formed by a single-aperture accel/decel

extraction-system which can be aligned independently of other source parts. This ion source consists three parts: a cathode chamber, which contains cathode filaments (tantalum wire), a discharge chamber where the ultra-high voltage is added on, and an extraction system. (see figure 2.2). Afterward, an intense (typically 10 mA at 25 KeV) argon ion beam was produced.

2.3 Sputtering chamber

Argon ion beam sputters metal cluster ions from a water cooled, metal target. The primary beam was collimated by an 8 mm aperture (denoted A1 in Fig. 1) which also serves to separate the ion source from the rest of the apparatus. The ion source was pumped indirectly, through and around A1, by a 500 l/s turbomolecular pump (Balzers TPU 510) which supports the specially designed sputtering chamber (MDC Vacuum Products). The 50° inclination between the primary and secondary beam lines correspond closely to the optimum ejection angle for material sputtered from a metal surface. [7]

2.4 Secondary beam line

The schematic of the secondary beam (figure 2.3) shows the route of the cluster beam containing different clusters from right after sputtering through the mass-selection process. Usually we float the whole line with –1.5 KV high voltage to increase the resolution of the secondary beam line.

2.4.1 Extraction lens: colutron 200-B lens system

Cluster cations sputtered from the target (normally maintained at 300-350 V) were extracted with a modified Colutron model 200-B lens system (L2 in Fig 2.1). It consists of an extraction lens in combination with an einzel lens. The lens system is attached to the Colutron Velocity Filters models 600-B, which serves the most important task: mass-selection of the metal clusters sputtered from the metal surface.

2.4.2 Wien Filter: Colutron 600-B lens system

The Wien filter is also known as velocity filter. The Colutron 600-B system, used in this system, consists of a magnet and a pair of deflection plates. The plates are mounted between the magnet poles to produce an electric field *E* perpendicular to the magnetic field *B*. Just as the name "velocity filter" implies, the mass-selection has been achieved by discrimination of the various cluster velocities. The velocity

$$v = \sqrt{2qV/m} \qquad (2.1)$$

of the charged cluster beams are obtained by accelerating the particles of mass m, charge q across a constant electric potential V. Obviously, different masses in the beam will be dispersed by the filter because of their different velocities.

Liquid cooling (Freon R22) added to the filter makes it possible for higher currents to produce higher magnetic field strength. For the deposition experiments described here, the Wien filter was operated at a magnetic field of about 2000 G (corresponding electric field: 130 V for most transition metal clusters) which gave a resolution ($M/\Delta M$) of approximately 6-7, i.e., sufficient to separate the desired clusters, for

example, dimers, from the atom and trimer and to ensure that oxides are not present.

2.4.3 10° degree bend and final lens

Only the selected ion beam can pass through the small aperture on the end of the filter. After mass separation, the selected ion beam was bent by 10° (using deflector plates D_2, mounted in a short bellows section) and then guided to the deposition region by two lenses L_3 and L_4 (see figure 2.4).

The 10° bend separates selected ions from the neutral sputtered products, whose flux may be comparable to or greater than that of the ions. In some earlier experiments, by depositing neutral silver clusters both with and without a 10° bend, we estimate that only about 0.1% of the neutral species are deposited in our experiments. [8]

2.5 Deposition region

The decisive specifications for our intended research is the ability to produce large, continuous (10-100 nA) currents of mass-selected transition metal (and other metal) clusters which can be subsequently decelerated (to < 10 eV) and deposited with low energy (<1 eV) electrons and excess rare gas (ratio:> 1000:1) as a solid matrix sample and under conditions of minimum fragmentation.

Secondary ion currents limit the number of neutral cluster species that can be trapped in a rare gas matrix. This in turn determines the minimum sensitivity requirements of the spectroscopic techniques applied to the analysis of the samples and, accordingly, the detail of the information extractable from these experiments, as for example resolution. Resolution is the performance characteristic that expresses the ability of a spectroscopic instrument to distinguish between closely spaced (in the frequency domain) spectral features. It also determines the degree of distortion introduced by the instrument in the shape of the spectral lines. Our research requires the observation of molecular spectral features well distinguished from each other and at the same time free of distortion in their relative intensities that might be caused by overlapping wings of spectral bands. Since resolution is intimately

related to signal intensity, optically dense samples are crucial. For example: visible absorption techniques generally need sample absorbances of 10^{-2} or better for adequate noise suppression; ESR techniques require collecting 10^{15}-10^{16} cluster species. For both examples, secondary ion currents of 10 nA (as discussed above) can produce useful samples following deposition times of about one hour.

2.5.1 Faraday cage

The deposition region (see figure 2.5) is encapsulated in a six-way cube (CU800-6, MDC Vacuum products). The cube is supported by the second Turbo molecular pump (TPU 510, Balzers Pfieffer, Germany Umbh). Selected ions were codeposited with Ar and electrons on a 45 × 8 × 1 mm polished CaF_2 plate (Maris-Delfour, Paris) mounted (using Wood's metal and an In gasket) to a closed cycle cryostat (APD Displex, 204SL/DMX-6). The cryostat temperature was measured by a Si diode in conjunction with a Scientific Instruments model 5500 temperature controller. Deposition temperatures were typically about 20 K. The CaF_2 substrate was largely enclosed by a "Faraday cage",

composed of two side plates (with openings for optical measurements), the lower half of the cryostat radiation shield, the electron source, and the last lens element of L4 which was closed by a 90% transmitting Ni mesh. This same lens element also incorporates a coaxial injector ring (eight 0.5 mm diam holes) for the matrix gas (99.9995% Ar, Alphagaz). The electron source consisted of a Philips electron microscope filament (0.13 mm tungsten, Philip Electronic design) on a ceramic base (Ladd Research Industries). This assembly was enclosed by a stainless steel box having an 8 × 1 mm slit positioned so that the electrons were introduced about 1-2 mm in front of the CaF_2 substrate. In order for sufficient, low-energy electrons to reach the matrix target, the filament was biased at –3 V with respect to the Faraday cage.

Ion currents could be monitored using a Faraday plate (not shown in the figure) situated near the deposition window. Since the cryostat is rotatable, the Faraday plate and the substrate could easily be adjusted in order to measure ion currents, to prepare matrix samples, or to record optical spectra. Even though the matrix and CaF_2 substrate are insulators, the potential in the deposition region can (to a large extent) be defined and so controlled by the voltage applied to the surrounding

Faraday cage. The difference in voltage (V_{dep}) between the target the Faraday cage determines the cluster deposition energy (eV_{dep}), which was usually held at approximately 10 eV in the experiments described here. (see Fig. 2.7 deposit curve of yttrium dimer) The kinetic energy distribution of the arriving ions, measured by applying a retarding potential to the Faraday plate, was centered close to $eV_{dep} = 0$ eV, had a half width of about 8 eV, i.e., comparable to that reported for sputtered ionic particles. Mass-selected currents (beam area about 1 cm^2) could be in the range of about 10-300 nA. The ratio of electron current to cluster ion current (as measured on the Faraday plate) was generally about 2:1.

The fragmentation of the clusters may be estimated by comparing the intensities of atomic excitation features in a dimer deposition with those obtained from depositions of the atom under similar conditions. In the earlier experiments on vanadium dimer [6] which was the first dimer studied in this system, we estimate that 10-15% of the vanadium dimers (neutral bond energy, 2.8 eV) are fragmented at eVdep = 10 eV. For trimers, in order to calculate absolute fragmentation values (oscillator strengths and fluorescence quantum yields are not well known for metal clusters in matrices) we use dimer/atom intensity ratios observed in

"high energy" trimer depositions. Since the dimer : atom emission ratio remains approximately constant over the range of 50 to 100 eV deposition energy, we assume that the trimer fragments as a dimer plus an atom, whose relative intensities thus provide a rough yardstick to calculate dimer fragmentation. [9] The fragmentation percentage has been controlled at or below this level at the following experiments on some other transition metal clusters. A dimer/atom excitation spectrum is included to illustrate the estimation of the fragmentation percentage of Yttrium dimer during the deposition. (figure 2.6)

2.5.2 Soft landing

In the earlier experiment on vanadium, since the dimer ionization potential (6.1eV) is relatively large compared to the bond energy (2.8 eV), we suppose that the neutralization step takes place on, or very near, the matrix surface. The effect we called "softlanding" takes place which enables the cluster to successfully land in the matrix, but not break into atoms. In subsequent experiments, we continue to use term

"softlanding" to describe the process of neutralization, codepositing, and landing on the matrices.

The use of the term "soft-landing" is perhaps misleading in the context of a metal aggregate impinging with about 10 to 20 eV on a Ar matrix whose cohesive energy is approximately 100 meV/atom. Under our experimental conditions, a metal cluster will dissipate its kinetic energy (KE) to the rare gas solid long before it interacts with any subsequent incoming (i.e. metal or Ar) particle. Thus, our depositions might properly be considered as a form of low energy sputtering. Since the cluster KE is about two orders of magnitude larger than the rare gas binding energy, such a process will also involve the displacement of a large number of matrix particles. This does not affect the quality of our absorption spectra, however, as these are quite similar to those observed following deposition at the thermal energies. Although the experimental fragmentation data points scatter considerably, there is a general tendency towards lower fragmentation when decreasing the deposition energy. We do not, however, have physically convincing models for the deposition process, nor do we have sufficient experimental data to correlate the fragmentation behavior to the binding energy of the cluster.

As long as translational energies are ten times (or more) larger than cluster bond strengths, the term soft-landing should be understood as probably involving a series of soft collisions which efficiently transfer the energy to the matrix.

2.5.3 Matrices

Matrices are usually made of a condensed rare gas, such as neon, argon, krypton, and xenon. The use of matrices was introduced by Pimental and his co-workers (Whittle, 1954) [10] These rare gases are chemically inert and optically transparent when cooled on a cold substrate usually at 14 K. The intermolecular forces in the matrices are small. Normally the rare gases crystallize in cubic close-packed (ccp) structures with a face-centered cubic (fcc) unit cell which is proved by x-ray diffraction studies. [11]

Matrices were grown at around 5-10 *u*m/hr with an Ar:metal dilution ratio of approximately 10^4:1, i.e., sufficient to ensure that the cluster remain well isolated both from each other and from any impurity species. The sample thickness could be tested when taking absorption

spectra, since the oscillator strength of the optical transition depends on the sample thickness. During deposition, the partial pressure of H_2O (the dominant background gas) in the cryostat chamber was generally about 5×10^{-9} Torr, as measured on a residual gas analzer (Leybold-Inficon, Quadruvac Q100). This translates into a better than 95% probability that a cluster will be surrounded by at least 12 nearest-neighbor argon atoms. (See figure 2.8)

The average density of vapor-deposited solids is about 1% less than the solid grown from the liquid, which indicates that the vapor-deposited solids are porous. [11] Therefore, unoccupied sites and imperfections in the matrices might affect the molecules embedded in it. It might lead to the matrix "site effects" which will be discussed in later chapter in lanthanum dimer Raman spectra.

We use units of nA-h (product of current and the deposition time in hours, 1 nA-h = 2.25×10^{13} particles) to measure the concentration of the sample. The density of neutrals in the matrix (N cm^{-2}) may be estimated from the gas-phase expression [12]

$$N = (2.6 \times 10^{19} / f\lambda^2) \int A(\lambda) d(\lambda) \qquad (2.2)$$

where $A(\lambda)$ is the measured absorbance, f is the (absorption) oscillator strength for the transition and λ is the wavelength in nm.

SCHEMATIC OF THE METAL CLUSTER DEPOSITION SOURCE

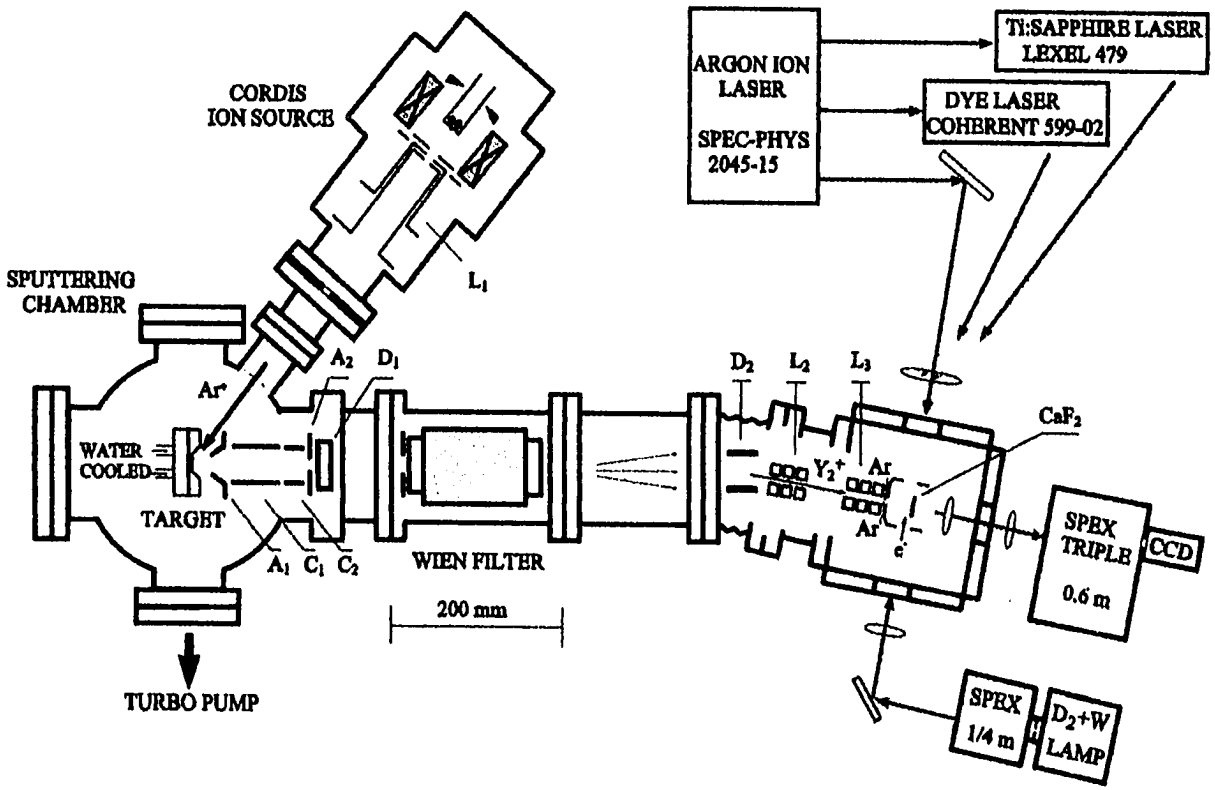

Fig. 2.1 CCNY mass-selected cluster beam deposition system

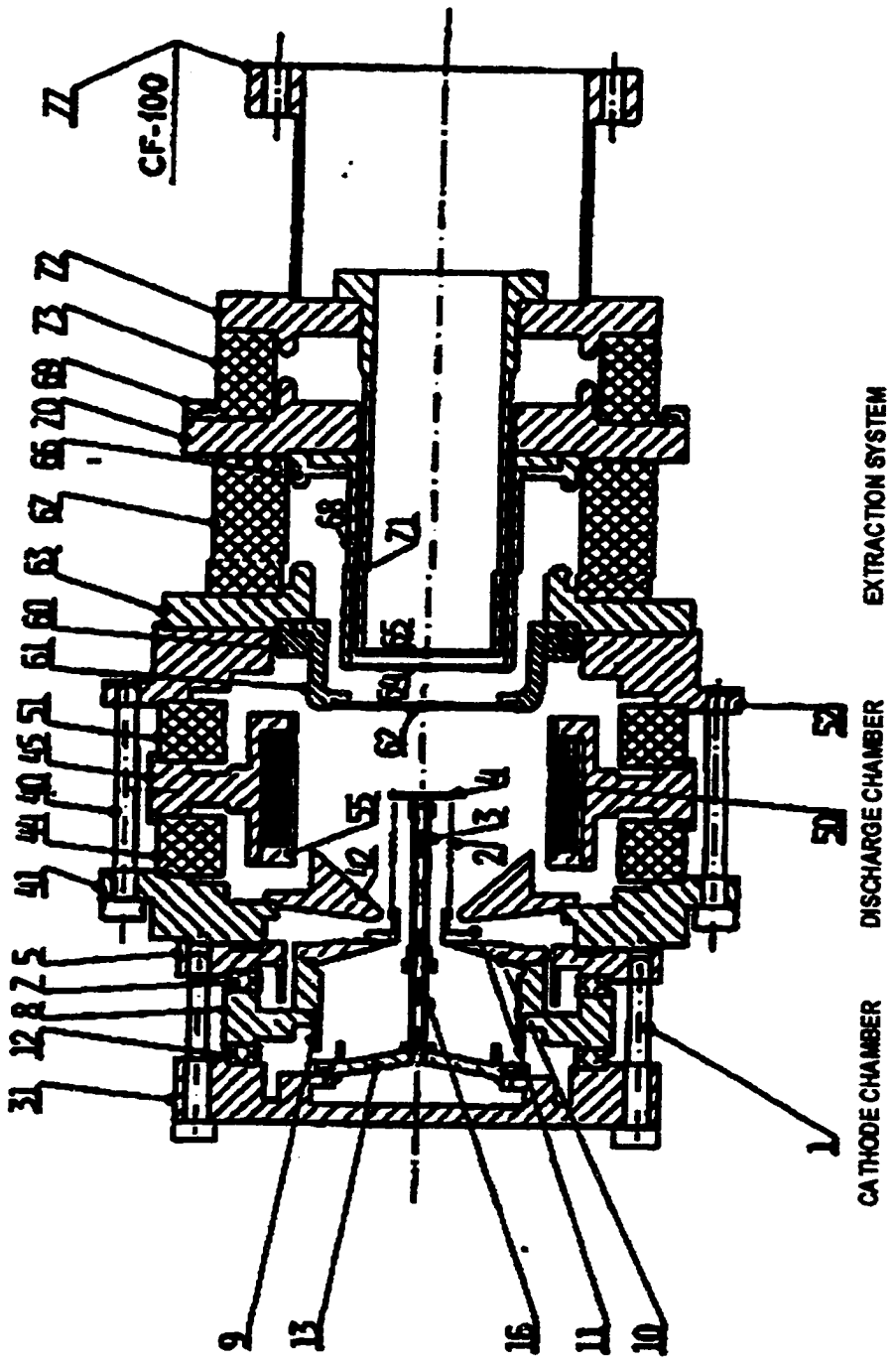

Fig 2.2 "CORDIS" ion source

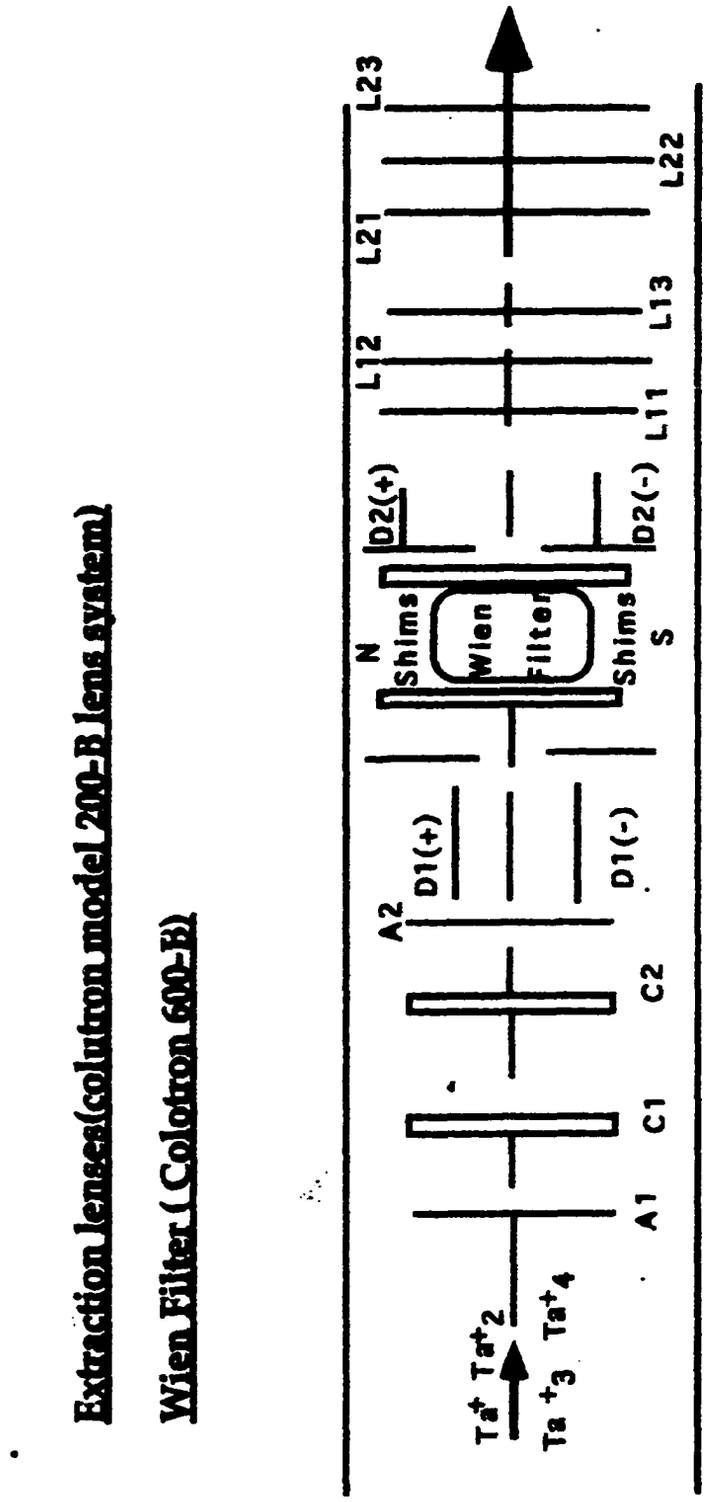

Fig 2.3 The schematic of the secondary beam

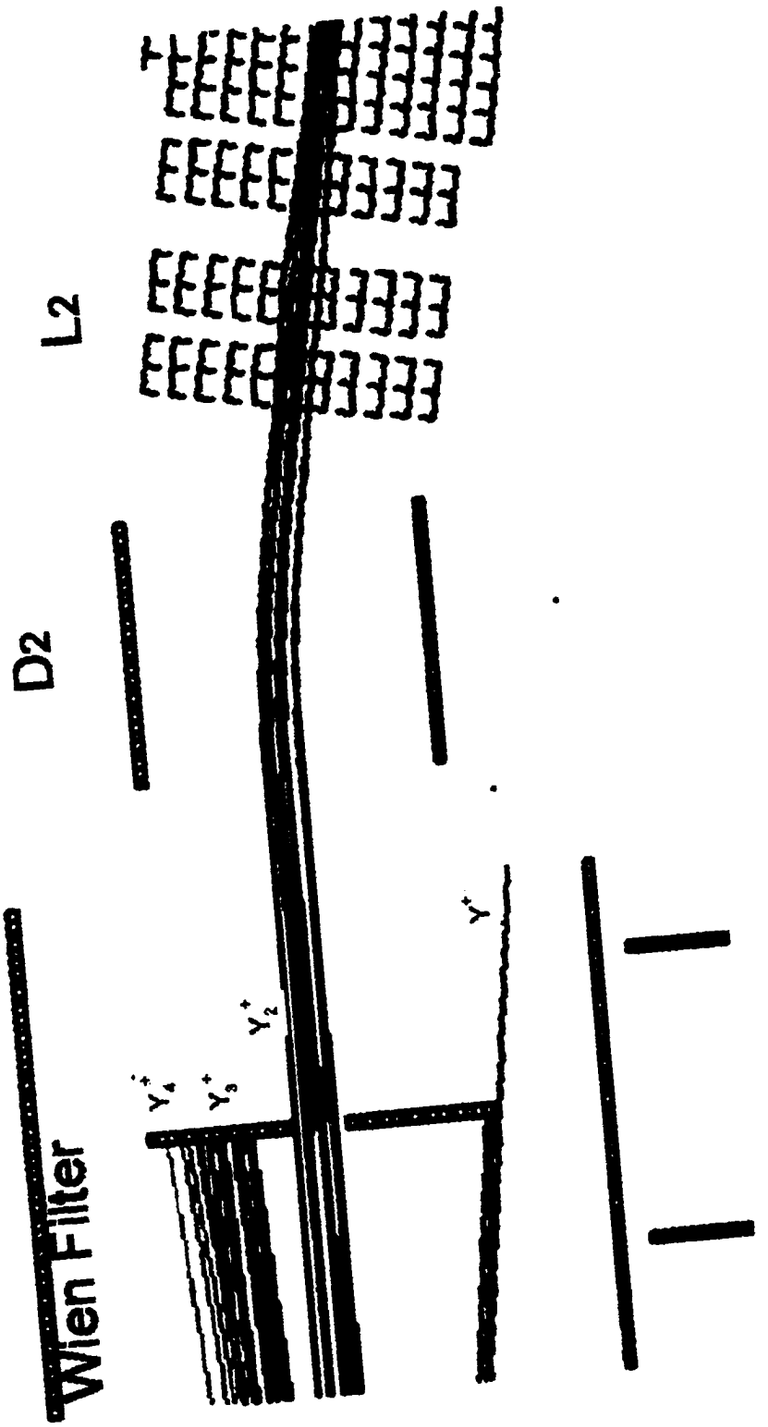

Fig. 2.4 The selected ion beam bent by 10° after mass separation

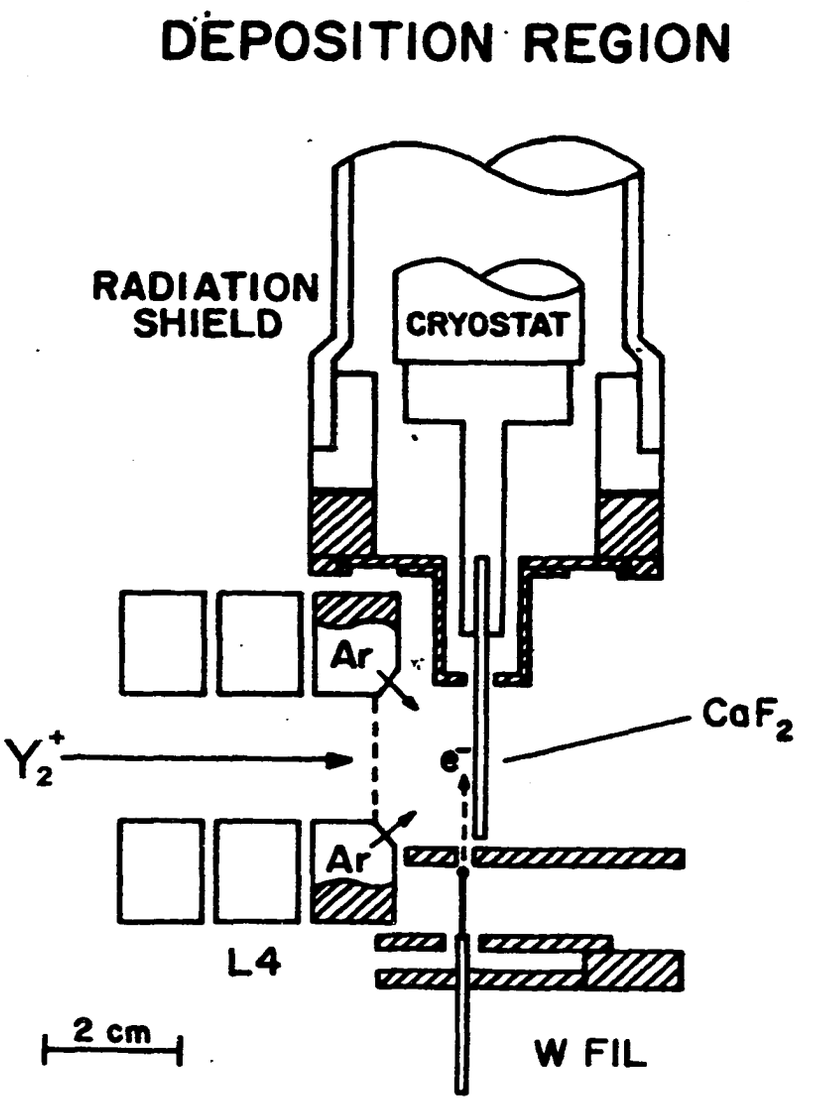

Fig 2.5 Deposit region

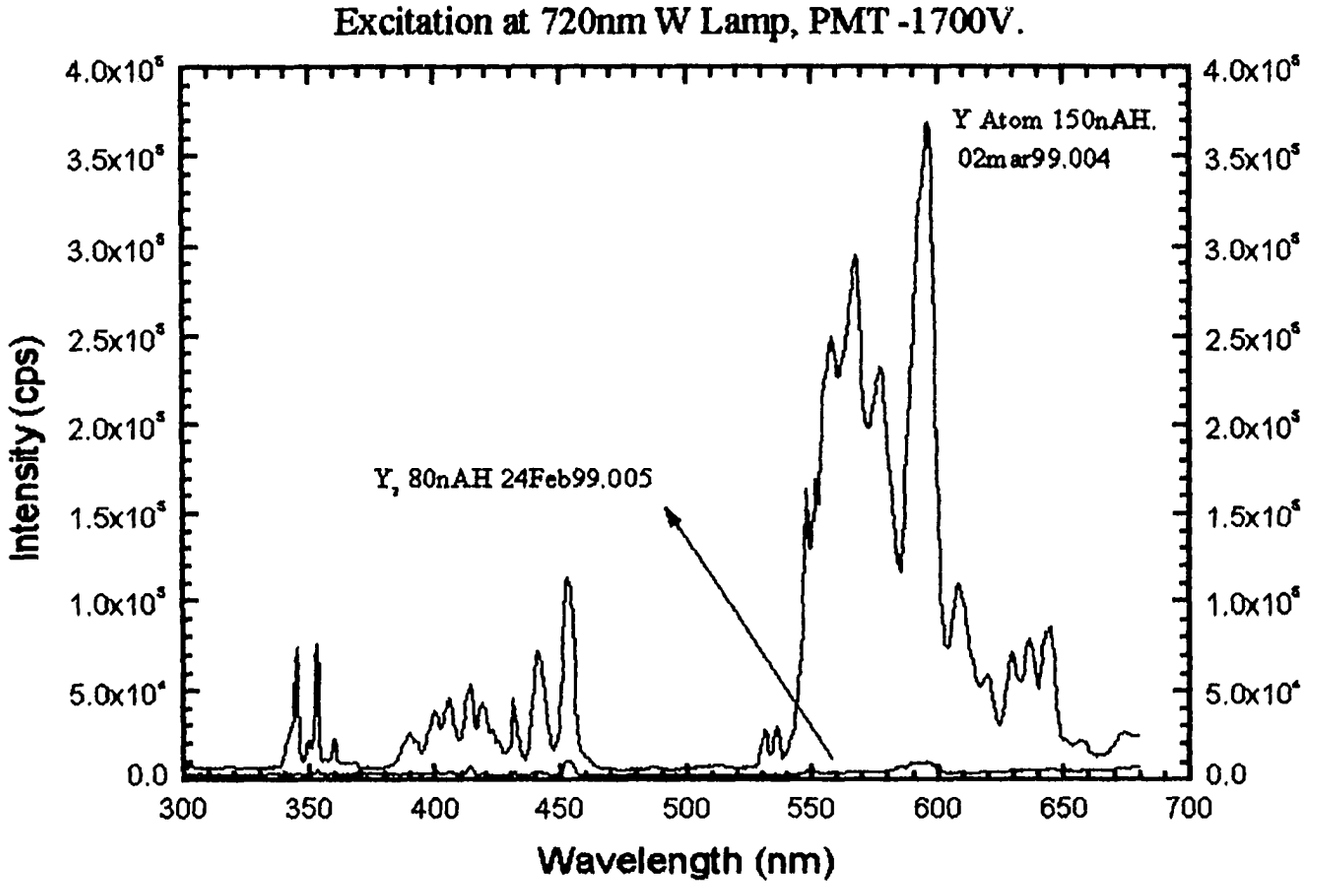

Fig. 2.6 Excitation SDS spectrum of Y atom and dimer deposited at similar condition. (Intensity of atomic features could be used to estimate the fragmentation percentage)

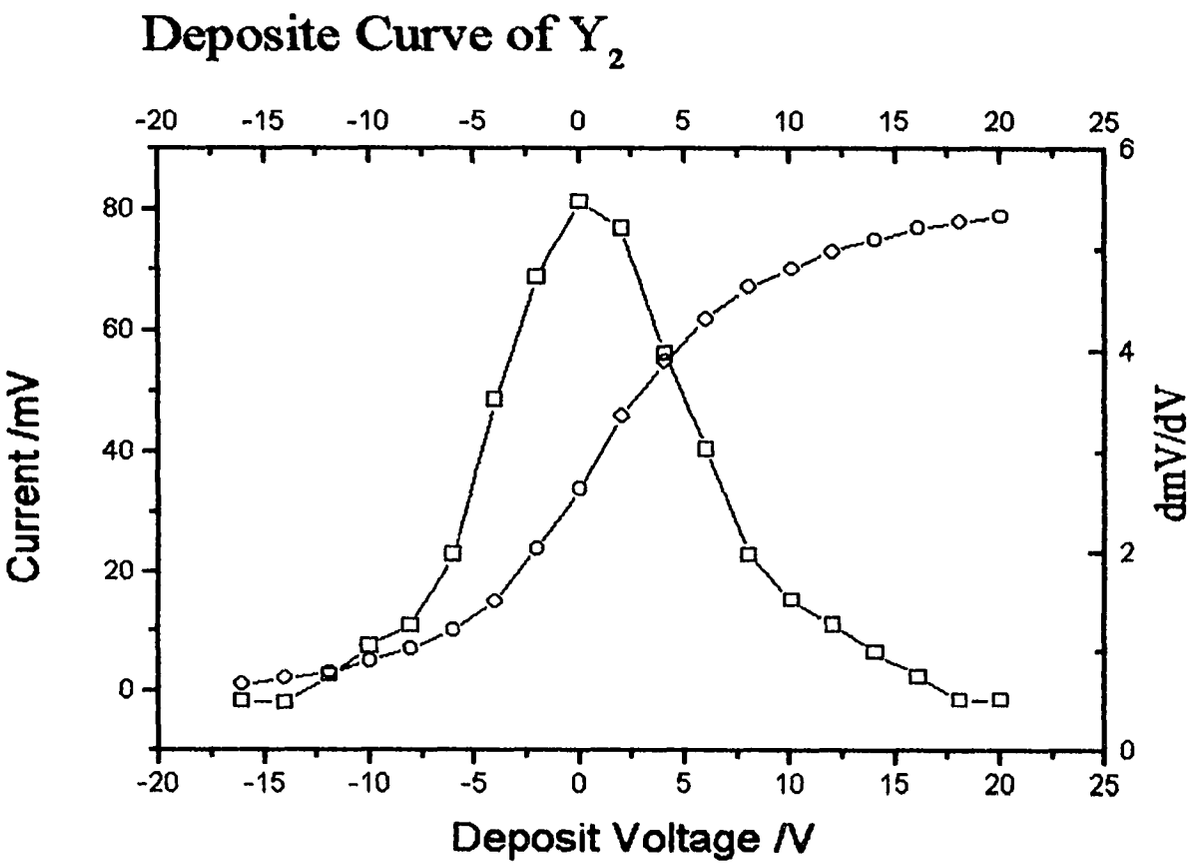

Fig. 2.7 Deposit curve of yttrium dimer. Circles are ion current of yttrium dimer measured on a Faraday plate,while Squares are differential of the current.

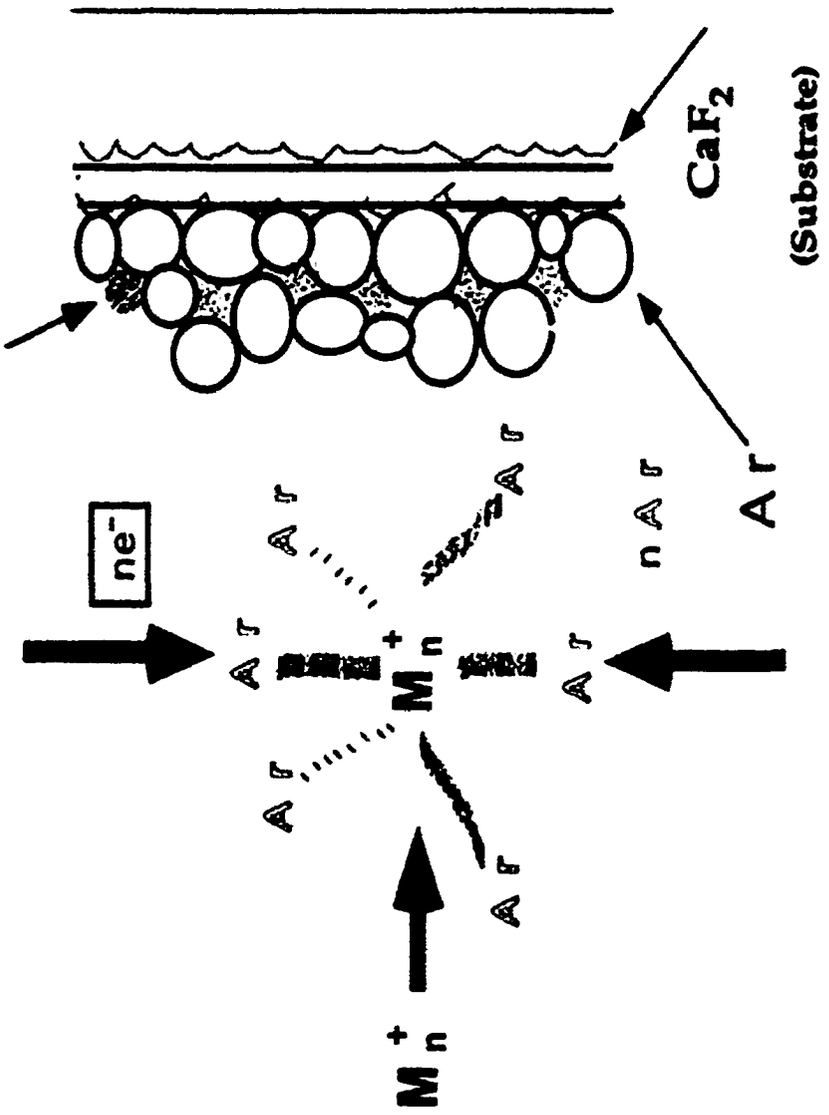

Fig. 2.8 matrix+cluster, during deposition (softlanding)

Chapter 3, Spectroscopy of metal clusters

3.1 Mass scan spectrum

A typical mass scan is obtained by applying a nonlinear voltage ramp to the power supply controlling the Wien filter magnetic field. Cluster ions which are accelerated through the secondary beam line can be monitored by reading the current of the positive ions meeting this plate, with dispersion sufficient to separate the selected cluster ions from other clusters from the atomic mass current. In this case the current on the Faraday plate is recorded as a function of the magnetic field on the Wien filter. Although the mass scales can be estimated from the known parameters of the Wien filter and the beam energy, we generally refine these scales using assigned cluster masses.

In fact we have efficiently used the mass scan spectrum to monitor the cluster types sputtered from the target, then select the desired one, and locate the suitable adjustable voltage on the Wien filter. Figure 3.1 and 3.2 shows the current of most transition metal clusters sputtered

from a target in our previous experiments. Figure 3.3 is mass scans of recent studies on yttrium and lanthanum.

3.2 "SDS": a special absorption spectroscopy

The importance of the Raman technique lies in its ability to provide structural information such as cluster vibraional frequencies, force constants, bond energies, etc. However, Raman spectroscopy is relatively insensitive and is currently feasible in these experiments only in case where the Raman signal is resonantly enhanced. In order to carry out such measurements it is first necessary to map out the optical absorption spectrum of the cluster. Normally this is accomplished by observing (as a function of wavelength) the light transmitted by reflected through the matrix sample. An alternative method, developed by Professor Lindsay, which we term "*Scattering Depletion Spectroscopy*" (SDS), involves detecting the light scattered at 90° to that incident. Thus, if the sample absorbs at a particular wavelength, the scattered light will be depleted at this wavelength and so (at least in

principal) also contains the absorption spectrum of the sample. In general scattering depletion spectra are recorded as the ratio of a "reference intensity" to a "signal intensity". The latter corresponds to light scattered from the cluster-rich center of the sample, whereas the former pertains to that scattered near an edge.

Even at as low as 13 K and 10^{-7} Torr, the matrices containing the sample are amorphous. As mentioned in chapter 2, our matrices are not unique and distribution of the clusters in the matrices is not homogenous. We can measure the dense cluster region in the center of substrates by at least 10^2 cps with a reference intensity of 2×10^6, characteristic of dilute perimeter of the substrate plate.

The absorption condition may be expressed as

$$\mathbf{R^{sds} = (1+\alpha_a/\alpha_s)\{[1 - exp(-\alpha_s)]/(1 - exp(-\alpha_a - \alpha_s)\}} \qquad (3.1)$$

where α_a and α_s are absorption and scattering coefficients, proportional to the number of absorbers/scatterers and the sample thickness.

We present SDS measurements for two sample matrices when we study a transition metal cluster: atomic metal in argon and clusters in argon. We measured resonance Raman spectra for cluster in argon, and

found that the corresponding Raman excitation profile closely mimics the absorption spectrum. .

For our matrices we found that the SDS technique is in fact somewhat more sensitive than conventional absorption measurements. Comparing the absorption spectrum of our lanthanum atomic deposition in argon with that of a similar deposition in another laboratory, it is clear that most of the atomic features are same in both spectrum, however, our SDS spectrum are much more sensitive. (See Figure 3.4 yttrium atomic SDS compared with a La atomic absorption traditional spectrum) For strongly scattering samples, SDS has advantage over normal absorption spectroscopy, with its flatter background.

This technique is accomplished by a special spectral device, including light source (tungsten and deuterium lamps), and a stepping motor controlled reflecting mirror. Light emitted from the lamp passes through a SPEX monomate, positioned to meet the sample plate at a right angle. Over 12 positions may be selected laterally across the substrate plate. Prior to recording SDS, an optical density profile is determined by recording a single beam spectra as a function of lateral position on the sample-holding substrate. After scanning the absorption

without the reference, the dense sites with highest absorption can be selected as sample sites, while the dilute sites with lower absorption could be used as reference sites. Approximately twice as much absorption was found in the center compared to the near the edge.

The SDS interface software was designed by Dr. George Sukenick and Dr. Zhengdong Hu in Quick Basic 4.0 and is run on a 386 PC. Since the position of light from the SPEX monomate must be determined by eye, the interface software controlls the stepping motor clockwise or anti-clockwise to set the reference and signal position. The schematic is shown on figure 2.1.

3.3 Excitation spectroscopy

As described in chapter 2, the fragmentation of clusters during the deposition could be estimated by calculating the relative intensity of the atomic features in the excitation spectrum of atom and clusters under similar experimental conditions. Also excitation spectrum provide a good view of the absorption and emission situation of the sample in certain wavelength regions.

The same optical arrangement as for absorption spectra is employed, however, there are two differences: first, the mirror mounted on the stepping motor is disabled so as to project light at only one particular lateral position on the substrate, which is similar to the taking of the absorption density profile; secondly, low pass filters are placed in an Oriel Corp. filter holder placed before the PMT. Filters normally used are from 300 nm to 700 nm.

3.4 Raman and Luminescence spectroscopy

When monochromatic radiation of wavenumber ν_0 is incident on systems like dust-free, transparent gases and liquids, or optically perfect transparent solids, most of it is transmitted without change, but, in addition, some scattering of the radiation occurs. If the frequency content of the scattered radiation is analyzed, there will be observed to be present not only the wavenumber ν_0 associated with the incident radiation but also, in general, pairs of new wavenumbers of the type $\nu'=\nu_0\pm\nu_M$. In molecular systems, the wavenumbers ν_M are found to lie principally in the ranges associated with transitions between rotational,

vibrational, and electronic levels. The scattered radiation usually has polarization characteristics different from those of the incident radiation, and both the intensity and the polarization of the scattered radiation depend on the direction of observation. Such scattering of radiation with change of frequency (or wavenumbers) is called Raman scattering, after the Indian scientist C. V. Raman who, with K. S. Krishnan, first observed this phenomenon in liquids in 1928. [1] The effect has been predicted on theoretical grounds in 1923 by A. Smekal. [2] Very shortly after the paper of Raman and Krishnan was published, Landsberg and Mandelstam in Russia reported the observation of light scattering with change of frequency in quartz; [3] and Cabannes and Rocard in France confirmed Raman and Krishnan's observations. [4]

In the spectrum of the scattered radiation, the new wavenumbers are termed Raman lines, or bands, and collectively are said to constitute a Raman spectrum. Raman bands at wavenumbers less than the incident wavenumber (i.e., of the type ν_0-ν_M) are referred to as Stokes bands, and those at wavenumbers greater than the incident wavenumber (i.e., of the type ν_0+ν_M) as anti-Stokes bands.

Classical treatment of the Raman effect is based on the theory that a fundamental frequency shall appear as a shift in the Raman spectrum when the amplitude of the dipole moment induced by the incident radiation changes during the vibration considered. The magnitude of the induced dipole moment P is given by:

$$|P| = \alpha \cdot |E|, \tag{3.2}$$

where E is the electric vector of the incident radiation of frequency ν and α the polarizability. In an unsymmetrical molecule, during all normal vibrations a periodic change of the polarizability takes place and, therefore, all normal frequencies appear in the Raman spectrum, that is, are Raman active. However, in symmetrical molecules it may happened that for certain vibrations the polarizability does not change, at least for small amplitudes.

From the *Schrödinger* equation of a system of N particles of coordinates x_i, y_i, z_i and masses m_i:

$$\Sigma_i(1/m_i)(\partial^2\psi/\partial x_i^2 + \partial^2\psi/\partial y_i^2 + \partial^2\psi/\partial z_i^2) + (8\pi^2/h^2)(E\text{-}V)\psi = 0 \tag{3.3}$$

where ψ is the wave function, E the total energy, and V the potential energy, we deduce the energy values of the harmonic oscillator i, given by

$$E_i = h\nu_i(v_i + \tfrac{1}{2}),\ v_i = 0, 1, 2\cdots \qquad (3.4)$$

where

$$\nu_i = (1/2\pi)\sqrt{\lambda_I} \qquad (\lambda_I = k/\mu_I) \qquad (3.5)$$

is the classical oscillation frequency of the normal vibration i, and v_i is the vibrational quantum number and k is the force constant and μ_I the reduced mass. In the most general case of degeneracies of the normal vibrations, the vibrational term values may be written conveniently

$$G(v_1, v_2, v_3\cdots) = \Sigma\, \omega_i(v_i + d_i/2), \qquad (3.6)$$

where $d_i/2$ is the degree of degeneracy of the vibration ω_i (d_i = 1 for non-degenerate vibration).

The Raman scattering transition moment is:

$$R = \langle X_i \mid \alpha \mid X_j \rangle \qquad (3.7)$$

where X_i and X_j are the initial and final states, respectively, and α is the polarizability of the molecule:

$$\alpha = \alpha_0 + (r - r_e)(d\alpha/dr) + \ldots \text{higher terms} \qquad (3.8)$$

where r is the distance between atoms and α_0 is the polarizability at the equilibrium bond length, r_e. Polarizability can be defined as the ease with which an electron cloud can be distorted by an external electric field. Since α_0 is a constant and $< X_i \mid X_j > = 0$, R simplifies to:

$$R = < X_i \mid (r-r_e)(d\alpha/dr) \mid X_j > \qquad (3.9)$$

The result is that there must be a change in polarizability during the vibration for that vibration to inelastically scatter radiation.

The polarizability depends on how tightly the electrons are bound to the nuclei. In the symmetric stretch the strength of electron binding is different between the minimum and maximum internuclear distances. Therefore the polarizability changes during the vibration and this vibrational mode scatters Raman light (the vibration is Raman active). In the asymmetric stretch the electrons are more easily polarized in the bond that expands but are less easily polarized in the bond that compresses. There is no overall change in polarizability and the asymmetric stretch is Raman inactive.

Since, for small amplitudes of the nuclei, a polyatomic molecule may be considered as a superposition of harmonic oscillators, the results for the harmonic oscillator approximation of diatomic molecules may be

utilized. Therefore, both in the infrared and Raman spectrum we have the selection rule:

$$\Delta v_i = \pm 1 \qquad (3.10)$$

for each normal vibration v_i. Since the oscillators in this approximation, are independent, no simultaneous jumps of two or more vibrations can occur. As for diatomic molecules, only those vibrations that are connected with a change of dipole moment can have $\Delta v_i = \pm 1$ for an infrared transition, and only those vibrations that are connected with a change of polarizability can have $\Delta v_i = \pm 1$ for a Raman transition. It is clear that the wave-number shifts of the Raman bands are equal to the actual vibrational frequencies (measured in cm^{-1})

$$v = \omega_i, \ |\Delta v| = \omega_i. \qquad (3.11)$$

In quantum theory, as in classical theory, the occurrence of a certain fundamental in Raman spectrum depends on the presence of a change of polarizability. If the lower state of a transition is the vibrationless ground state (v_1=0, v_2=0, ···) the eigenfunction ψ_v'' is totally symmetric. The eigenfuction of a state in which only one vibration is singly excited has the symmetry type of that vibration. Therefore, for a 1-0 transition of a vibration v_i (fundamental) the product $\psi_v'\psi_v''$ has the symmetry

type of the vibration ν_i. In another words, *a vibration is a active as a fundamental in the Raman effect if it behaves with respect to all symmetry operations permitted by the symmetry of the molecule in the same way as at least one component of the polarizability.* [5]

The harmonic oscillator approximation for the vibration is a reasonably good approximation to real molecular potential curves only in the region of small displacements from equilibrium at the bottom of the potential. This is adequate for describing the $1 \leftarrow 0$ fundamental, but not for transitions involving any higher levels. The potential curve rises more steeply than a parabola as $r \rightarrow 0$, as coulombic repulsion between the nuclei becomes more significant and less steeply as $r \rightarrow \infty$. Indeed, the potential must eventually approach a limiting, finite value corresponding to separated atomic states, and generally approaches this limit with a long-range attractive behavior such as r^{-6} (arising from van der Waals or dispersion forces), rather than anything like r^2. This finite energy between the minimum of the potential and the separated atoms is the dissociation energy of the molecule, D_e.

The effect of anharmonicity on the vibrational energy levels of a molecule depends on the detailed shape of the potential. It is convenient to represent the levels in terms of a series in v+1/2:

$$G_v = \omega_e(v+1/2) - \omega_e x_e(v+1/2)^2 + \omega_e y_e(v+1/2)^3 + \omega_e z_e(v+1/2)^4 + \cdots. \quad (3.12)$$

The center frequency of the 1→0 band is slightly shifted,

$$\nu_0 = \omega_e(7/2-1/2) - \omega_e x_e(9/4-1/4) + \cdots = \omega_e - \omega_e x_e + \cdots. \quad (3.13)$$

The ratio $x_e = \omega_e x_e/\omega_e$, is called the "anharmonicity factor". The effect of anharmonicity on vibrational energy levels and spectra is, primarily, that the energy levels are no longer exactly equally spaced, as in the harmonic oscillator, but get closer and closer together as v increases. The consequences of the anharmonicity are: (1) the selection rule holds only for a harmonic oscillator; the overtone bands can have appreciable intensity (2) the overtones are not exactly at $2\nu_0$, $3\nu_0$, and so on, but at slightly lower frequencies (3) the "hot bands" (v=1 → v=2, v=2 → v=3, and so on) are shifted slightly to the red of the fundamental (v=0 → v=1) band.

If we cut the series off after the first anharmonicity term,

$$\Delta G_{v+1/2} = \omega_e - 2(v+1)\omega_e x_e \quad (3.14)$$

the spacing decreases linearly with v, then a linear extrapolation of $\Delta G_{v+1/2}$ should yield the exact number of vibrational levels in the potential, and D_0^0, the dissociation energy from the v = 0 level, should be obtained simply by summing the $\Delta G_{v+1/2}$ values read off the linear graph:

$$D_0^0 = \sum_{V=0}^{V=V\max} \Delta G_{v+1/2}. \qquad (3.15)$$

The dissociation energy from the bottom of the potential, D_e, is obtained simply by adding the zero point energy to D_0^0:

$$D_e = D_0^0 + \tfrac{1}{2}\,\omega_e - \tfrac{1}{4}\,\omega_e x_e. \qquad (3.16)$$

If we substitute (3.14) for $\Delta G_{v+1/2}$ and carry out the sum, we find that

$$D_e = \omega_e x_e^2 / 4\omega_e x_e. \qquad (3.17)$$

While transitions for which one $\Delta v_i > 1$ or for which several $\Delta v_i \neq 0$ (overtone and combination bands respectively) are in general much weaker than the fundamentals, they may yet be observed in the Raman effect by using sufficiently long exposure times. Overtone and combination bands for which $|\Delta v_i| = 2$ or $\Sigma|\Delta v_i| = 2$, that is, transitions in which either one vibration changes by two quanta or two vibrations by

one quantum, are also called binary combinations; those for which $|\Delta v_i|$ = 3 or $\Sigma|\Delta v_i|$ = 3 are also called ternary combinations; and so on. Corresponding to the anharmonicity, the spectrum consists of a number of progressions Δv_i = 0, 1, 2, starting at every fundamental, binary combination, and so on, and consisting of nearly equidistant bands of very rapidly decreasing intensity. However, this decrease is not always quite regular if the molecule has symmetry, since certain overtone and combination bands may be forbidden by the rigorous selection rules. In fact it may happen in certain cases that a fundamental may be forbidden while certain overtone and combination bands involving the same vibration are allowed. In the case of degenerate vibrations the upper states of the overtone bands are split into a number of sublevels whose species are obtained from the point group table. Therefore, the overtone bands consist in general in a number of "sub-bands" which lie close together. But only those sublevels combine with the ground state whose species agree with that of at least one component of the polarizability.

Raman line intensities are proportional to:

$$R \propto \nu^4 \cdot \Sigma\nu \cdot I \cdot \exp(-E_i/kT) \cdot C$$

where ν is the frequency of the incident radiation, $\Sigma\nu$ is the Raman cross section (typically 10-20 cm^2), I is the radiation intensity, $\exp(-E_i/kT)$ is the Boltzmann factor for state i, and C is the analyte concentration.

If a scattering system has an absorption band close to the excitation frequency, resonance Raman scattering results. The intensity of resonance Raman scattering is usually many orders of magnitude greater than normal Raman scattering. The availability of a range of excitation frequencies from laser sources and the development of tunable laser sources has resulted in a growing exploitation of this form of Raman scattering. An obvious, but important, application of resonance Raman scattering is to use the intensity enhancement to enable spectra to be obtained from low concentrations of material, i.e., rare-gas matrices containing small amount of metal clusters.

Virtually every cluster source produces a distribution of particle sizes at low density. Therefore, spectroscopic techniques must be extremely sensitive and involve some inherent size selectivity to be useful for these kinds of experiments. Cluster geometry and the nature of cluster chemical bonding are the fundamental framework on which practical applications of clusters are based. Therefore, the understanding

of unusual catalytic activity, conductivity, or optical properties ultimately requires a knowledge of cluster structure. Thus spectroscopy studies continue to be a primary focus in cluster research, and new spectroscopic techniques are under investigation in a number of laboratories. Since 1990, Resonance Raman spectroscopy studies have been employed on transition metal clusters combined with mass-select ion techniques. [6]

In fluorescence, the incident photon is completely absorbed and the molecule concerned is thereby raised to an excited electronic level. After a certain lifetime in this upper state, the molecule undergoes a downward transition and thereby reradiates light of a frequency lower than that which it had absorbed. This mechanism is radically different from that of the Raman effect, in which the photon as a whole is never absorbed, but rather perturbs the molecule and induces it to undergo a vibrational or rotational transition. The essential difference is shown by the fact that fluorescence can be quenched by adding a species that is able to take away the energy of the molecule by collisions after it has absorbed the incident photon, but before it has had time to reradiate. No

such quenching is possible for the Raman effect, because this does not involve the actual attainment of an excited intermediate level.

Matrix samples may be interrogated by excitation and fluorescence spectroscopy, however, transition metal clusters show a notable lack of fluorescence except for a few examples, e.g., Group IB clusters, Mo_2 [7, 8], and Pt_2. In chapter 4 luminescence spectroscopy of Pt_2 will be discussed.

At very low temperature, the wavelength of vibrational transitions of a guest isolated in a cold inert host is observed to shift by less than 1% of the transition energy from the wavelength of the same transition when the guest species is in the gas phase. The shift arises because the excited state of the guest interacts with the host to a different extent than does the ground state of the guest. (see figure 3.5) The shift is a measure of the relative difference in interaction energy, but unfortunately, it does not give a measure of the absolute interaction energy of the host with either state of the guest. Depending on the relative magnitude of the interactions involved, the wavelength of the transition may be shifted either to longer or to shorter wavelength. [9]

Accordingly Raman spectroscopy is relatively sensitive probe of these species, provided that the exciting laser is resonant with an

absorption band. As a consequence, it is first necessary to map out the cluster absorption spectrum (discussed in 3.2) and then to have available both a wide range of laser wavelengths and a correspondingly versatile detection system. A fixed wavelength monochromator and notch filter combination is not suitable. In our laboratory, we have lasers (large frame argon ion, standing wave dye and CW titanium sapphire) which cover (almost continuously) a 275 – 1000 nm range of wavelenghts. As a detection system we originally had been using a double ¼ m monochromator combined with either a Hamamtsu R 943-02 photomultiplier tube, or (for wavelengths beyond about 800 nm) a low noise (4 Hz dark count) silicon diode detector. Currently Raman and emission spectra are collected with a SPEX 0.6m Triplemate Spectrometer and detected by a liquid nitrogen cooled CCD detector (SPEX model "Spectrum One") with DM3000R software. A schematic is shown on figure 3.6.

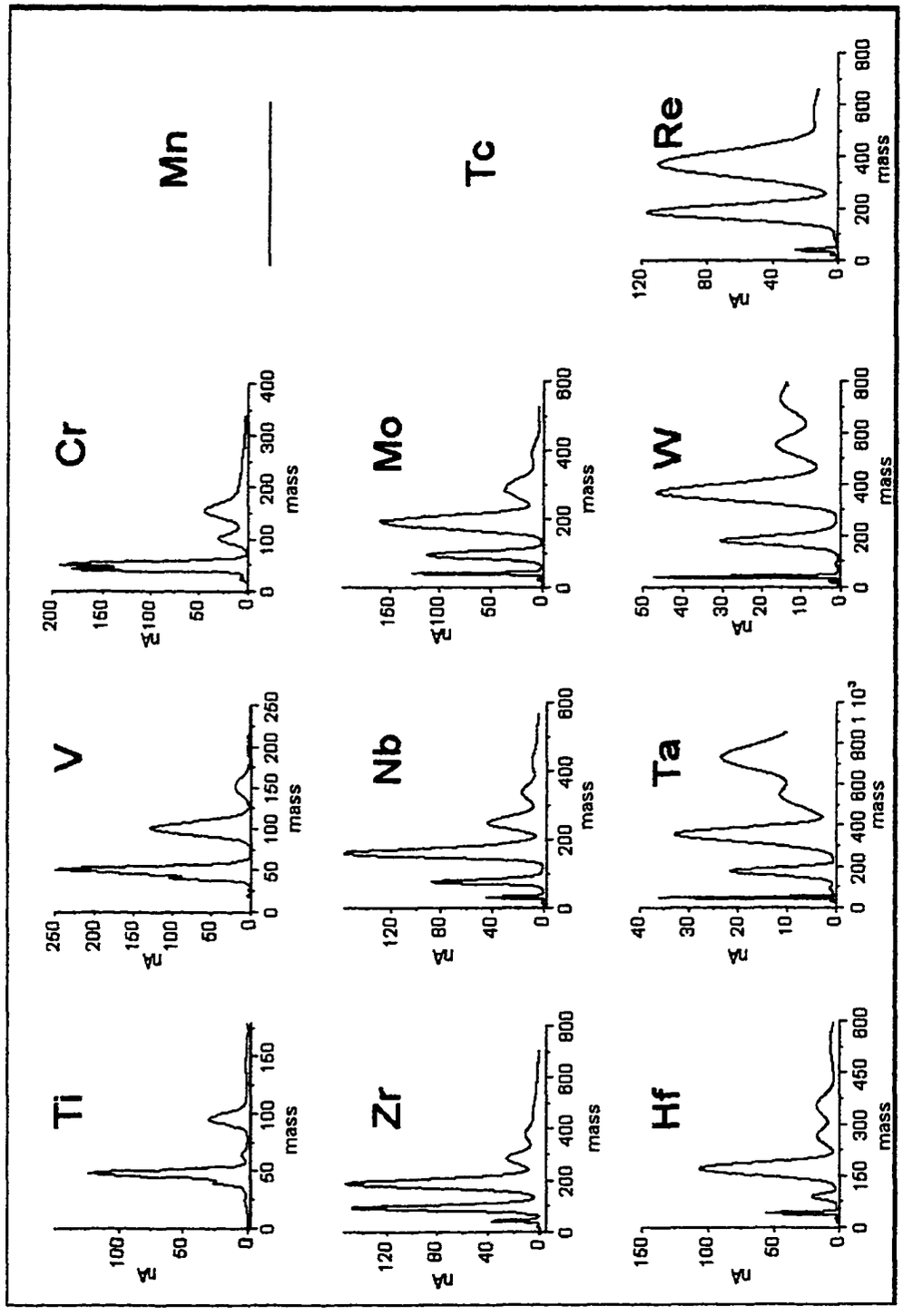

Fig. 3.1 Some early transition metal sputtering mass scan spectrum

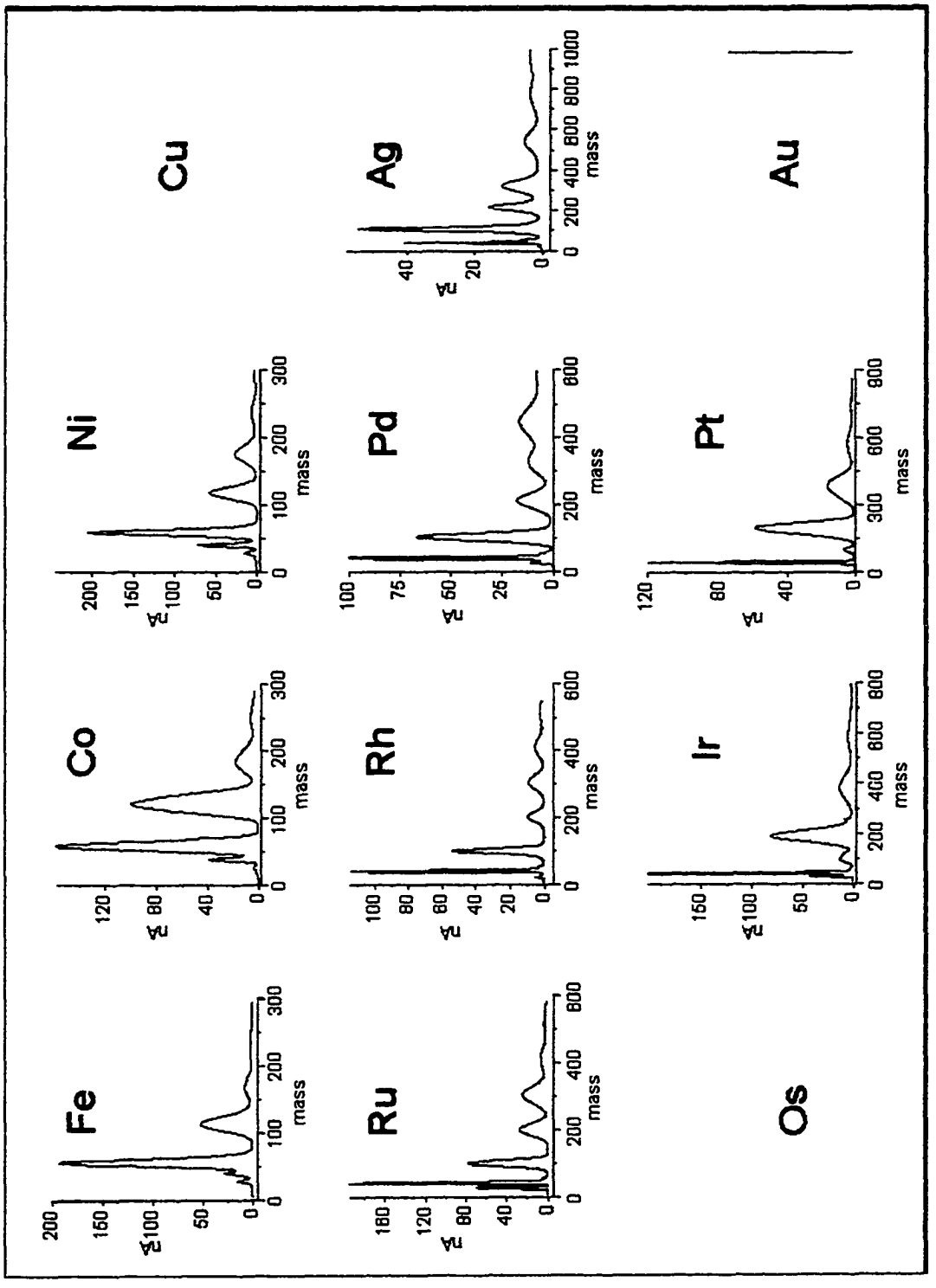

Fig. 3.2 Some late transition metal sputtering mass scan spectrum

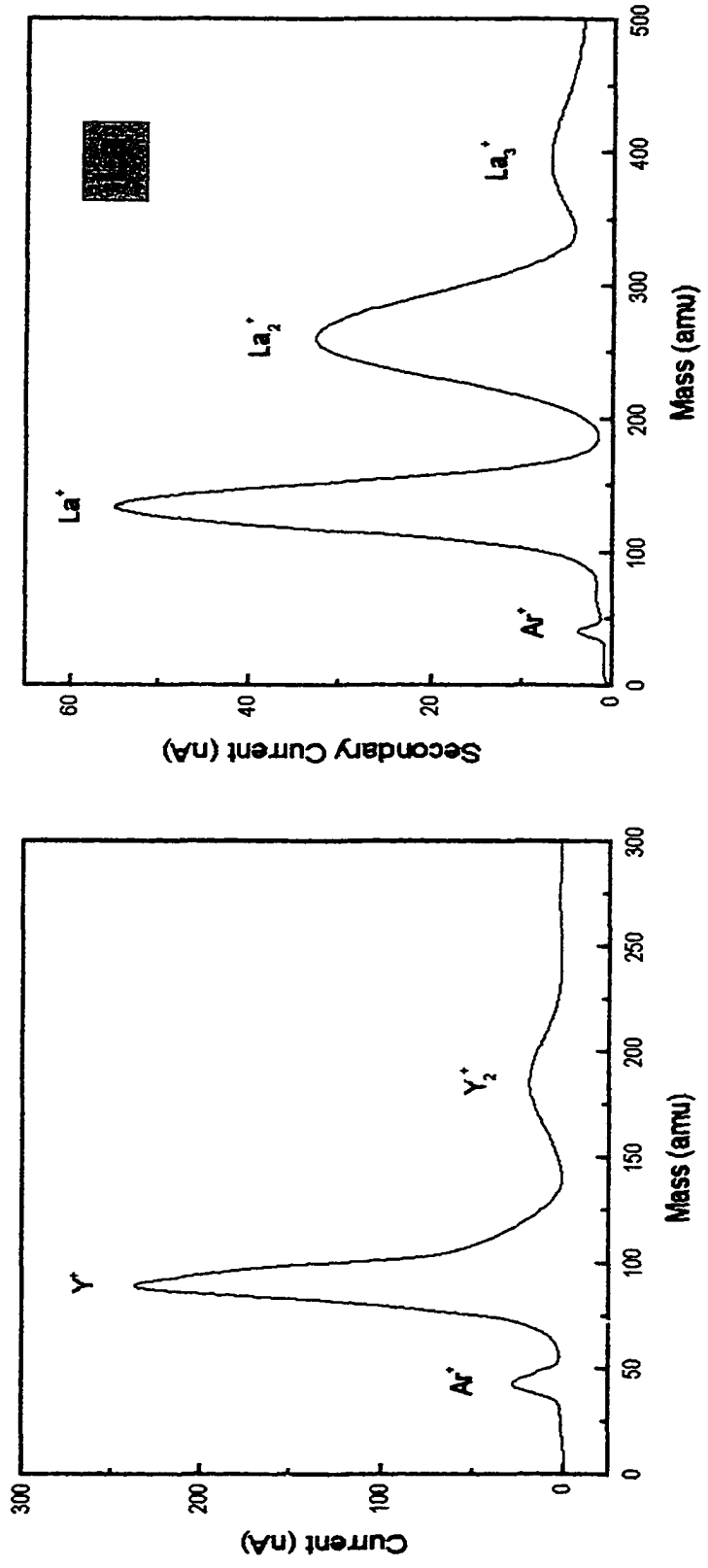

Fig. 3.3 Mass spectrum of yttrium and lanthanum

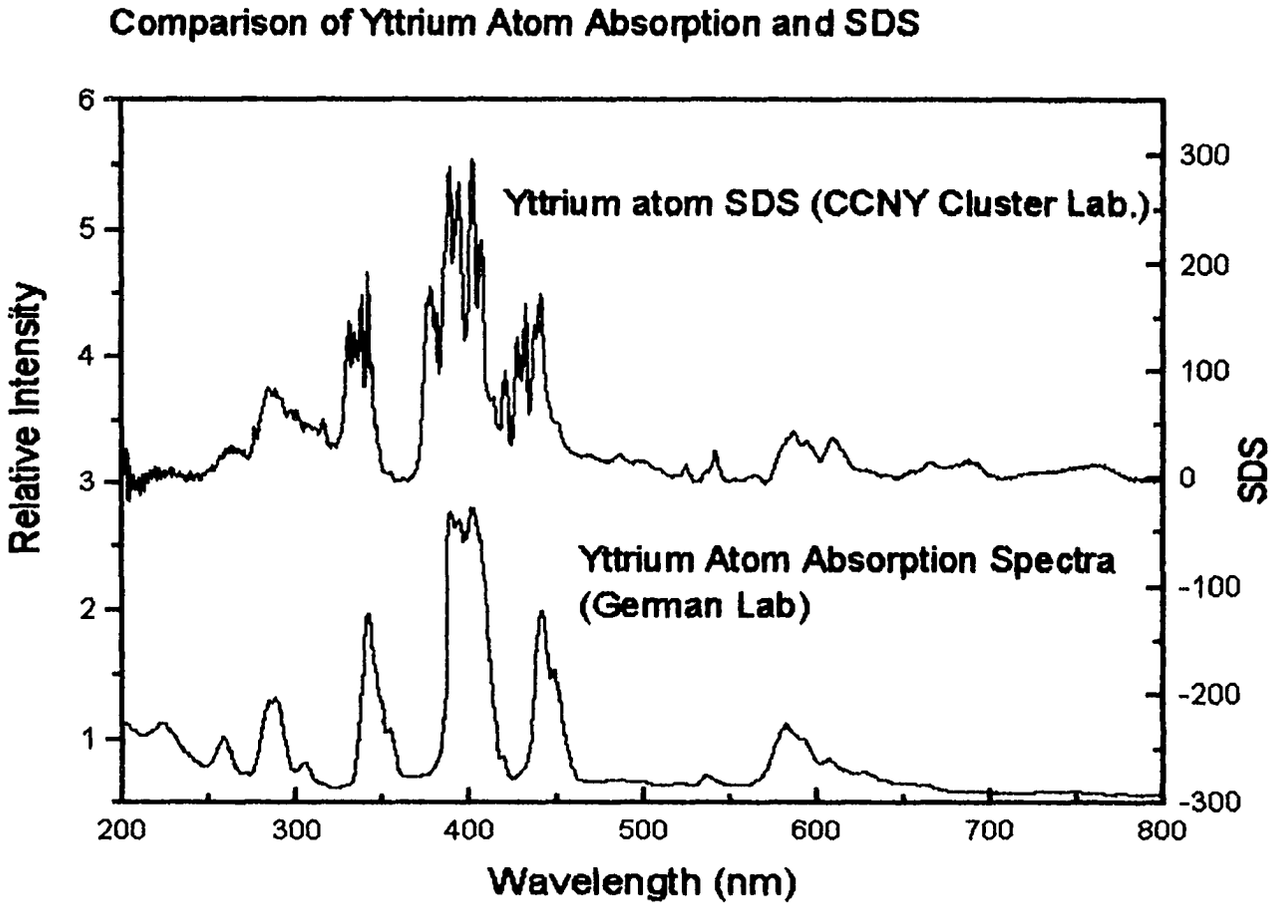

Fig. 3.4 SDS of yttrium atom (upperside) compared with yttrium atomic absorption in argon matrices

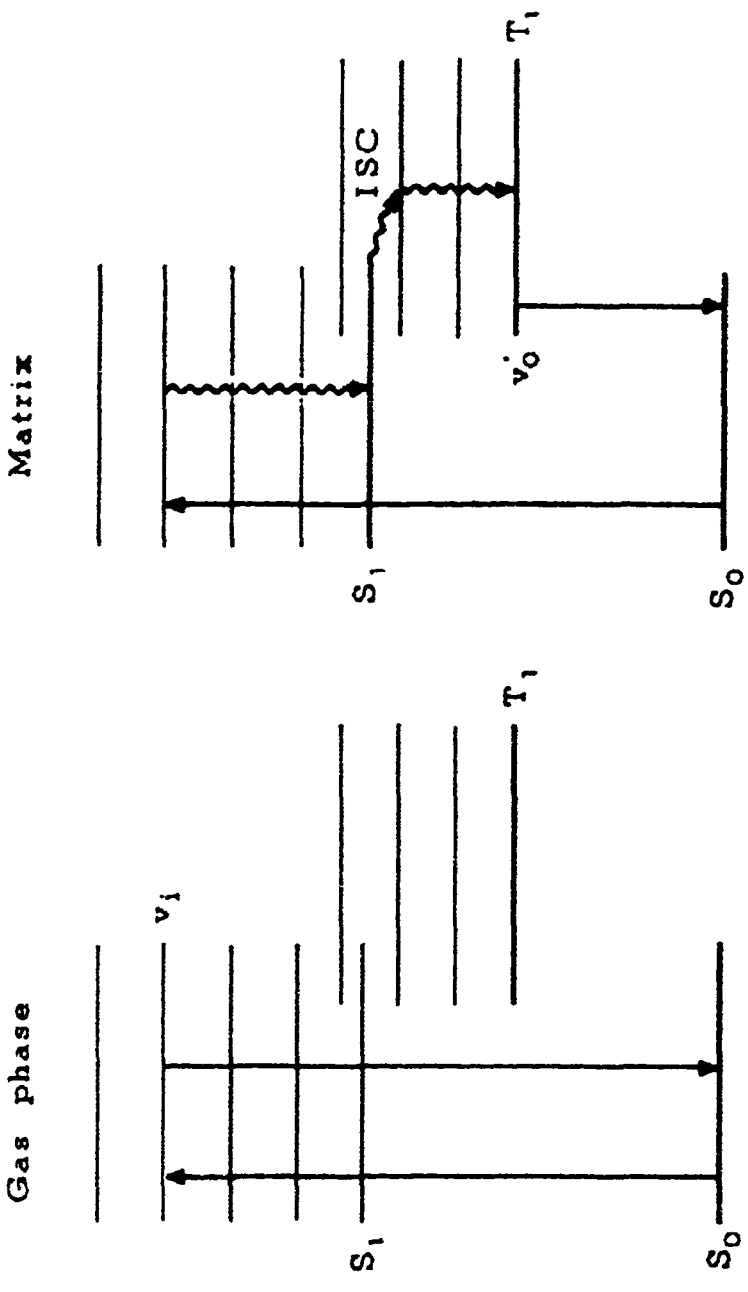

Fig. 3.5 Emission of molecules in matrix: Red shift arise from the interaction with matrix. a) gas phase; b) in matrix at 20 K

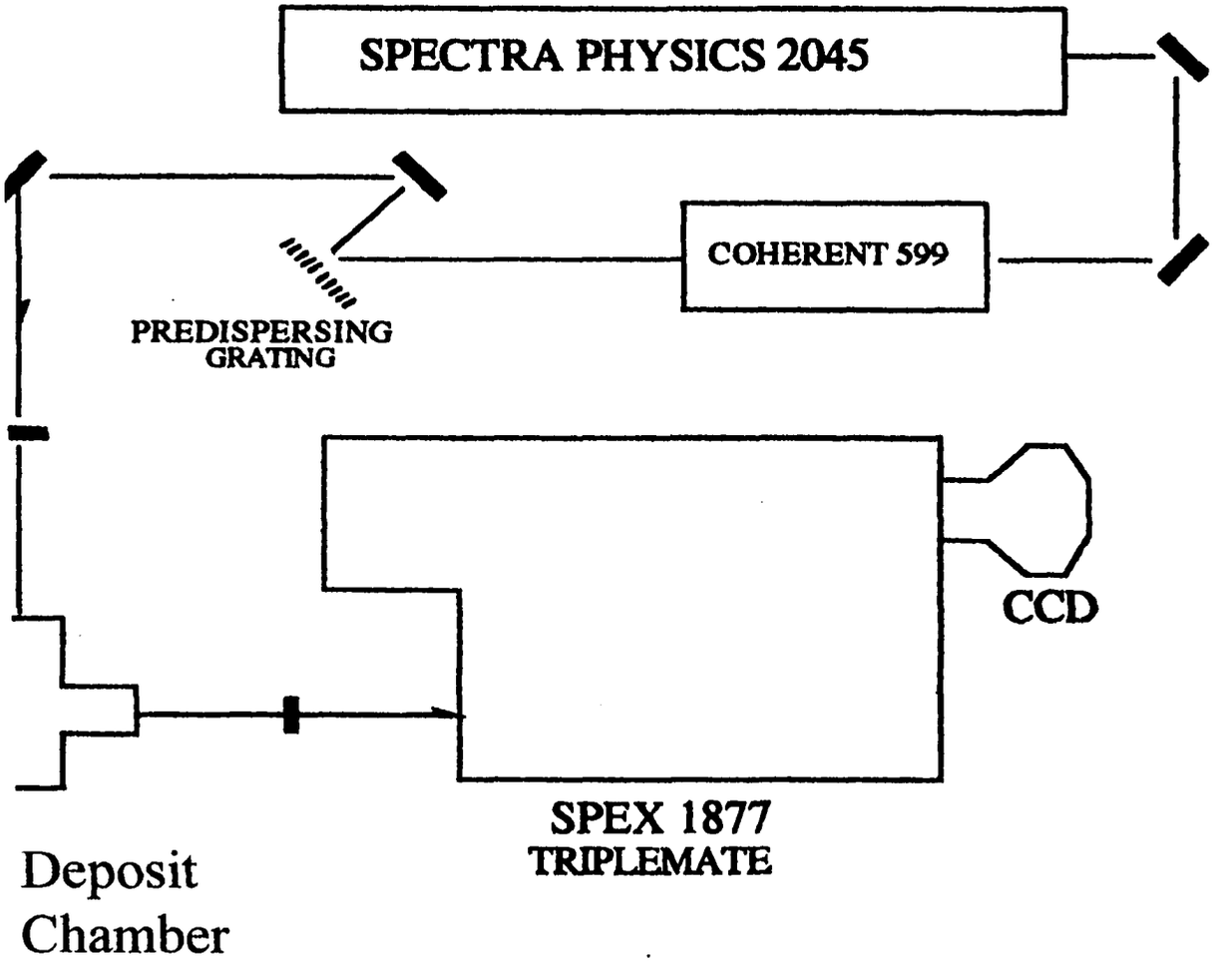

Fig. 3.6 Raman spectrum schematic

Chapter4 , Transition metal clusters

4,1 Luminescence Spectra of Mass-selected Pt_2 in Argon

I. Introduction

The dimer of platinum has been the subject of several recent experimental and theoretiacl studies. Jansson and Scullman [1] obtained an optical absorption spectrum in rare gas matrices. Photoelectron spectra [2] as well as resonant two-photon ionization spectra [3] have been carried out by Balasubramanian. [4] Our interest stems from resonance Raman spectra studies in our laboratory of various transition metal dimers such as Co_2, [5] Ni_2, [6] Re_2, [7] Rh_2, [8] and Ru_2. [9] Of particular interest in these studies is the degree to which d-orbitals contribute to bonding. Accurate values for the ground state force constants derived from the Raman frequencies have been invaluable in these determinations. The only previous ground state data for Pt_2 comes from the phtoelectron spectra of Ho et al. [2] from which a vibrational frequency of 215 ± 15 cm^{-1} was obtained. In order to enable careful comparisons of force constants

across the periodic table, we initiated an attempt to obtain a more accurate value for this parameter by searching for resonance Raman spectra, utilizing our mass-selected ion cluster deposition technique. Although no Raman spectrum was observed, we did obtain a sharp, intense luminescence spectrum, on which we report here.

II. Experimental Section

The CCNY cluster deposition source has been described in detail elsewhere. [10] Briefly, an argon ion beam (typically 15 mA at 25 KeV) sputters a cooled, platinum target (Alfa Aesar, 99.9%). The sputtered products are extracted by electrostatic lenses, mass-selected using a Wien filter, bent by 10° to eliminate neutrals, and then guided into the deposition region. Platinum dimer (or atomic) ions were then codeposited with argon gas and electrons onto a ~14 K substrate, composed of a CaF_2 plate. Ion currents under soft landing conditions could be measured on a Faraday plate in the deposition region and were Pt^+ (48 nA), Pt_2^+ (7 nA), and Pt_3^+ (3 nA). Prior to deposition, the selected ions were simultaneously slowed to 10 eV by a surrounding

"Faraday cage". Matrices were grown at about 4-6 μm/h with an Ar:metal ratio of approximately 10^4:1. Emission spectra were recorded using the visible output of an argon ion laser (Spectra Physics model 2045) pumping a titanium-sapphire laser. Scattered light was collected at 90° into a Spex 1877E 0.6 m Triplemate Spctrometer and detected by a liquid nitrogen cooled CCD detector (Spex model "Spectrum One") with DM300R software.

III. Results and Analysis

Absorption features, useful as a guide for finding resonance Raman (or other) spectra, were observed. However, earlier work by Jansson and Scullman and by Taylor et al. [3] indicated that Pt_2 absorbs in the 800-900 nm region, thus providing a starting point in a search for spectra. Although no Raman transitions were observed, [11] we found several sharp fluorescence features (see Figure 4.1.1) when pumping in the 800-815 nm region. The measured fluorescence frequencies are given in Table 1 and were obtained by averaging data at 38 different excitation wavelengths (22 in the case of the 0-4transition). The Figure 1 spectrum consists of a fairly strong progression ($v' = 0 \rightarrow v''$) in the

lower stated vibrational frequency average $\omega_e'' = 197.4 \pm 3.3$ cm^{-1}) and (see insert) a much weaker progression ($v' \rightarrow v'' = 0$) in the emitting state with an average frequency of $\omega_e' = 179.2 \pm 0.6$ cm^{-1}. No sequence features were observed. Isotope effect were not observed, as (predicted) splittings in the fluorescent spectra are only about 0.5 cm^{-1}, i.e., much less than the approximately 5 cm^{-1} half-widths of these lines. Annealing of samples to 25 K led to no change in the observed spectra. One further emission occurs at 10,852 (2) cm^{-1}, but this is largely excited between 12,500 and 13,000 cm^{-1}, which is an entirely different fluorescence excitation profile from that (see below) of the transitions shown in Figure 1. The average lower state frequency *is* $\omega_e'' = 197.4 \pm 3.3$ cm^{-1}, which is within experimental error of the ground state frequency (215 ± 15 cm$^{-1)}$ reported by Ho *et al.*.. [2] Our lower state vibrational separations do not fall off monotonically, but rather $\Delta G (v'' + ½)$ *increases* between $v'' = 1$ and 2 before decreasing for v'' = 3 and 4. Although this effect is small (and might be argued to arise from measurement errors), this pattern of vibrational energy separations is quite robust, persisting in all of the several methods that we used for analyzing the data. Accordingly, it seems likely that the lower state vibrational levels are perturbed by a

nearby state, which is not too surprising for, as pointed out by Taylor et al., [3] "with 157 molecular states present within 0.2 eV of the lowest dissociation threshold, it is likely that perturbations between these states will be significant." The Table 4.1.1 data suggest a perturbing state with origin near $v'' = 2$ (i.e., at approximately 400 cm^{-1}) and a vibrational frequency close to that of the perturbed state.

Figure 4.1.2 shows the measured (filled circles) fluorescence excitation profile (emission intensity *vs* excitation wavelength) for the 0-0 band of Pt_2. Excitation profiles for the 0-1 through 0-3 transitions are essentially identical to the Figure 4.1.2 result. Sufficient detail is observed to indicate a vibrational progression, but the spacing is slightly uneven indicating a possible overlap of several electronic transitions. This is consistent with the high-resolution gas-phase absorption spectrum of Pt_2, [3] where several overlapping systems (denoted I, II, etc.) were observed in a region corresponding to our matrix spectrum. In order to compare our results with those in the gas phase, we carried out a simulation of the matrix excitation spectra using the data for systems I-VI given in Table 4.1 of ref 3. Since the lowest gas-phase transition (the 0-0 band of system I) occurs at 11, 426 $cm^{-1,}$ whereas our observed

origin is 11, 929 cm^{-1} (i.e., 503 cm^{-1} to the blue), all the ref 3 transitions were shifted by a constant 503 cm^{-1}, but the ω_e and $\omega_e\chi_e$ values determined from the high-resolution spectra were maintained. Each line was given a Gaussian profile with a width of 103 cm^{-1}, as determined from the lowest frequency line of the matrix spectrum, which is relatively isolated from the rest. The relative intensities of the first few transitions *within* each of systems I-IV were kept the same as those in the gas-phase spectrum (Figure 4.1 of ref 3), but it was found necessary to adjust the relative intensities *among* each of these systems. Thus, we found the best fit with system III most intense, rather than I or II as observed in the gas phase. [12] The stick spectrum in Figure 4.2 gives the best fit intensities for each of the contributing lines, and the solid line is the overall result of our simulation. The correspondence between the two data sets is surprisingly good, indicating the possibility that the absorption spectrum in the matrix arises from the same transitions as are observed in the gas phase. However, we have made the rather questionable assumption of a constant matrix shift for the electronic origins of each of the six systems involved. Given the relatively broad line widths and the fact that these systems have roughly comparable

vibraional spacings, other fits with carrying matrix shifts are also possible.

IV. Discussion

The origin of absorption (excitation) differs from that of emission by nearly 1200 cm^{-1}, which indicates that the first excited state in absorption is not the same as that responsible for emission. The fact that ω_e' for our emitting state (179.2 cm^{-1}) does not obviously correspond to any of the ω_e; of systems I-VI in the gas-phase analysis [3] supports this idea. Since no absorption from the ground state to the emitting state is observed, it is most likely that this process is formally forbidden. The lack of direct emission in the matrix from the states of system I-VI indicates that radiationless processes depopulating these states is rapid by comparison with emission lifetimes.

For molecules with weak spin-orbit coupling, where spin may be regarded as a good quantum number, we would presume that the multiplicity of the emitting state (populated by intersystem crossing) differs from that of the ground state and from any of the excited states

involved in absorption. However, for Pt_2 spin-orbit coupling is expected to be very large, and only Ω (= Λ + Σ) is a good angular momentum quantum number. Although the assignment of Ω for the dimer ground state is not certain, calculations by Balasubramanian [4] predict this to be $^3\Sigma_g^-(0_g^+)$ arising largely from two δ_u^2 configurations (total weight 62%) plus two δ_g^2 configurations (total weight 32%). If this is correct, then our results can only be explained by the existence of a manifold of states to which spectroscopic transitions are forbidden from the ground state, but which are accessible by means of rapid radiationless transitions. Balasubramanian predicts a low lying state 5_u, which is only 614 cm^{-1} above the ground state (predicted vibrational frequency: 193 cm^{-1}), and another state of symmetry 4_u at 1074 cm^{-1} (predicted vibrational frequency: 240 cm^{-1}). Both these states are candidates for assignment as our lower state, although the 5_u is more likely due to its proximity to the predicted ground state and the fact that predicted vibrational frequency more closely matches ours. If either 4_u or 5_u corresponds to our lower state, the matrix-mediated intersystem crossing would involve a rather significant change in Ω.

Recently Pinegar *et al.* [13] have reported on the gas-phase fluorescence of jet-cooled Pt dimers. These authors found a ground state vibrational frequency of 222.5(7) cm^{-1}, and a nearby excited state at 2884(3) cm-1 whose vibrtional frequency is 197.0 (3) cm^{-1}. In addition they discovered a metastable state with a vibrational frequency of 210.9(8) cm^{-1} but were unable to determine the position of this state with respect to the ground state. Their ground state vibrational frequency differs by 25 cm^{-1} from that of our lower state, a shift too large to be explained by a matrix effect. There are several possible explanations for this discrepancy. One is that we are not observing emission to the ground state but only to the lowest state in a different manifold, which then rapidly converts to the actual ground state by radiationless transitions. In this case, our lower state must lie within 1299 cm^{-1} of the ground state. Another possibility is that Pinegar *et al.* are not observing emission to the ground state. Since their studies are carried out in the gas phase at low pressures, there is a possibility that their initial sample is in a metastable state (which should be plentiful in this molecule) as opposed to the true ground state. Indeed a metastable state was observed when exciting close to the expansion source, and

even though their apparent ground state was seen to remain much farther downstream, this does not rule out the existence of an even longer lived metastable state. The third possibility is that Pinegar *et al.* are indeed observing the true ground state, but the dimer ground state in an argon matrix is different from that in the gas phase. Although our measured frequency is almost identical to that of the gas-phase excited state as 2884 cm^{-1}, this is not the most probable candidate for our lower state as this would imply that matrix effects cause an energy decrease of at least 1683 cm^{-1}, which is unlikely. Furthermore, transitions from the manifold of systems I-VI to the 2884 cm^{-1}state are clearly allowed in the gas state, while they are forbidden to the state which we observe. It is conceivable that our lowest state coincides with the metastable state observed by Pinegar *et al.*, but the electronic origin of this state is unknown. In any case, there is still not sufficient experimental evidence to distinguish which of the above explanations for the discrepancy between the gas-phase and matrix results is most probable.

Table 4.1.1: Measured transition frequencies for Pt_2 in argon, with estimated uncertainties (1 standard deviation) in parentheses

Assignment (v'→v'')	**Frequency (vacuum cm^{-1})**	**ΔG(v'' + ½)**
0-0	10,730.5(6)	198.3(1)
0-1	10,532.2(6)	201.6(16)

Assignment (v''→v')	**Frequency (vacuum cm^{-1})**	**ΔG(v'' + ½)**
0-0	10,730.5(6)	179.6(7)
1-0	10,910.1(4)	178.8(6)

Figure 4.1.1 Laser fluorescence spectrum of Pt_2 in an argon matrix (sample content 45 nA-h) showing progressions in the lower state ($\nu' \rightarrow \nu'' = 0$). The excitation wavelngth is 815.4 nm for both spectra.

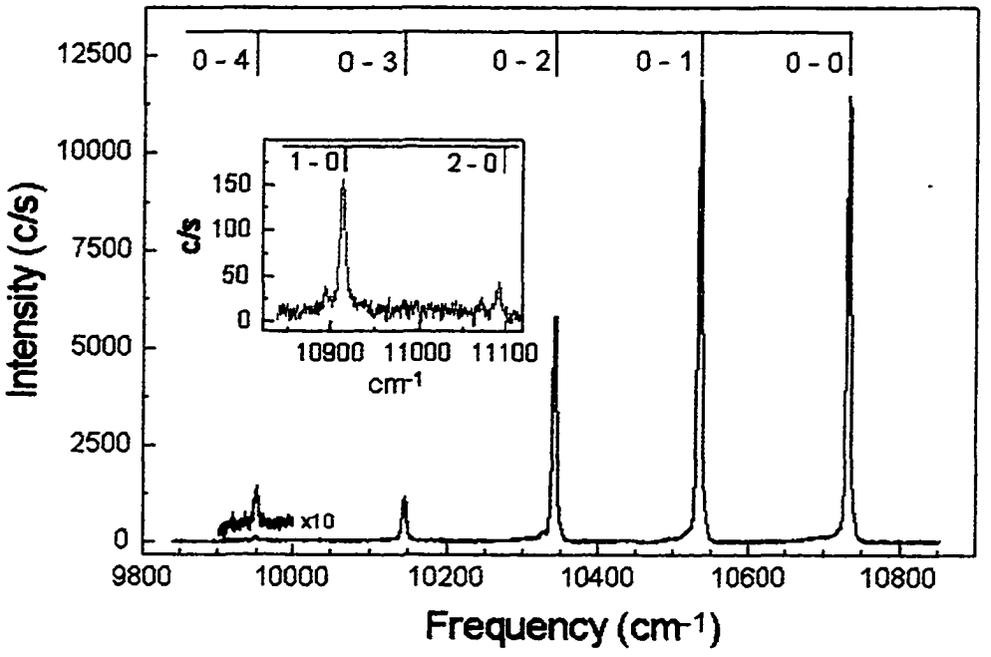

Figure 4.1.2 Emission excitation profile (filled circles) of the 0-0 band of Pt_2 in argon. Also shown is a fit to the matrix profile (solid line) using gas-phase data (shifted by 503 cm^{-1}, see text) from ref 3. Each transition was given a Gaussian line shape with a width of 103 cm^{-1} and an intensity as shown in the stick spectrum.

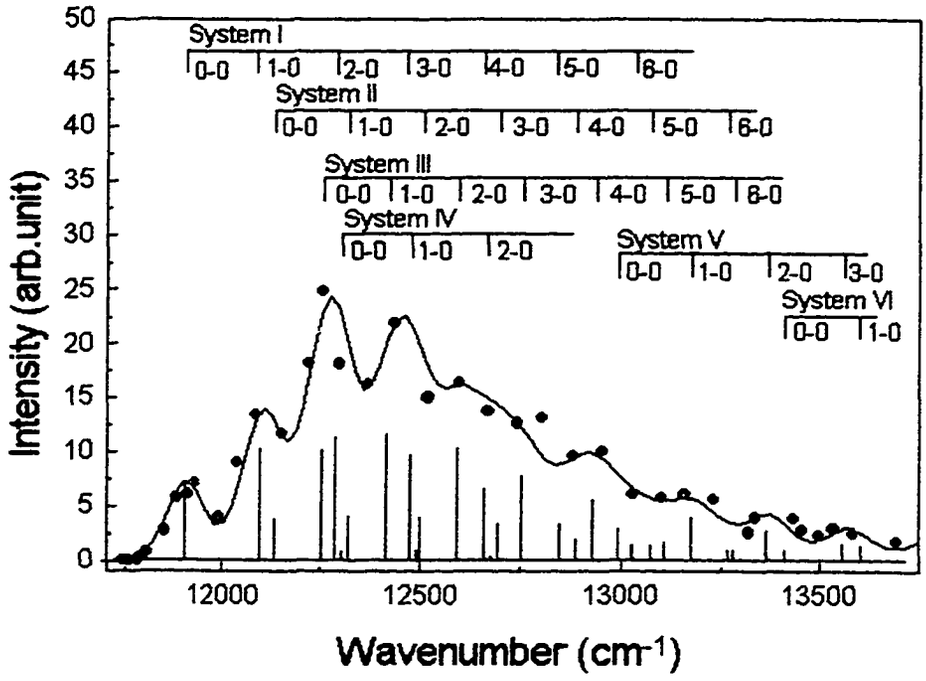

4.2 Absorption, resonance Raman, and Raman excitation spectra of hafnium trimers

I. Introduction

Almost no work, either experimental or theoretical, has been published on the clusters of hafnium. To our knowledge, only a Raman spectrum of the dimer exists. [1] In that work we utilized our mass-selection cluster beam to isolate dimers, which enabled unambiguous absorption and resonance Raman spectra to be obtained. Several transitions were observed in the visible region, and by pumping into the band at 620 nm a long progression in the ground-state vibration was observed. In this work we extend these results to the trimer of hafnium. Using mass selection we are able to isolate Hf_3 in argon matrices in sufficient quantities to observe several broad absorption peaks in the 605-620 nm region. Using a dye laser to pump in this region, we obtain a surprisingly rich and complex resonance Raman spectrum. The ground electronic state is shown to have a strong, linear Jahn-Teller interaction.

In addition we are able to identify five low-lying excited electronic states each with their own vibronic structure.

II. Experiment

The CCNY cluster deposition source has been described in detail elsewhere. [2] Briefly, an argon ion beam (typically 15 mA at 25 KeV) sputters a cooled, hafnium target (H. Cross, 97.0%). The sputtered products are extracted by electrostatic lenses, mass0selected using a Wien Filter, bent by 10° to eliminate neutrals and then guided into the deposition region. Hafnium trimer (or dimer or atomic) ions were then codeposited with argon gas and electrons onto a ~14 K substrate, composed of a CaF_2 plate. Ion currents under soft landing conditions could be measured on a Faraday plate in the deposition region and were: Hf^+ (85 nA), Hf_3^{2+} (13 nA), Hf_2^+ (14 nA), and Hf_3^+ (6 nA). The mass spectrum is shown in Fig. 4.2.1. The position of the Ar^+ peak at 40 amu is useful for calibration. Note that both the +1 and +2 charged species of Hf_3 appear. All the spectra reported here result from deposition and neutralization of Hf_3^{2+}. When Hf_3^+ was deposited, no absorption or

Raman spectra were observed. In order to check whether we were observing the Raman spectra of ions instead of neutrals, we tried depositing both Hf_3^{2+} and Hf_3^{+} without electrons. No spectra were observed under these conditions. Furthermore, since the charge/mass ratio of Hf_3^{2+} is the same as for Zr_3^{+} and since Zr is the major impurity (3%) in Hf metal, we compared the observed spectra with those previously obtained [3] for Zr_3^{+}. There is no match, and our conclusion is that we are indeed observing the spectrum of Hf_3. We have no explanation as to why spectra are not observed when depositing Hf_3^{+} in the presence of electrons under our conditions. One possibility is that the molecular geometry of neutralized Hf_3^{+}, differs from that of neutralized Hf_3^{2+}, resulting in different spectroscopes. As seen below, the Raman spectra are characteristic of a trimer, and the observed fundamental frequencies are just what would be expected for the trimer of hafnium on the basis of the dimer frequency. Thus, despite our inability to observe a spectrum when depositing Hf_3^{+}, we believe that the species observed when depositing Hf_3^{2+} is indeed the hafnium trimer.

Prior to deposition, the selected ions were simultaneously slowed to 10 eV by a surrounding "Faraday cage". Matrices were grown at about 4-6 μm/hr with an Ar:metal ratio of approximately 10^4:1. By comparing the intensities of known atomic excitation features in a trimer deposition with those obtained from depositions of the atom and dimer under similar conditions, the trimer fragmentation is estimated to be less than 2%. Matrix samples were interrogated *in situ* using both absorption and Raman spectroscopy. As previously reported, [4] the absorption measurements were made by collecting the light at 90° to that incident, a technique we term "scattering depletion spectroscopy" (SDS). The SDS spectrum of Hf_3 is shown in the top panel of Fig. 4.4.2. Raman spectra were recorded using the visible output of an argon ion laser (Spectra Physics model 2045) pumping a dye laser with Rhodamine 6G. Raman excitation profiles were obtained by observing the Raman spectra while tuning the dye laser in small steps through the absorption region 604-620 nm. Scattered light was collected at 90° into a Spex model "Spectrum One") with DM300R software. All Raman results were calibrated using the CaF_2 (substrate) line at 330 cm^{-1}.

III. Spectra and analysis

The absorption spectrum of Hf_3 (top panel of Fig. 4.2.1) consists of several broad, featureless peaks that were simulated using overlapping Gaussians (maxima at 606, 610, 615, and 619 nm). At this stage little can be said as to the nature of the transitions involved, but excitation profiles will provide some information below. However, this spectrum can be used as a guide for resonance Raman excitation. We first analyze the Raman spectrum, assigning vibrations of the ground and several low-lying excited states. Then we examine the Raman excitation profiles in an attempt to obtain more detailed information as to the nature of the excited states.

A. Raman spectra

In Fig. 4.2.3 we show a typical Raman spectrum recorded with excitation at 618.8 nm for the 100-500 cm^{-1} region and at 606.0 nm for the 500-900 cm^{-1}. Usually in trimer spectra we expect to see two (for D_{3h}) or at most three (for C_{2v}) fundamentals. [5] However, many more lines are observed than can be explained in this way. The observed

frequencies, averaged over many (up to 28) scans, at different excitation wavelengths are listed in Table I with one standard deviation uncertainties in parentheses. Careful examination of the observed spectral lines indicates that a frequency interval of 143-152 cm^{-1} is commonly obtained. Ozin and MacIntosh [6] have suggested that force constants of higher clusters (n>2) may be obtained from that of the dimer by simple distribution among the various bonds and we have found this to be a reliable guide. [7,8] Assuming a central force field, the totally symmetric fundamental frequency for a trimer should be observed at approximately $\sqrt{3}/2=0.866$ times the dimer frequency. For dihafnium the fundamental frequency is 176 cm^{-1} predicting a trimer frequency of 152 cm^{-1}, so it is likely that the observed intervals (143-152 cm^{-1}) correspond to the totally symmetric vibration. Note also that for several of the low-lying excited states, a fundamental is observed ~103-108 cm^{-1}. In trimers of D_{3h} symmetry, the ratio of totally symmetric to nontotally symmetric frequencies is $\sqrt{2}=1.41$ which is close to the ratio of the two frequency values observed here. Accordingly, we may designated these fundamentals as (at least approximately) of either a_1' or e' symmetry. (Sometimes for notational

simplicity we use the shorthand *a* or *e*.) With this assignment, and assuming a number of low-lying electronic states origins at 319.0, 413.4, 609.6, 642.8, and 785.4 cm^{-1} designated *A*, *B*, *C*, *D*, and *E*, respectively) and with the aid of excitation profiles, it is possible to assign of almost all the observed lines in our spectra.

We assign the lines at 142.8 and 278.1 cm^{-1} as the n_a=1 and 2 lines of the totally symmetric ν_a vibration of the ground state which we designate as *X*. In the region of the 142.8 and 278.1 cm^{-1} lines there are in fact clusters of four lines, which are shown in Fig. 4.2.4. Each set of clusters displays almost the same spacing which is quadratically increasing. These components may be interpreted as due to pseudo rotation caused by a strong, linear Jahn-Teller effect in the ground state. They may be fit to the expression $E=\alpha j^2$ where $|j|$ the total vibronic angular momentum, takes on values of ½, 3/2, 5/2, 7/2, and the best fit to α (average of n_a=1 and 2 data) is 1.9 ± 0.5 cm^{-1}. With this interpretation we may assign the X ground state to arise from a state of E' symmetry (in the D_{3h} limit), although in the strong Jahn-Teller coupling limit, the molecule must strictly speaking be considered fluxional, without fixed geometry. In Table 4.2.1 we use the notation

(n_a, n_e, j) to represent the number of quanta in (respectively) the totally symmetric (a_1') and doubly degenerate (e', in the limit of zero a Jahn-Teller effect) vibrations and the pseudorotational angular momentum, αj^2. In the low-lying excited electronic states (A, B, C, D, and E) no evidence is observed for a strong Jahn-Teller interaction of the type observed in the X state.

The first excited A state has an origin at 319.0 cm^{-1}. The line at 471.3 cm^{-1} is interpreted as the ν_a fundamental which is at 152.3 cm^{-1} above the origin. The line at 421.7 cm^{-1} lies 102.7 cm^{-1} above the origin and we interpret this transition as having one quantum of excitation in the ν_e vibration. Thus the ratio of ν_a/ν_e (1.48) is close to that expected (1.41) for D_{3h} symmetry, implying that the A state has an equilateral geometry. The origin of the B state is 413.4 cm^{-1}. The transition at 555.1 cm^{-1} is assigned to a ν_a vibration having a frequency of 141.7 cm^{-1}. Since no nontotally symmetric mode is observed, no information as to the geometry of this state may be inferred. The C state, with origin at 609.6 cm^{-1}, has a vibronic level at 726.3 cm^{-1} (116.7 cm^{-1} above the origin) which most likely corresponds to the ν_e fundamental. Although this deviates somewhat from the nontotally symmetric frequencies

observed in the other states, we base this assignment on the close similarity of the excitation profiles observed for both lines (see Table I). It is possible to account for this deviation by postulating that the *C* state has a C_{2v} geometry with a large distortion from equilateral geometry. The *D* state, with origin assigned as 642.8 cm^{-1}, shows a totally symmetric fundamental (ν_a) at 149.5 cm^{-1} (absolute frequency 792.3 cm^{-1}) with one quantum of excitation in a ν_a mode (ω=150.3 cm^{-1}) of an E state having an origin at 785.4 cm^{-1}, the 894.1 cm^{-1} line is most likely a ν_e vibration (ω=108.7 cm^{-1}). Although both the 785.4 and 894.1 cm^{-1} lines are too weak to provide a reliable excitation profile (see next section), the ν_a/ν_e ratio of 1.38 indicates a that the E state also has D_{3h} symmetry.

The properties of the low-lying states of Hf_3 are summarized in Table 4.2.2.

B. Raman excitation profiles

At this state it is worth noting that several distinct types of excitation profiles are observed, examples of which are shown in Fig. 4.2.2. A detailed examination of the profiles indicates that they correspond very

closely to the four optical transitions (top panel of Fig. 4.2.2, broken lines) at 606, 610, 615, and 619 nm. The Raman excitation profiles were also simulated using overlapping Gaussians and these data are summarized in columns 3-6 ("Excitation profile at wavelength") of Table I. For each Raman line, we indicate either *s* (strong), *w* (weak), or leave blank (for intensity too weak to measure).the *s* or *w* represent the relative intensity of a peak *within the profile*, whereas the column 2 entries marked relative intensity indicate the *relative intensity* of a Raman transition with respect to the other lines for 606 nm excitation. For several very weak lines, no reliable profile could be determined. Furthermore, the utility of this data is sometimes marred by the interference of weak fluorescence, which creates occasional ambiguities. It had been hoped to be able to classify each of the profiles into a few distinct types, but that proved to be difficult due to the considerable variety of distinct overall profiles observed. Several special features can be noted, however. A few lines (274.5, 278.1, 319.0, 606.6, 726.3, and 785.4 cm^{-1}) have most of their intensity in the 606 nm transition. Several others (298.2, 301.9, 751.2, and 792.3 cm^{-1}) are distinguished by their strength at 615 nm (with or without contributions at 619 nm).

Otherwise, no simple patterns are discerned. The similarity, even uniqueness, of the 751.2 and 792.3 cm^{-1} line profiles may be taken as confirmation that they belong to the same state. In the previous section we utilized the similarity of the 609.6 and 726.3 cm^{-1} lines to infer that these were related. Also noteworthy is the fact that the origins of the *A*, *C*, and *E* states all have considerable intensity at 606 nm but weak or no intensity at 615 nm, while *B* and *D* are strong at both 606 and 615 nm.

Considerably more information could, in principle, be gleaned from the excitation profile data, if we could be sure that the excited states were free from strong vibronic interactions. Since all four excited transitions are allowed from the E' (j = 1/2) ground state, in the D_{3h} limit they must be vibronically either A_1', or A_2', E', or E''. Both of the observed ground-state profiles having $j = 3/2$ (146.9 and 283.4 cm^{-1}) show strong intensity at 615 nm. Since $j = 3/2$ states are either A_1' or A_2' this implies that the 615 nm excited state must by either E' or E'' (since transitions A_1', $A_2' \rightarrow A_1'$, A_2' are forbidden). With the exception of the 301.9 cm^{-1} line, assigned as X (2, 0, 7/2), all transitions for which $j \neq 3/2$ do not show intensity at 615 nm. Since these must be vibronically E', to which transitions should be allowed from all possible excited state

symmetries, we obtain contradictory results, unless we assume strong vibronic distortion in the excited state. Then we might expect all transitions to be governed by the less stringent C_{2v} selection rules. We would then seek an explanation of the intensities in terms of Franck-Condon factors, but this is beyond our ability given the current data.

IV. Discussion

We have obtained detailed structural and electronic information concerning several states of hafnium trimer, apparently the first study of any sort on this molecule. The ground state arises from E' symmetry in the D_{3h} limit, but is strongly Jahn-Teller distorted. Conventionally, it is stated that strong spin-orbit coupling tends to quench Jahn-Teller effects.[9] Hafnium is a third row transition metal and would be expected to show strong spin-orbit effects. We must conclude therefore that either the quenching effect is not as large as normally believed, or that the ground state is of low spin (e.g., a singlet), with little or no spin-orbit coupling. The ground-state configuration of the Hf atom is $6s^2 4f^{14} 5d^2$ so the trimer has an even number of electrons. Thus a singlet ground state is possible. At this state, few transition metal trimers have been

characterized, so possibilities for detailed comparisons are scant. We have shown that the ground states of both Zr_3 [3] and Nb_3 [5] have D_{3h} symmetry, although in both cases there is little or no vibronic distortion. On the other hand Cu_3 [10] is well known to be a fluxional molecule in the ground state and is perhaps the best model for the present case.

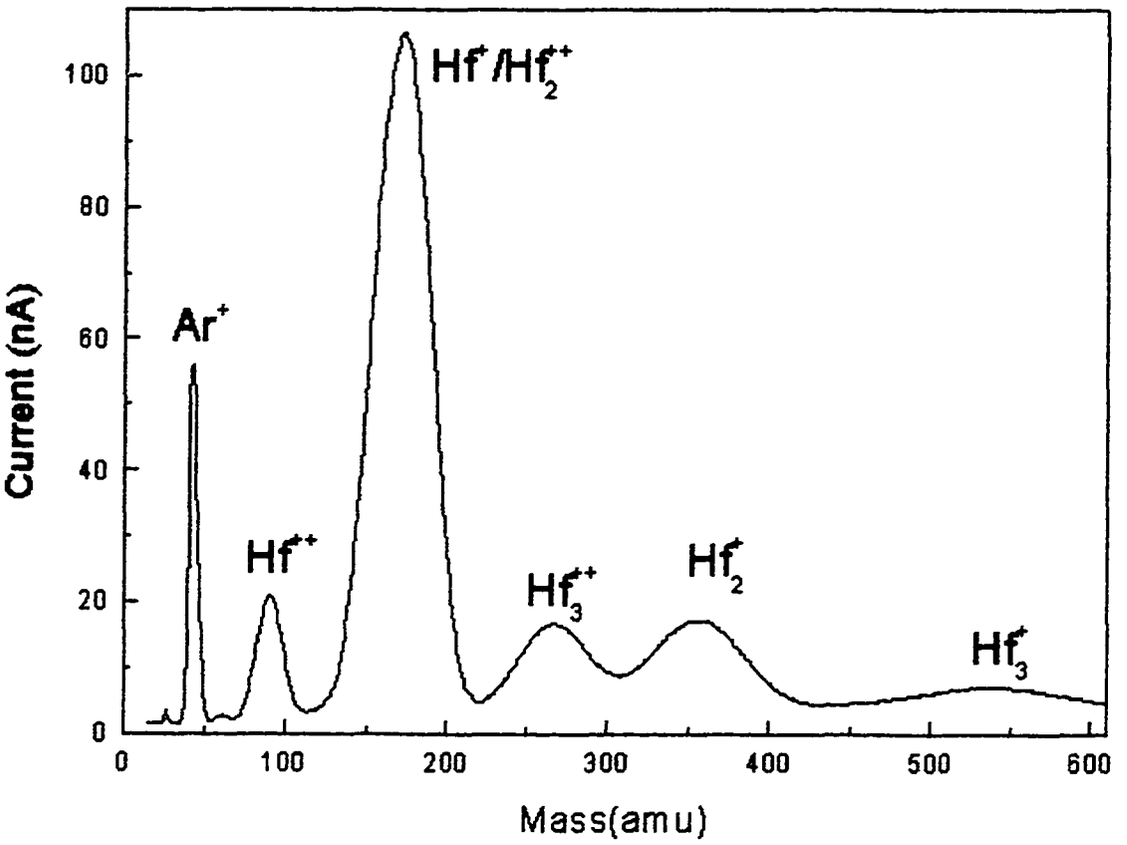

Fig. 4.2.1. Mass spectrum of sputtered Hf metal obtained by scanning the Wien filter magnetic field. Note peaks at mass/charge ratios corresponding to both Hf_3^{2+} and Hf_3^{+}.

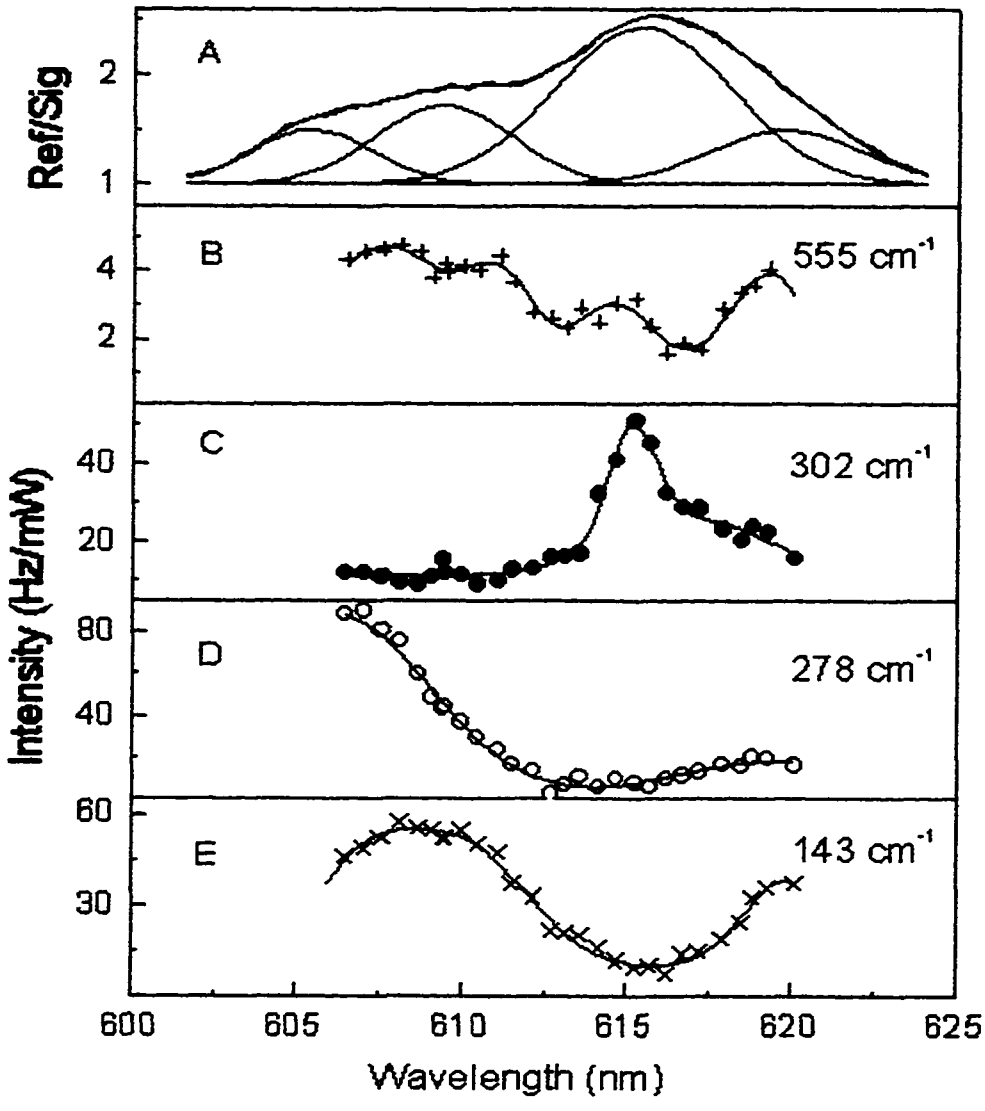

Fig. 4.2.2. Absorption (SDS) spectrum of Hf_3 in an argon matrix at 14 K (top panel, A) and excitation profiles of the 555, 302, 278, and 143 cm^{-1} lines (panel B-E, respectively). The excitation profiles clearly indicate at least four optical transitions (see text), as confirmed by the best fit Gaussian profiles (broken lines, top panel) to the absorption spectrum.

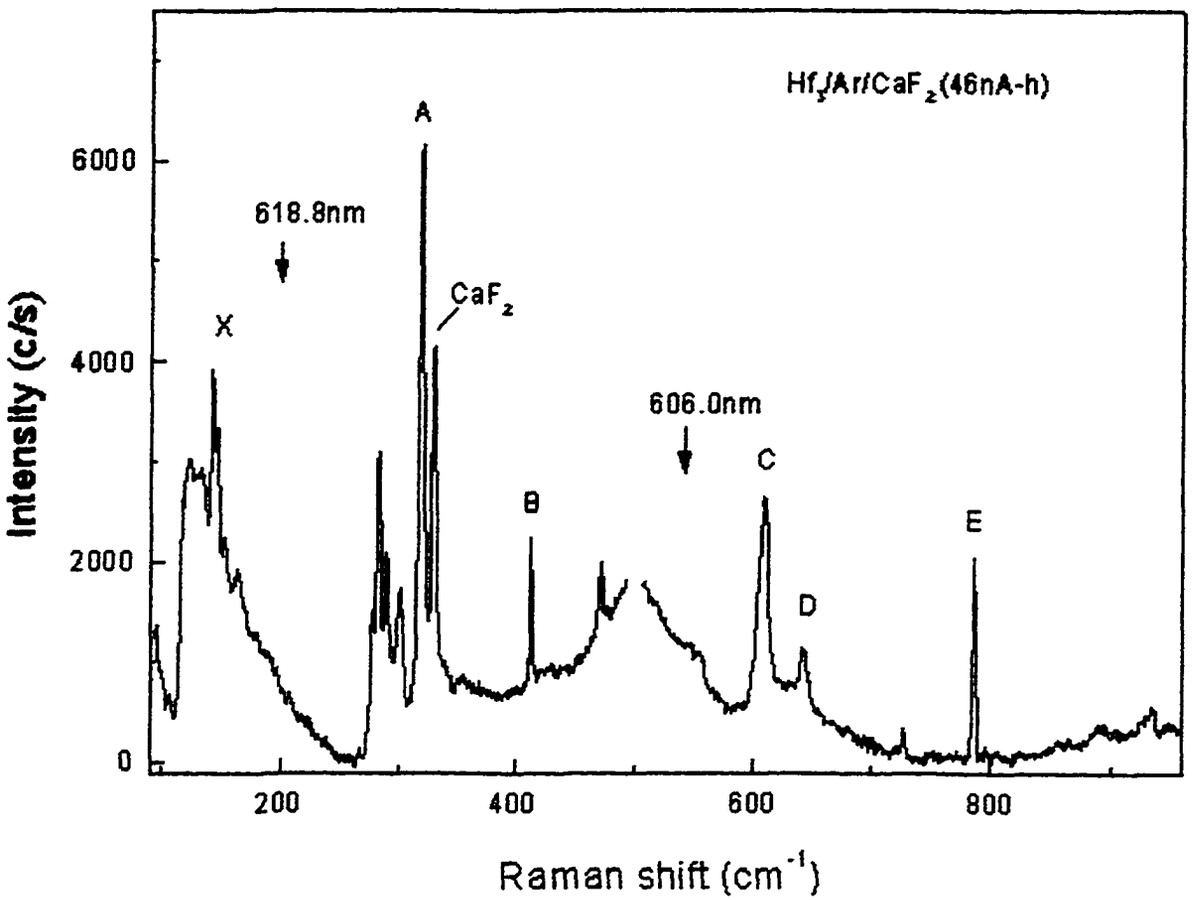

Fig. 4.2.3. Resonance Raman spectrum of Hf_3 in an argon matrix excited by 618.8 nm radiation for the range 100-500 cm^{-1} and by 606.0 nm radiation for the range 500-850 cm^{-1}. The origins of the *X* and *A-E* states are indicated.

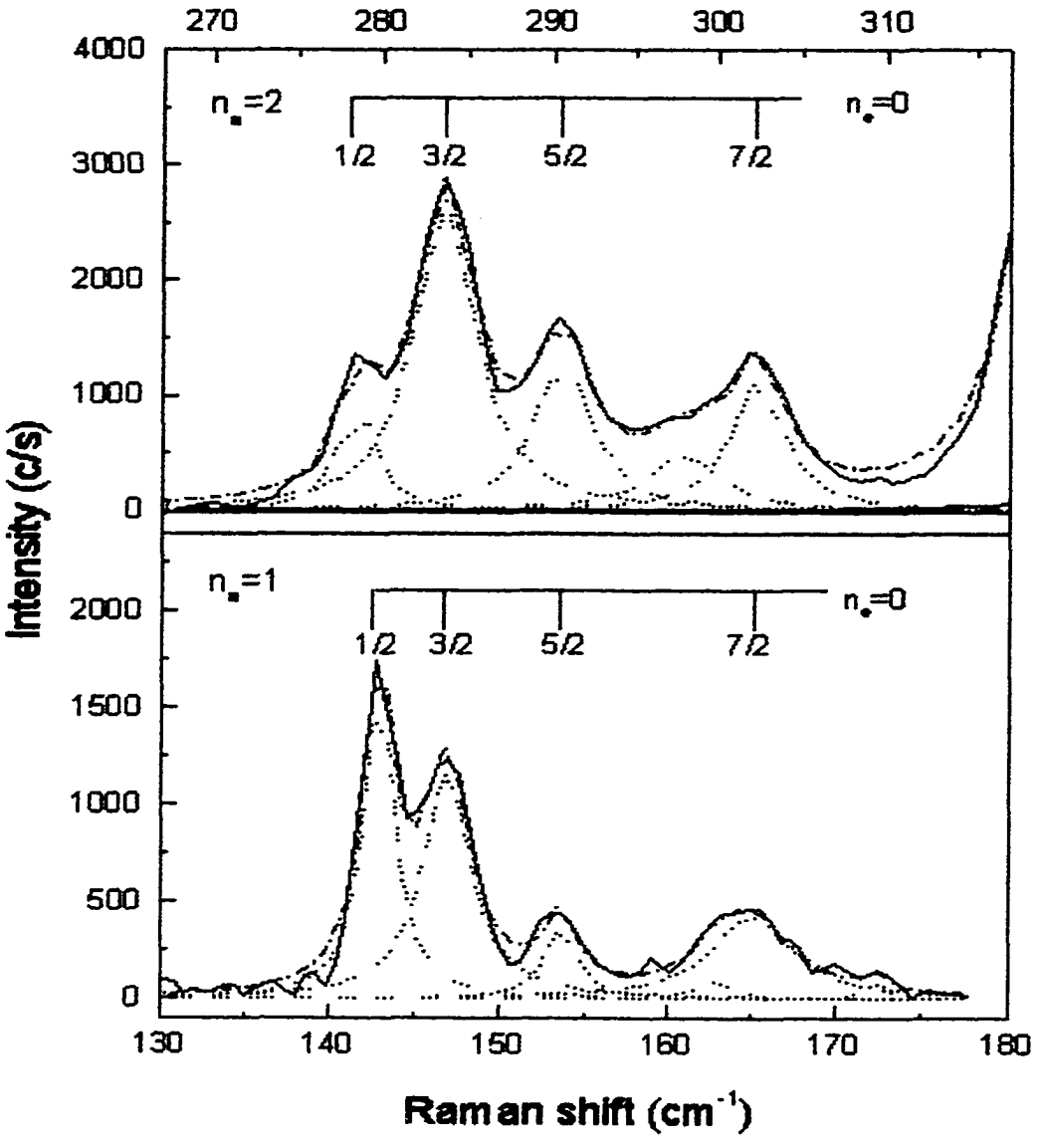

Fig. 4.2.4. Detail of the clusters of lines originating near 143 cm^{-1} (bottom panel) and 278 cm^{-1} (top panel) denoted (see the text) $X(1, 0, ½)$ and $X(2, 0, 1/2)$, respectively. Each group of lines contains a progression of transitions assigned (see text) by $j = \pm 1/2$ through $j = \pm 7/2$.

Table 4.2.1. Observed frequencies (column 1 data, uncertainties in parentheses) and intensities of the resonance Raman lines of Hf_3. Excitation profiles (columns 3-6) show intensity at wavelengths 606, 610, 615, and 619 nm, where s or w indicate strong or weak intensity *within* each profile (no entry means transitions were weak). Relative intensities in column 2 pertain to excitation *at 606nm*, although these vary (column 3-6 data) at different excitation wavelengths. Assignments (last column, see text) are to either the $X(n_a, n_e, j)$ ground electronic state, or to the $A(n_a, n_e)$-$E(n_a, n_e)$ low-lying electronic states.

Frequency	**Relative**	**Excitation Profile at wavelength**				
(cm^{-1})	**Intensity**	606 nm	610 nm	615 nm	619 nm	**Assignment**
142.8 (2)	m	s	s		s	X(1,0,1/2)
146.9 (2)	w	s	w	s	s	X(1,0,3/2)
154.2 (11)	w	s	w	w	s	X(1,0,5/2)
1655 (9)	w	s	w		w	X(1,0,7/2)
278.1 (6)	m	s	w		w	X(2,0,1/2)
283.4 (3)	m	w	s	s	w	X(2,0,3/2)
291.1 (5)	w	w	w	w	s	X(2,0,5/2)
301.9 (6)	w			s		X(2,0,7/2)
319.0 (3)	vs	s	w	w	w	A(0,0)
413.4 (6)	m	s	s	s	s	B(0,0)
421.7 (12)	w	s	s	s	s	A(0,1)
471.3 (3)	w	w	w	s	s	A(1,0)
555.1 (9)	w	s	s	w	s	B(1,0)
609.6 (5)	m	s	w			C(0,0)
642.8 (5)	w	s	w	s	s	D(0,0)
726.3 (12)	w	s	w			C(0,1)
751.2 (7)	vw			s	s	D(0,1)
785.4 (2)	w	s	w	w	w	E(0,0)
792.3 (7)	vw			s	s	D(1,0)
894.1	vw					E(0,1)
935.7	vw					E(1,0)

Table 4.2.2. Summary of the properties of the low-lying states of Hf_3, where T_0 denotes the electronic term value and ν_a, ν_e are totally symmetric and degenerate vibrational frequencies, respectively. Uncertainties are given in parentheses.

Designation	T_0 (cm^{-1})	Symmetry	ν_a (cm^{-1})	ν_e (cm^{-1})
X	0	D_{3h}[a]	142.5 (1)[b]	
A	319.0(3)	D_{3h}	152.3 (4)	102.7 (19)
B	413.4(6)		141.7 (11)	
C	609.6(5)			116.7 (13)
D	642.8(5)	D_{3h}	149.5 (9)	108.4 (9)
E	785.4(2)	D_{3h}	150.3	108.7

[a]Jahn-Teller distorted state. The values for α in the linear Hahn-Teller energy expression $E = \alpha j^2$, are 1.88(2) and 1.95 (9) cm^{-1} for $n_a = 1$ and 2, respectively.

[b]Origin of the 1 ν_a progression; the 2 ν_a origin occurs 135.9 (7) cm^{-1} higher in energy.

4.3 Spectroscopy of Yttrium Dimers in Argon Matrices

I. IN TRODUCTION

In the past two decades, research on transition-metal clusters has attracted a number of theoretical and experimental scientists[1]. It is clear that an understanding of the multiple-metal bonding often observed in the ground states of transition metal dimers depends on accurate determination of crucial structural parameters such as vibrational frequencies, force constants, dissociation energies, etc. Work has been carried out in this regard by this and other laboratories on several second row transition metal dimers (Zr_2[2], Nb_2[3], Mo_2[4], Ru_2[5], Rh_2[6], Pd_2[7], and Ag_2[8]). However, relatively little work has been carried out on the dimer of yttrium. In this paper we report the first matrix isolation optical absorption and resonance Raman spectra of Y_2.

Samples of Y_2 are obtained by mass selection after sputtering a metal target with high energy Ar ions. This ensures discrimination against spectral interference from atoms and higher clusters of Y, as well as various oxides of Y. We observe a weak, broad optical transition

near 485nm. Exciting with Ar^+ laser radiation in this region enables us to obtain a sharp resonance Raman Spectrum with a long progression of overtones. Spectral analysis gives ω_e=185.5(7) cm^{-1}, with $\omega_e x_e$= 0.38(5) cm^{-1}, leading to a spectroscopic dissociation energy of D_e = 2.8(4) eV. Comparison of our results with several *ab initio* calculations confirms the assignment of the ground state to be $^1\Sigma_g^+$.

II. EXPERIMENT

The City College of New York (CCNY) metal cluster deposition source has been described in previous publications[2,3,9]. Briefly, an intense (typically 15mA at 25keV) argon ion beam from a CORDIS ion source sputters on a water cooled yttrium target (Alfa, 99.9%) maintained at 300V. Secondary ions are extracted with a modified Colutron model 200-B lens system and then mass selected using a Wien filter (Colutron 600-B) in conjunction with an approximately 175mm free drift distance and a 6.5mm diameter aperture. The mass resolution is 6~7, enough to discriminate against possible oxide contaminants. After mass selection, the ion beam is bent by 10° using two electric

plates to eliminate neutrals and then guided and focused to the deposition region by two einzel-like lenses.

Yttrium dimer ions were codeposited with Ar and electrons (generated from a heated tungsten filament) on a polished CaF_2 substrate (~14K). Matrices were grown at ~5μm/hour with an Ar:metal dilution ratio of approximately 10^4: 1. The deposition region was surrounded by a "Faraday Cage" whose potential with respect to the sputtering target controls the kinetic energy (10eV in this experiment) of deposited ions. Ion currents under "soft landing" conditions were approximately: Y^+ (250nA), Y_2^+ (25nA). By comparing the intensity of known atomic excitation features in a dimer deposition with those obtained from deposition of atom under similar conditions, the fragmentation ratio of dimers is estimated to be 10%.

Matrix samples were interrogated *in situ* using both absorption and Raman spectroscopy. As previous described [2, 3, 9], for the absorption measurements, both deuterium and tungsten lamps were employed as excitation light sources, dispersed by a single 1/4 m monochromator, reflected by a plane mirror (controlled by a stepping motor), which allows the light to be scanned across the 8mm wide sample. The

absorption measurements were made by collecting the light scattered at 90° to that incident, a technique termed "Scattering Depletion Spectroscopy (SDS)" [3].

After obtaining absorption spectra, the Raman spectra were measured by exciting the sample with appropriate laser wavelength within the absorption region. In this experiment on Y_2, the visible output (457.9nm-514.5nm) of an argon ion laser (Spectra Physics model 2045) was employed. The scattered light was collected at 90^0 and focused into a Triplemate Spectrometer (Spex 1877E, 0.6m). The scattered light was detected with a liquid nitrogen cooled CCD system (Spectrum One + CCD30 + DM3000R Software). The resolution of the detection system on Y_2 experiment was set about $2cm^{-1}$ (at 500nm). The Raman shifts of Y_2 were calibrated using the CaF_2 (substrate) line[10] at $330cm^{-1}$.

III. SPECTRA AND ANALYSIS

Figure 4.3.1 shows a typical Raman spectrum (excited with 488nm) for Y_2 in argon matrix (14K, dimer content ~75nAH) and as an

inset, a portion of the absorption spectrum (SDS) of the same sample compared with several excitation profiles.

The SDS shows a broad weak band centered at 485nm, and closely parallels the excitation profile, which further confirms its assignment to the yttrium dimer.

Resonance Raman spectra of Y_2 were obtained at five different argon ion laser emissions in the visible region (465.5~496.5nm). Up to ten Stokes transitions were observed and the average value of these measurements give the Raman shifts, which are listed in table 4.3.1.

Analysis of these data by standard techniques[11] (linear fit of $\Delta G_{v+1/2}$ vs v) gives ω_e =185.5(7) cm^{-1}, with $\omega_e x_e$ = 0.38(5) cm^{-1}, leading to a spectroscopic dissociation energy of D_e = 2.8(4) eV, and the force constant k_e=0.90(1) mdyne/Å. Attempts to obtain higher anharmonic corrections ($\omega_e y_e$) failed to improve the standard deviation, so it may be safely inferred that such corrections are negligible.

Note that several of the observed Raman lines are accompanied by one or more weaker satellite lines. Since there are no isotopes that need to be considered, it is most likely that they are due to site effects in the

Ar matrix. Similar effects have been observed in other dimer spectra[3]. We have used only the most intense line in each group for our analysis.

IV. DISCUSSION

It is of interest to compare our measured value of the force constant k_e for Y_2 with those of other members of the second row transition metal dimers. These are given in table 4.3.2.

As can be seen the force constants increase almost linearly from left to right. The ground state atomic configurations are (Y) $5s^2 4d^1$, (Zr) $5s^2 4d^2$, (Nb) $5s^1 4d^4$, (Mo) $5s^1 4d^5$. However, in transition metals, bonding is usually more favorable if at least one atom has an s^1 configuration, requiring some promotion energy. Thus considering a configuration $5s^1 4d^m$ (m=2-5), the force constant is proportional to the number of *d* electrons involved in bonding. A complementary, nearly linear decline in force constant was observed[5-7] in the series Ru_2, Rh_2, Pd_2 indicating a configuration $5s^1 4d^m$ (m=7-9). We can conclude that, at least for the second row transition metal dimers, each d-electron

available for bonding makes a nearly equal additional contribution to the bond order.

Of several previous publications on Y_2 only one is experimental, Verhaegan, Somoes and Drowart [12] determined the bonding energy using the third law analysis of the high temperature Knudsen effusion mass spectrum. Their result was D_0 (Y_2) = 1.62 ± 0.22 eV, in sharp disagreement with our spectroscopic value of 2.8 ± 0.4eV. The third law technique suffers from the requirement that ω_e and r_e must be known, as well as the electronic partition function, and the results are often unreliable. However, the spectroscopic technique also has difficulties, in that a Morse potential is assumed to govern the nuclear motion. In transition metals this assumption is not always even close. This is caused by the fact that, where both s-s and d-d bonding is important, due to their disparate spatial extensions, *d*-orbitals often have considerably different dissociation ranges than *s*-orbitals. The best example of this is the case of Cr_2 [13], where serious deviations from a Morse potential are observed and the spectroscopic value of D_e is misleading. However, on Y_2 it is most likely that the bond order is small, perhaps near one. Thus, only one electron pair is involved in dissociation, and the above effect

of different s and d bonding will not be important. We also have observed regular behavior all the way up to ninth harmonic (n=10). We feel, therefore, that our value is more likely to be correct.

Most of the remaining work on Y_2 has been theoretical. Walch and Bauschlicher [14] have carried out a complete active-space multiconfiguration-self-consistent field (CAS-MCSCF) calculation followed by configuration-interaction (CI). Their results indicate that the ground state is $^5\Sigma_u^-$ ($5s\sigma_g^2 5s\sigma_u^1 4d\sigma_g^1 4d\pi_{xu}^1 4d\pi_{yu}^1$) which stems from the $5s^24d^1+5s^14d^2$ atomic configurations. A nearby, low-lying state (Te = 0.87 eV) is the $^1\Sigma_g^+$ ($5s\sigma_g^2 4d\pi_{xu}^2 4d\pi_{yu}^2$) state arising from the $5s^14d^2+5s^14d^2$ configurations. In similar calculations in Sc_2 this latter lies considerably higher that in Y_2 which indicates larger contributions of *d*-electron bonding in the second row. Dai and Balasubramanian [15] have carried out similar complete active space self consistent field (CASSCF) calculations followed by multi-reference configuration interaction (MRSDCI) in which both single and double excitations are considered. Up to 2.6 million configurations are included in this calculation. Their results are quite similar to those of Walch and Bauschlicher (see table 3). Comparison of the SCF calculations both

with and without CI contributions show that increasing CI lowers the relative energy of the higher state considerably (to Te = 0.55eV). In conjunction with the lack of observable ESR spectrum [16], Dai and Balasubramanian conclude that the $^1\Sigma_g^+$ state is most likely the ground state. Our Raman results (see table 4.3.3) are consistent with this conclusion. The experimental value for ω_e of 185.5 cm^{-1} is quite close to that of 180cm^{-1} in the CASSCF+MRSDCI calculation of Dai and Balasubramanian for the $^1\Sigma_g^+$ state. Similarly our D_e = 2.8(4) eV compares favorably with their value of 3.09 eV for the same state.

The theoretical results are listed and compared with this work in table 4.3.3.

Another argument is that the $^1\Sigma_g^+$ state has short –r (bond length) feature and the determination of r_e value would be helpful for determining the ground state. Using our experiment data, we tried to determine the r_e of the ground state of Y_2. Badger's [a] rule is employed here on the forth row metal diatomic molecules as Weisshaar [b] did on the third row elements. Unfortunately, only a very few experimental data (listed in table 4.3.4) have been available up till now, especially of the bond length r_e. The normal Badger's rule has the format: $k_e (r_e - d_{ij})^3 =$

C, here d_{ij} is a constant that is different depending one the row number of the periodical table and C may be taken as the same for all molecules (C = 1.86 mdynÅ^2 if k_e is in mdyn/Å and r_e , d_{ij} in Å).

In an attempt to determine the constant d_{44} and C for the forth row metal diatomic molecules, a linear least squares fitness was employed to five pairs of ω_e, r_e values (see table 4.3.4 and Fig 4.3.2), leading to d_{44} = 1.09Å and C=3.41mdyn Å^2 (linear correlation coefficient is 0.998). Using our experimental result ω_e=185.5cm^{-1}, the bond length of Y_2 is calculated out to be 2.65Å, which is a little bit shorter than Dai's result (r_e=2.76 Å). This result is another support for our presumption: that $^1\Sigma_g^+$ is very likely candidate for the ground state.

Table 4.3.1. Raman frequency shifts (cm^{-1}) for Yttrium dimers in argon matrices

v"	1	2	3	4	5	6	7	8	9	10
Raman Shift (cm^{-1})	186.5	369.1	551.8	733.7	915.5	1096.3	1276.6	1457.3	1635.3	1813.1
Std.Dev.	0.6	0.4	0.7	0.7	0.7	0.7	0.4	0.6	1.0	1.3

Table 4.3.2. Ground state vibrational frequencies (cm^{-1}) & force constants (mdyne/ Å) for several second row transition metal dimers.

	Y_2 (this work)	Zr_2 (2)	Nb_2 (3)	Mo_2 (4)
ω_e (cm^{-1})	185.5	305.7	420.5	477.1
k_e (mdyne/Å)	0.90	2.51	4.84	6.43

TABLE. 4.3.3. Comparison of theoretical and thermodynamic results for low state parameters of Y_2 with spectroscopic data (this work)

Authors (Ref)	Method	Low state	*Re* (Å)	ω_e (cm^{-1})	*De* or D_0 (eV)	Te (eV)
Dai and BalasubraManian (15)	CASSCF + MRSDCI	$^5\Sigma_u^-$**	3.03	172	2.56	0.0
		$^1\Sigma_g^+$	2.76	180	3.09	0.55
Walch and Bauschlicher. (14)	CI	$^5\Sigma_u^-$**	3.03	171	2.44	0.00
	CI	$^1\Sigma_g^+$	2.74	206	2.93	0.87
	CASSCF	$^1\Sigma_g^+$	2.73	205	1.74	
Verhaegan, Somoes, and Drowart (12)					1.62±0.22	
This work	Isolated matrix			185.5±0.7	2.8±0.4	

**: Assigned to be the ground state.

Table 4.3.4. Experiment data of the third row metal diatomic molecules

Molecular	State	ω_e (cm^{-1})	r_e (Å)	$k_e^{-1/3}$ (mdyn/Å)$^{-1/3}$	Ref
Mo_2	$X^1\Sigma_g^+$	477.1	1.938	0.537	(19)
Mo_2	$A^1\Sigma_u^+$	449	1.937	0.560	(19)
Ag_2	$X(O_g^+)\,^1\Sigma_g^+$	192.4	2.531	0.949	(20,1)
Ag_2	$A(O_u^+)\,^1\Sigma_u^+$	155.3	2.655	1.095	(20,1)
Sr_2	$B^1\Pi_u$	80.4	3.85	1.816	(21)

Fig. 4.3.1 Resonance Raman and absorption (SDS compared with excitation profile, left) for Y2 in an argon matrix

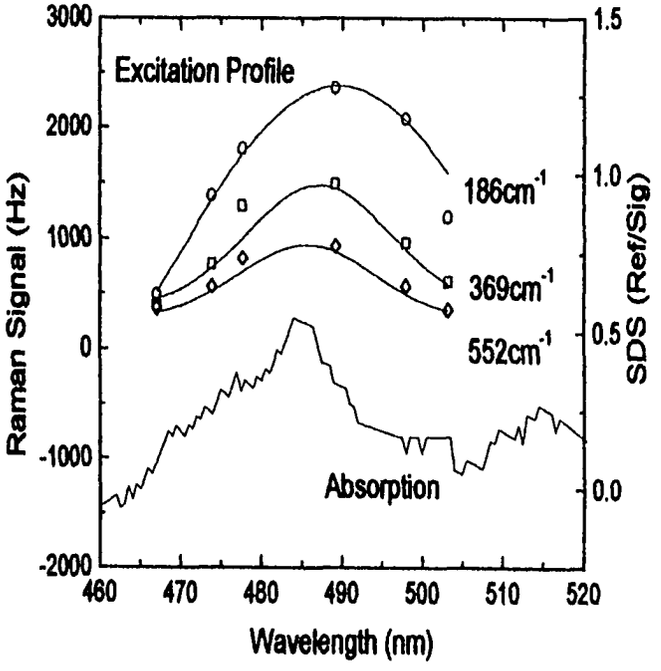

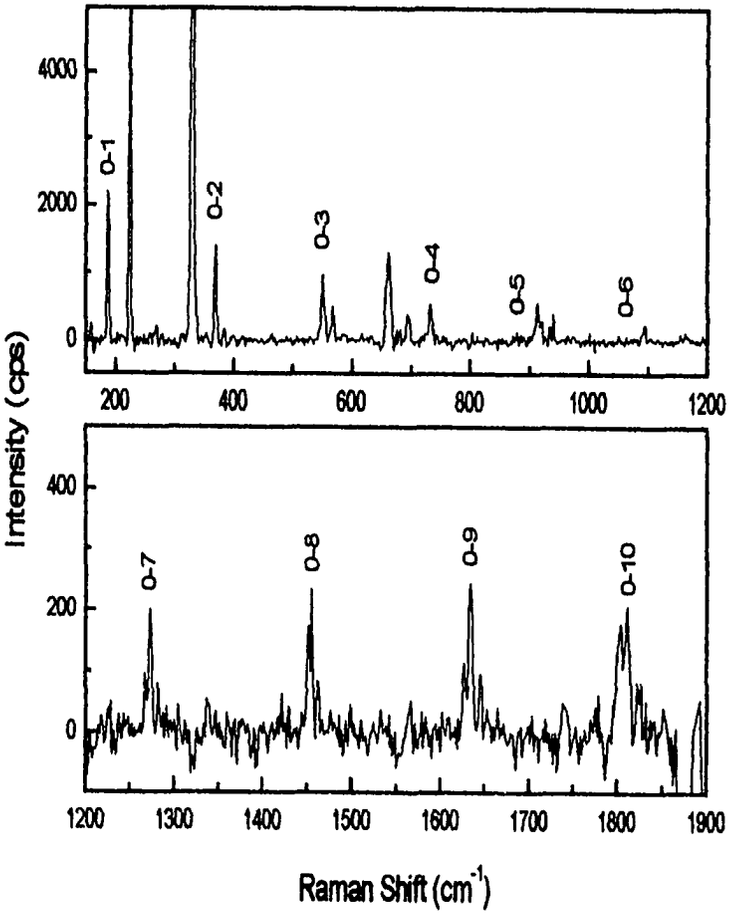

113

114

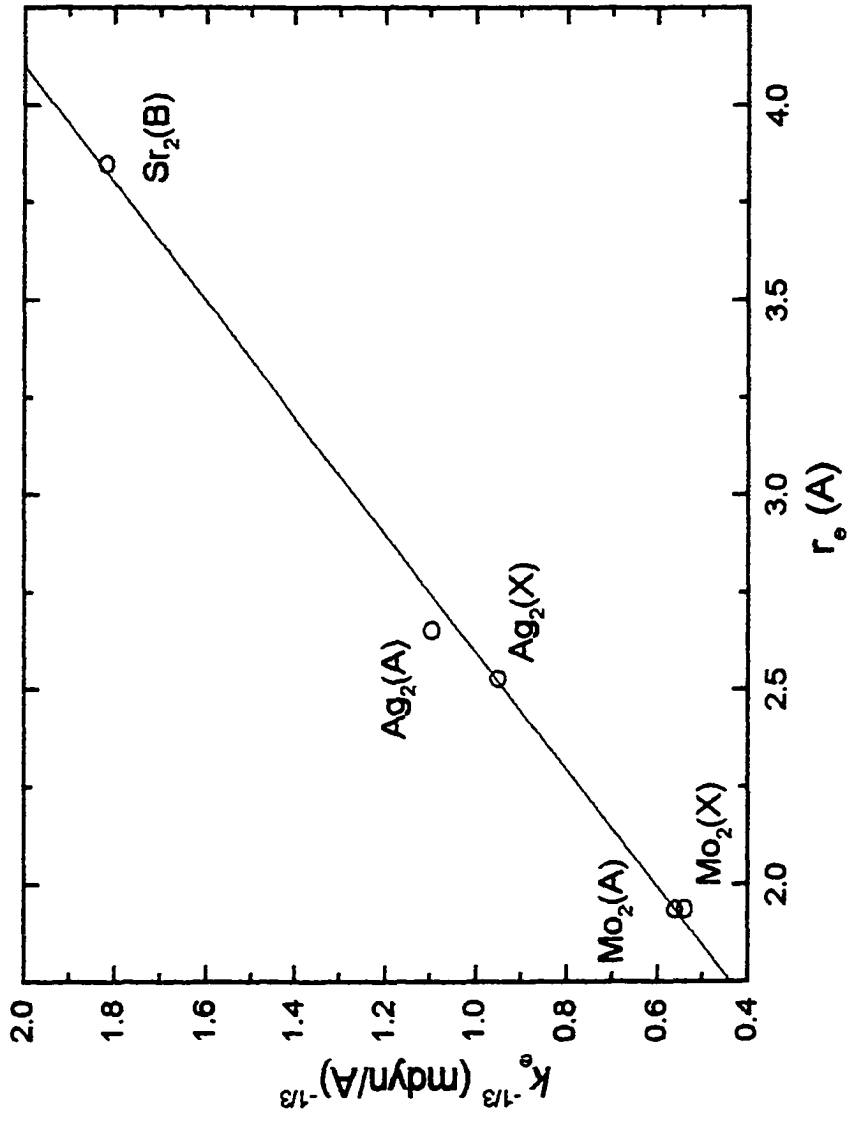

Fig.4.3.2 Badger's rule plot of $k_e^{-1/3}$ vs r_e for metal diatomics from the forth row of the periodic table as indicated.

4.4 Absorption, Resonance Raman and Raman Excitation Spectra of Lanthanum Dimers in Argon Matrices

I. INTRODUCTION

Having reported the result of measurements of Raman and absorption spectra of numerous transition metal dimers, (including Ni_2, [1] Ru_2, [2] Rh_2, [3] etc.), we have recently concentrated our studies on the 3B group transition metal dimers: yttrium [4] and lanthanum dimers. It is interesting to study the lanthanum dimers not only because they have seldom been investigated before, but also due to the wide interest in *5d* orbital bonding properties. Lanthanum dimer also provides the opportunity to examine the effect of *4f* orbitals on neighboring dimer bonding.

Very few experimental and theoretical results are available for La_2. [5] The only experimental datum on La_2 was obtained by Verhaegen et al. [6] by high-temperature Knudsen effusion mass spectrometry in 1963. The absolute entropy method was used to determine $D_0^\circ(La_2)$ =

2.50 ± 0.22 eV. The only other piece of information available about La_2 is the failure of Knight et al. [7] to observe an ESR spectrum attributable to La_2. Dolg, Stoll and Preuss [8] have carried out calculations for La_2 using SCF as well as configuration interaction calculations including all single and double substitutions (CISD). All results were approximately corrected for size-consistency errors (+ SCC) using the Langhoff-Davidson formula. They considered 13 low-lying electronic states as possibilities for the ground state. Bond lengths r_e (Å), vibrational constants ω_e (cm^{-1}) and term energies T_e (eV) were derived from their calculations.

In this chapter we report the observation of resonance Raman spectra and the absorption (scattering depletion) spectrum of La_2 in argon matrices. From the Raman spectrum, we measured the Stokes lines at Raman shift 237.5 (5) cm^{-1}, 469.4 (6) cm^{-1}, 699.1 (9) cm^{-1}, and 928.1 (7) cm^{-1}. These data give $\omega_e = 239.0 \pm 2.2$ cm^{-1} with $\omega_e \chi_e = 1.4 \pm 0.4$ cm^{-1}. The resulting spectroscopic dissociation energy is $D_e = 1.3(4)$ eV.

II. EXPERIMENT

The CCNY cluster deposition source has been described in detail elsewhere. [9] Briefly, an intense (typically 15 mA at 25 keV) argon ion beam from a CORDIS ion source sputters lanthanum cluster ions from a water cooled, lanthanum target (Alfa Aesar 99.9 % (REO)) maintained at about 300 V. Secondary ions were extracted with a modified Colutron model 200-B lens system and then mass-selected using a Wien filter (Colutron 600-B) in conjunction with an approximately 175 mm long drift space and a 6.5 mm diameter aperture. After mass separation, the ion beam is bent by 10° (in order to eliminate neutral sputtered products) and then guided to the deposition region by two einzel-like lenses. Lanthanum dimer (or atomic) ions were then codeposited with argon gas and electrons onto a $\approx$ 14 K CaF_2 substrate. Ion currents under "soft landing" conditions could be measured on a Faraday plate in the deposition ergion and were approximately: La^+ (55 nA), La_2^+ (30 nA), La_3^+ (8 nA). Prior to deposition, the selected ions were simultaneously slowed to 10 eV by a surrounding "Faraday cage".

Matrices were grown at about 5-7 μ/h with an Ar : metal ratio of approximately 10^4:1.

By comparing the intensities of known atomic excitation features in a dimer deposition with those obtained from depositions of the atom under similar conditions, the dimer fragmentation is estimated to be about 15%.

Matrix samples were interrogated *in situ* using both absorption and Raman spectroscopy. As previously described, the absorption measurements were made by collecting the light at 90° to that incident, a technique we term "Scattering Depletion Spectroscopy" (SDS). Raman spectra were recorded using the visible output of an argon ion laser (Spectra Physics model 2045). Scattered light was collected at 90° into a Spex 1877E Triplemate Spectrometer (0.6 m) and detected by a liquid nitrogen cooled CCD detector (Spex model "Spectrum One") with DM3000R software.

III. SPECTRA AND ANALYSIS

The insert in Fig. 4.4.1 shows the "scattering depletion" (absorption) spectrum of La_2, which consists two broad transitions centered at 490 nm and 540 nm. No other features attributable to La_2 were observed. The spectrum was obtained following a 3 hour deposition of La_2^+ (50 nA h) at a deposition energy of 10 eV. The broken lines in this insert are Raman excitation profile obtained by dividing the Raman intensity (the sum of the 3 Raman lines in each incited laser line) by the laser power. The remainder of Fig. 4.4.1 shows the resonance Raman spectrum of La_2 when excited at 501.7 nm. A line due to the CaF_2 (at 330 cm^{-1}) substrate is also in evidence. The spectra we obtained by four excited Argon CW laser lines (488.0 nm, 496.5 nm, 501.7 nm, 514.5 nm) consist of a single progression of almost equally spaced lines. Each member of the progression can be seen to consist of a closely spaced triplet. The Raman spectrum may be assigned to the first through fourth Stokes transitions of the lanthanum dimer. The observed Raman frequency shifts are listed in table 4.4.1. Some Raman transitions were obscured by very intense atomic fluorescence features at other argon laser CW lines. Since there is no expected isotope effect, the three Raman lines in each member of the progression indicates a "site effect"

of dimer molecules in argon matrices. A similar but less characteristic "site effect" spectrum was obtained in previous studies of niobium dimers. [10] We also recorded the spectrum while annealing the sample to steps of temperature from 16 K to 40 K (see fig. 4.4.2). The annealing was controlled by a Scientific Instruments model 5500 temperature controller. In each set of Raman transition, the middle of the three lines clearly seen in the 16 K spectrum, disappears when temperature exceeds 20 K while the other two lines remain until the temperature reaches 32 K. These features remain until the matrix evaporates at temperatures higher than 36K. From the annealing spectrum we see there are most likely two stable sites with slightly different potential energy at low temperatures for lanthanum dimers in the matrix. The vibrational constants, obtained by analysis of the resonance Raman spectrum are ω_e = 239.0 (22) cm^{-1} with $\omega_e x_e$ = 1.4(4) cm^{-1} and D_e = 1.3(4) eV .

IV. Discussion

The observed vibrational frequency for La_2 leads to an experimental force constant of k_e=2.34(1) mdyne/Å. The corresponding

values for Sc_2 [11] and Y_2 [12] are 0.756 and 0.90 mdyne/Å respectively. This trend is marked contrast to the tendency of the third row dimer force constant to decrease in comparison to the corresponding first and second row dimers. A good example of this effect shows readily in the adjacent column: Ti_2 (2.35 mdyne/Å), Zr_2 (2.511 mdyne/Å) and Hf_2 (1.63 mdyne/Å). (For a more complete chart of transition metal dimer force constants [13], or refer to http://www.sci.ccny.cuny.edu/~lombardi/). The same anomaly is apparent if we compare force constants along the same row. In the first and second row of transition metal dimers the group 3B force constants are lower than those of the adjacent 4B, 5B and 6B force constants. For La_2 in the third row, the force constant is higher than that of Hf_2. This anomaly is most likely due to the increased bonding afforded by the relatively low promotion energy for La. The ground states of Sc, Y, La and Lu all have a d^1s^2 configuration leading to a ^2D ground state. All have a nearby d^2s^1 configuration (^4F state) which is much more favorable for bonding. The La ^2D-^4F promotion energy (0.36 eV) is much lower than that of Lu (2.33 eV) which itself is much more similar to that of Hf ^3F-^5F ($5d^26s^2$-$5d^36s^1$ 1.94 eV). We thus expect La_2 to exhibit stronger bonding than either Y_2, Lu_2 or Hf_2.

The only work on La_2 is a calculation by Dolg, Stoll and Pruess [8]. They carry out a quasi-relativistic *ab initio* study of lanthanide elements using pseudopotentials to account for relativistic effects. In all cases fixed integral $4f$ occupation numbers were used. They predicted two low-lying states for La_2. The lowest is a $^5\Sigma_u^+$ $(\sigma_g^1\sigma_u^1\sigma_g^1\pi_u^2)$, with r_e=3.247 Å, and ω_e=130 cm^{-1}. The first excited state which lies only 0.11eV higher than the putative ground state is $^1\Sigma_g^+$ $(\sigma_g^2\pi_u^4)$ with r_e=2.830 Å, and ω_e=167 cm^{-1}. Lack of observation of an ESR spectrum [7] is an indication that most likely the singlet state is indeed the ground state. Our observed force constant would also tend to support the singlet state as the ground state, although both calculated states display frequencies considerably lower than that observed.

Note that the observed decrease in force constant for third row dimers is contrary to what would be expected by considering the "Lanthanide contraction". As electrons are added to the *f* shell, the ionic radius of the lanthanide is reduced due to the inability of additional f electrons to effectively shield each other from the increasing nuclear charge. If this were the only effect, we would expect Hf_2 to have a

shorter bond length and higher force constant than Zr_2. We thus might expect Lu_2 to be more comparable to Hf_2 than La_2. Lu has configuration $4f^{14}5d6s^2$ and Hf has just one more *d* electron. Dolg, Stoll and Preuss [8] calculate a $^1\Sigma_g^+$ $(\sigma_g^2\sigma_u^2\sigma_g^2)$ ground state for Lu_2 with r_e=3.78 Å and ω_e=74 cm^{-1}. The much weaker vibrational frequency, corresponding to a bond order near 1, is in sharp contrast to the likely bond order of 2-3 for the lowest calculated states of La_2.

Our value for the spectroscopic dissociation energy (1.3(4) eV) is derived from the Kratzer relationship ($D_e = \omega_e^2/4\omega_e\chi_e$). This is considerably lower than that (2.50(0.22) eV) obtained by Verhagen et al. [6] using third law analysis of the high temperature Knudsen mass spectrum. This latter technique suffers from the need for accurate values of ω_e and r_e as well as knowledge of the electronic partition function. At best, these must be guessed, and the results have in the past been unreliable [5]. In almost all cases, as here, they have been too high. The spectroscopic technique also has difficulties, especially when both *s* and *d* orbitals are involved in bonding. If the separation of *s*-electrons takes place at a different distance than that of *d*-electrons, we might expect

serious deviations from a presumed Morse-like potential on which the Kratzer relation depends. Despite this difficulty, we feel that the spectroscopic technique, being more direct, is more likely to be accurate. The calculations cited above are certainly much closer (1.06 eV) to our results.

Table 4.4.1 Raman frequency shifts (cm^{-1}) of dilanthanum in an argon matrix.

λ_{ex} (nm)	v'' = 1			v'' = 2			v'' = 3			v'' = 4		
Mean	237.5	240.6	244.7	469.4	474.9	482.2	699.1	707.6	718.9	928.1	939.4	954.1
(σ)	0.5	0.7	0.7	0.6	0.6	0.4	0.9	0.8	0.7	0.7	0.4	0.5

125

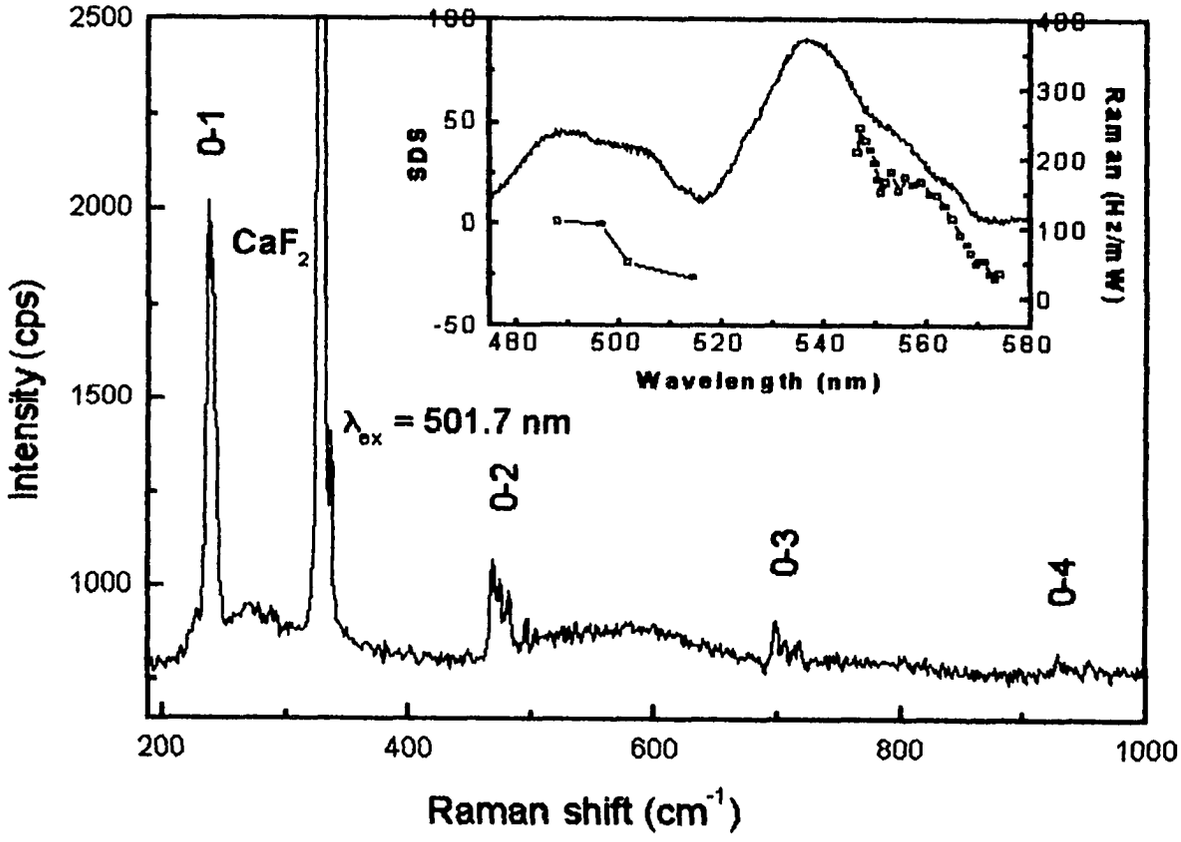

Fig. 4.4.1: Raman spectra of dilanthanum in an argon matrix. Insert: SDS and Raman excitation profile.

126

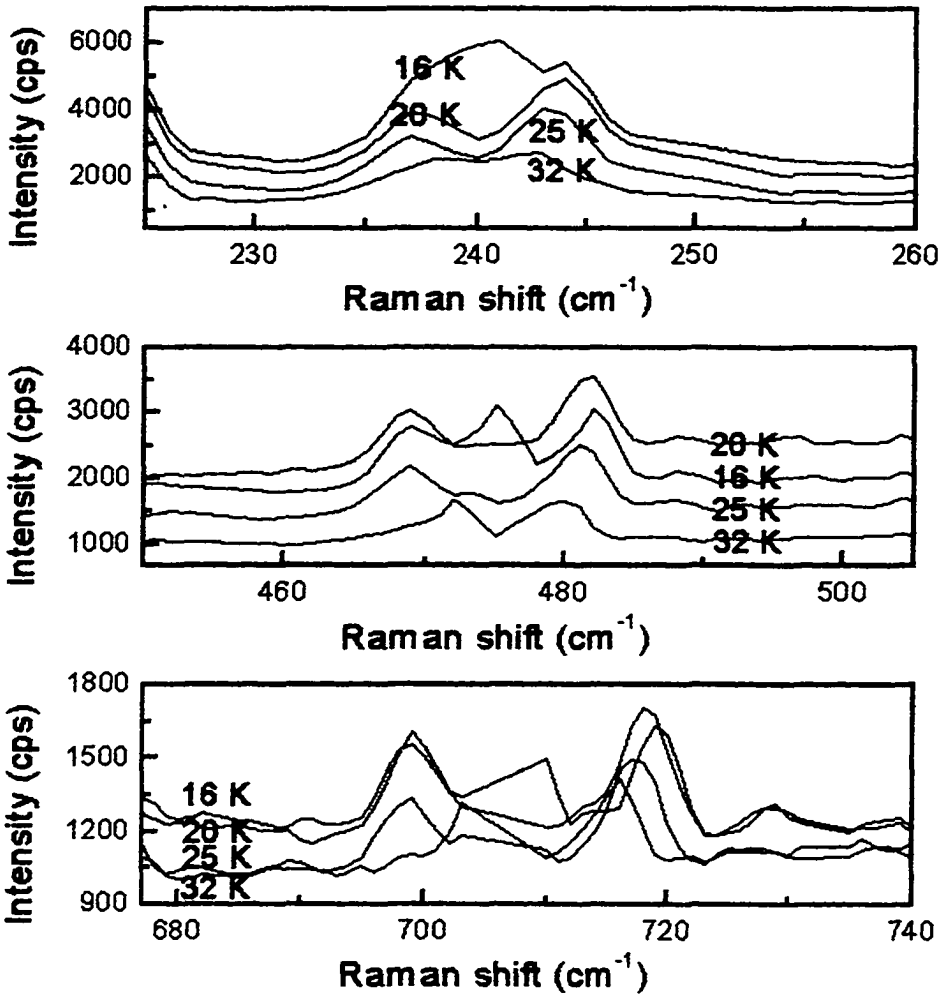

Fig.4.4.2. Raman spectrum of lanthanum dimers during annealing the argon matrices.

Chapter 5, Summary and possible future research in this field

After nearly 10 years of studies on transition metal clusters, the CCNY cluster laboratory has achieved excellent results on vibrational constants, bonding energy, cluster structure, etc. Almost all the transition metal dimers have been measured using MI and the mass-selected technique by Raman or luminescence spectroscopy except Os, Ir and Tc. Also, several trimers and tetramers have been successfully deposited and measured by Raman spctrum. (check http://www.sci.ccny.cuny.edu/ ~lombardi for reference)

Table 5.1 summarizes all ground state force constants data (in mdyne/Å) known for homonuclear transition metal diatomic species. The elements underlined were done by CCNY cluster laboratory. The remaining data come from other spectroscopic measurements either in low temperature matrices or from the gas phase, more recently in elegant molecular beam experiments.

Chemical bond formation is most favorable when at least one of the interacting atomic moieties has an open s-shell configuration s^1d^m as

opposed to s^2d^{m-1}. If s^1d^m is not the ground state, bonding can still take place but at the cost of a certain promotion energy. The dimer bond strength is largely depend on the amount of overlap between the atomic *d* orbitals. If $\langle r_{(n+1)s}\rangle/\langle r_{nd}\rangle$ is small this means that the *d* orbital electron contributes to a strong bond. The strong bonding of the group 6B is influenced by the overlap of *d* orbitals. The force constants for the early transition metal dimers are much larger than those of the later elements. This effect arises from a combination of the greater *d*-orbital contraction (small overlap) in the heavier elements of a particular period and the natural tendency for more antibonding orbitals to be filled in a dimer composed of atoms whose *d* orbitals are more than half filled. For those elements with a half-filled or filled *d*-shell (Mn and group 2B) the bonding is described as van der Waals in nature.

Compared with the fact that many experimental data have been found in the gas phase or matrices for 3*d* series, little is known either experimentally or theoretically about diatomics formed from the 4*d* and 5*d* series. Theoretical progress has been impeded by difficulties in treating the weak, multiple *d-d* bonding of the transition metal elements. Furthermore one has to worry about the problem of relativity.

Relativistic effects become quite important in the later half of the 4d transition series and remain important throughout the 5d transition series. It was shown in chapter 4 that some theoretical calculation results were far different from our experimental results, especially in treatment on lanthanum dimers.

An interesting result comes from our experiment on lanthanum dimer. We have tried to include all the ground states force constants into a simple plot in the form of periodic table. (See figure 5.1) The bond order is calculated by taking the 1B group bond as standard 1. A general tendency of bond order is that it increases from left to right then drops down linearly. There is an exception on lanthanum bonding. We assumed that it should be lower than the experimental data. However, it is higher than yttrium and scandium. In chapter 4, we noted that the ground states of Sc, Y, La and Lu all have a d^1s^2 configuration leading to a ^2D ground state. All have a nearby d^2s^1 configuration (^4F state) which is much more favorable for bonding. The La ^2D-^4F promotion energy (0.36 eV) is much lower than that of Lu (2.33 eV) which itself is much more similar to that of Hf ^3F-^5F ($5d^26s^2$-$5d^36s^1$ 1.94 eV). We thus expect La_2 to exhibit stronger bonding than either Y_2, Lu_2 or Hf_2. The

reason cann be surmised from the effect of the *f* orbitals. Indeed, we are considering the involvement of the *f* orbitals in the dimer bonding of the lanthanide dimers. The only difference besides the atomic number between La and Lu is that La has empty *f* orbitals while Lu has closed *f* shells. This is the reason we are interested in lanthanide series.

In the future experiment, we will try to study Lu_2. We expect that the bonding of the lutetium dimer is considerably weaker than lanthanum. Furthermore, more lanthanide dimers will be a great challenge for the cluster studies. The results of lanthanide clusters could provide us with a better understanding the role of *f* electrons in bonding formation. In the studies of Gd, Van Zee, Li and Weltner have found the ground electronic state is $^{19}\Sigma$ from the ESR spectrum of Gd_2. Such high spin multiplicity is unbelievable if we consider only *s* and *d* electrons involved in the bonding. [1] Therefore, Gd dimer will also be a good choice for our next deposit.

For the trimer, we have a much more unexplored field. Yttrium trimer is a good candidate for near future study. From our deposit record on yttrium dimers, yttrium trimer sputtering yields are not very high. Weltner and copworkers have observed the matrix-isolated electron spin

resonace (ESR) spectra of Y_3. [2] Dai and Balasubramanian employed CASSCF followed by MRSDCI calculation, and found two nearly degenerate electronic states with D_{3h} geometries as candidates for the ground state of Y_3. [3]

Table 5.1 DIMERS FORCE CONSTANTS (mdyne/Å)

3B	4B	5B	6B	7B	8B	8B	8B	1B
Sc_2[a] 0.76	Ti_2[b] 2.35	V_2[e] 4.33	Cr_2[h] 3.52	Mn_2[k] 0.094	Fe_2[a] 1.48	Co_2[o] 1.51	Ni_2[q] 1.16	Cu_2[t] 1.33
Y_2 0.90	Zr_2[c] 2.51	Nb_2[f] 4.84	Mo_2[i] 6.43	Tc_2	Ru_2[n] 3.59	Rh_2[p] 2.45	Pd_2[r] 1.38	Ag_2[u] 1.18
La_2 2.34	Hf_2[d] 1.63	Ta_2[g] 4.80	W_2[j] 6.14	Re_2[l] 6.66	Os_2	Ir_2	Pt_2[s] 2.23	Au_2[v] 2.12

* Underlined dimers done by CCNY cluster laboratory

a. Moskovits, M; Dilella, D. P.; Limm, W. J. Chem. Phys. 1984, 80, 626.Using ω_e=238.9cm^{-1}.

b. Cosse, C; Fouassier, M.; Mejean, T.; Tranquille, M.; Dilella, D. P.; Moskovits, M. J. Chem. Phys. 1980, 73, 6076. Using ω_e =407. 9cm^{-1}.

c. Hu, Z.; Zhou, Q.; Lonbardi, J. R.; Lindsay, D. M. In Physics and Chemistry of finite System:from Clusters to crystals; Jena, P., Khanna, S. N., Rao, B. K., Eds., Kluwer Academic: Dordrecht, the Netherlands, 1992; p969.Using ω_e =305.7cm^{-1}.

d. Z. Hu, J-G. Dong, J. R. Lombardi, and D. M. Lindsay, J. Chem. Phys. 97, 9263 (1993). Using ω_e =176.2cm^{-1}.

e. Hu, Z.; Shen, B; Zhou, Q; Deosaran, S.; Lombardi, J. R; Lindsay, D. M.;Harbich, W. J. Chem. Phys. 1991, 95, 2206. Using ω_e =536.9cm^{-1}.See also ref b.

f. Hu, Z.; Shen, B; Zhou, Q; Deosaran, S.; Lombardi, J. R; Lindsay, D. M. Proc. SPIE 1992, 1599, 65. Using ω_e =420.5cm^{-1}.

g. Hu, Z.; Shen, B.; Lombardi, J. R.; Lindsay, D. M. J. Chem. Phys. 1992, 96, 8757. Using ω_e =300.2cm^{-1}.

h. Casey, S. P.; Villalta, P. W.; Bengali, A. A.; Cheng, C. L; Dick, J. P.; Fenn, P. T.; Leopold, D. G. J. Amm. Chem. Soc. 1991, 11 3, 6688. Using ω_e =479cm^{-1}.

i. Efremov, Y. M.; Samoilova, A. N.; Kozhukhovsky, V. B.; Gurvich, L. V. J. Mol. Spectrosc. 1978, 73, 430. Using ω_e =477.1cm^{-1}.

j. Z. Hu, J-G. Dong, J. R. Lombardi, and D. M. Lindsay, J. Chem. Phys. 1992, 97, 8811. Using ω_e =336.8cm^{-1}.

k. Bier, K. D.; Haslett, T. L.; Kirkwood, A. D.; Moskovits, M. J. Chem. Phys. 1988, 89, 6. Using ω_e = 76.4 cm^{-1}.

l. Z. Hu, J-G. Dong, J. R. Lombardi, and D. M. Lindsay; Harbich, W. J. Chem. Phys. 101, 95, (1994). Using ω_e = 348.4 cm^{-1}.

m. Haslett, T. L.; Moskovits, M. J. Mol. Spectrosc. 1989, 135, 259. Using ω_e = 299.5cm^{-1}.

n. Huaiming Wang, Yifei Liu, Robert Craig, Hanae Haouari, John R. Lombardi, and D.M. Lindsay J.Chem.Phys. J.Chem.Phys. 106, 6534 (1997). Using ω_e =347.1cm^{-1}.

o. J-G. Dong, Z. Hu, J. R. Lombardi, and D. M. Lindsay. J. Chem. Phys. 101, 9280 (1994).Using ω_e =296.8cm^{-1}.

p. Huaiming Wang, Yifei Liu, Robert Craig, Hanae Haouari, John R. Lombardi, and D.M. Lindsay. J. Chem. Phys. 106, 2101 (1997). using ω_e = 283.9cm^{-1}.

q. H Wang, H. Haouari, R. Craig, J. R. Lombardi, and D. M. Lindsay. J. Chem. Phys. 104, 3420 (1995). Using ω_e=259.2cm^{-1}.

r. Ho, J.; Ervin, K. M.; Polak, M. L.; Gilles. M. K.; Lineberger, W. C. J. Chem. Phys. 1991, 95, 4845. Usinq ω_e = 210cm^{-1}.

s. Ho, J. Ph.D Thesis, University of Colorado, Boudler, 1991. Using ω_e = 215cm^{-1}.

t. Rohlfing, E. A.; Valentini, J. J. J.Chem.Phys. 1986, 84, 6560. Using ω_e =266.4cm^{-1}.

u. Huber, K. P.; Herzberg, G. Constants of diatomic Molecules; Van Nostrand: New York, 1979.

v. same as ref S. using ω_e =190.9cm^{-1}.

Figure 5.1 Dimer bond order vs transition metals.

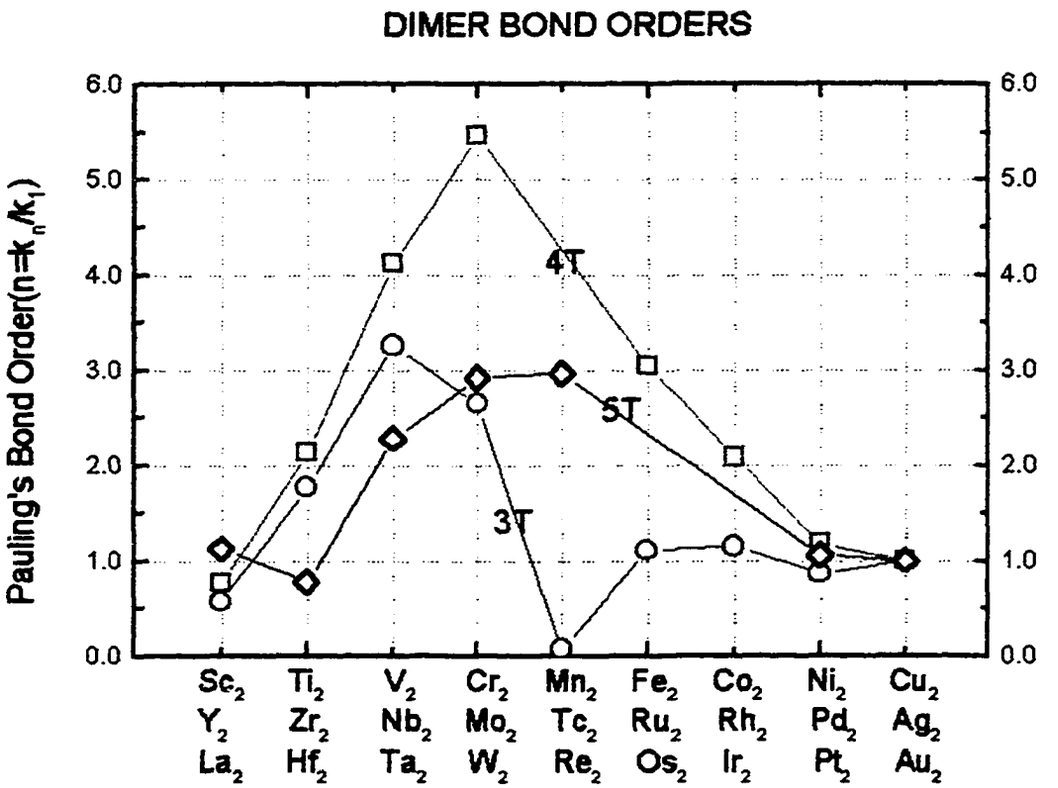

Bibliography

Chapter 1:

1, *Thirteenth International School*, Erice, Sicily (1987). See. *Elemental and molecular Clusters*, ed. By G. Benedek *et al.* (Springer-Verlag, New York, 1988).

2, *Fifth International Meeting on Small Particles and Metal clusters*, Konstanz, Germany, 1990. See: Zeits. Phys. **D19**, (1991); *Sixth International Meeting on Small Particles and Metal clusters*, Chicago, Illinois, 1992. See: Zeits, Phys. **D26**, (1993)

3, International Symposium on the Physics and Chemistry of Small Clusters, *NATO Adcanced Workshop*, Richmond, Virginia (1991). See: *Physics and Chemistry of Finite System: From Clusters to Crystals*, edited by P. Jena and S. N. Khanna and B. K. Rao (Kluwer, Dordrecht, 1992)

4, *Symposium on Clusters and Cluster Assembled Materials*, Materials Research Society Meeting, Boston (1990). See: MRS Symposium Series **206**, (1991)

5, *First International Conference on Nuclear and Atomic Clusters*, Turku, Finland (1991); *Second International Conference on Nuclear and Atomic Clusters*, Santorini, Greece (1993).

6, *Transition Metal Molecules*, W. Weltner and R. J. Van Zee, Ann. Rev. phys. Chem. **35**, 291 91984).

7, *Clusters of Transition Metal Atoms*, M. D. Morse, Chem. Rev. 86, 1049 (1986).

8, *Metal Clusters*, edited by M. Moskovits (Wiley, New York, 1986).

9, *Spectroscopy and Dynamics*, edited by M. A. Duncan, Advances in Metal and Semiconductor Clusters (JAI press, Greenwich CT, 1992).

10, For example: T. H. Maugh, Science **219**, 474, 1413(1983); **220**, 592(1983).

11, A. L. Robinson, Science **185**, 772(1974); **194**, 1150 (1976).

12, J. H. Sinfelt, Science **195**, 641 (1977); Acc. Chem. Res. 10, 15 (1977).

13, J. Haggin, Chem. & Eng. News, Pg. 32, Jan. 18 (1993).

14, J. F. Hamilton and P. C. Logel, J. Catal. **29**, 253 (1973); Phtoto. Sci. Eng. **18**, 507 (1974); J. F. Hamilton, J. de Phys. **C2**, 181, (1977).

15, G. A. Somorjai, Acc. Chem. Res. 9, 248 (1976).

16. For example, Jacox reports that "the argon-matrix shift for most diatomic
molecules is less than 2% ". See: M. E. Jacox, J. Molec. Spectrosc. **113**, 286 (1985).

17. Z. Fu, G. W. Lemire, Y. M. Hamrick, S. Taylor, J-C. Shui and M. Morse, J. Chem. phys. **88**, 3524 (1988).

18. K. LaiHing, P. Y. Cheng and M. A. Duncan, Z. Phys. **D13**, 161 (1989).

19. C. Wang, S. Pollack, D. Cameron and M. M. Kappes, J. Chem. Phys.
93,3787 (1990).

20. See, for example: W. Harbidi, S. Fedrigo, F. Meyer, D. M. Lindsay, J.
Lignieres, J. C. Rivoal and D. Kreisle, J. Chem. Phys. **93**, 8535 (1990).

21. Z. Hu, B. Shen, Q. Zhou, S. Deosaran, J. R. Lombardi, D. M. Lindsay and W. Harbich, J. Chem. Phys. **95**,2206 (1991).

22. Z. Hu, B. Shen, Q. Zhou, S. Deosaran, J. R. Lombardi and D. M. Lindsay, Proc. SPIE **1599**,65 (1992).

23. S. P. Walch and C. W. Bauschlicher, in *Comparison of ab initio Quantum Chemistry,* ed. By R. J. Bartlett (Reidel, Boston, 1985).

24. Z. Hu, Q. Zhou, J. R. Lombardi and D. M. Lindsay, in *Physics and Chemistry of Finite System,* ed. by P. Jena et al. (Kluwer, Dordrecht, 1992), pg. 969.

25. C. W. Bauschlicher, H. Partridge, S. R. Langhoff and M. Rosi, J. Chem.
Phys. **95**, 1057(1991).
26. *Optical and Raman Spectroscopy of Mass-Selected Rhenium Dimers in Argon Matrices,* Zhendong Hu, jian-Guo Dong, John R. Lombardi, D. M. Lindsay and W. Harbich, J. Chem. Phys. **101**,95,(1994).

27. D. G. Leopold, T. M. Miller and W. C. Lineberger, J. Am. Chem. Soc. **108**, 178 (1986).

28. Z. Hu, Bo Shen, J. R. Lombardi and D. M. Lindsay, J. Chem. Phys. **96**,8757 (1992).

29. Z. Hu, J-G. Dong, J. R. Lombardi and D. M. Lindsay, J. Chem. Phys. **97**,8811 (1992).

30. *Optical and Raman Spectroscopy of Mass-Selected Hafnium Dimers in Argon Matrices,* Zhendong Hu, Jian-Guo Dong, John R. Lombardi, and D. M. Lindsay, J. Phys. Chem., **97**, 9263 (1993).

31. F. A. Cotton and R. A. Walton, *Multiple Bonds between Metal Atoms,* Wiley, New York (1982).

32. A. J. L. Hanlan and G. A. Ozin, Inorg. Chem. 16, 2848 (1977); G. A. Ozin and A. J. L. Hanlan, Inorg. Chem. 18,1781 (1979).

33. K. jansson and R. Scullman, J. Molec. Spectrosc. 61, 299 (1976).

34. J. Ho, PhD Thesis, *Negative Ion Laser Photoelectron Spectroscopy of Mass Selected Small Metal Clusters,* University of Colorado, Boulder (1991).

35, T. G. Dietz, M. A. Duncan, D. E. Powers, and R. E. Smalley, *J. Chem. Phys.* **74**, 6511(1981).

36, R. E. Smalley, Laser Chem. **12**, 167(1983); D. E. Powers, S. G. Hansen, M. E. Geusic, D. L. Michalopoulos, and R. E. Smalley, *J. Chem. Phys.* **78**, 2866(1982)

37. Knight, W. D.; Clemenger, K.; de Heer, W. A.; Saunders, W. A.; Chou, M. Y.; Cohen, M. L. *Phys. Rev. Lett.* **1984**, 52, 2141.

38. W. Krätschmer, L.D. Lamb, K. Fostiropoulus, D.R. Huffman, *Nature* **1990**, 347, 354.

39. Bondybey, V. E.; English, J. H. *J. Chem. Phys.* **1980**, 73, 42; **1982**, 76, 2165; **1984**, 80, 568.

40. Dietz, T. G.; Duncan, M. A.; Liverman, M. G.; Smalley, R. E. *J. Chem. Phys.* **1980**, 73, 4816.

41. Hopkins, J. B.; Langridge-Smith, P. R. R.; Morse, m. D.; Smalley, R. E. *J. Chem. Phys.* **1983**, 78, 1627.

42. Ervin, K.; Loh, S. K.; Armentrout, P. B. *J. Am. Chem. Soc.* **1984**, 106, 1161; Loh, S. K; Hales, D. A.; Lian, L.; Armentrout, P. B. *J. Chem. Phys.* **1989**, 90, 5466; Loh, S. K.; Lian, L.; Armentrout, P. B. *J. Am. Chem. Soc.* **1989**, 111, 3167.

43. Jarrold, M. F.; Illies, A. J.; Bower, M. T. *J. Am. Chem. Soc.* **1985**, 107, 7339.

44. Hettich, R. L.; Freiser, B. S. *J. Am. Chem. Soc.* **1987**, 109, 3537.

45. Brucat, P. J.; Zheng, L-S.; Pettiette, C. L.; Yang, S.; Smalley, R. E. *J. Chem. Phys.* **1986**, 84, 3078.

46. Geusic, M. E.; Jarrold, M. F.; McIlrath, T. j.; Freeman, R. R.; Brown, W. L. *J. Chem. Phys.* **1987**, 86, 3862.

47. Ray, U.; Jarrold, M. F.; Bower, J. E.; Kraus, *J. S. Chem. Phys. Lett.* **1989**, 159, 221; *J. Chem. Phys.* **1989**, 91, 2912.

48. Geusic, M. E.; Morse, M. D.; O'Brien, S. C.; Smalley, R. E. *J. Chem. Phys.* **1985**, 82, 590. Trevor, D. J.; Whetten, R. L.; Cox, D. M.; aldor, A. *J. Am. Chem. Soc.* **1985**, 107, 518. Richtsmeier, S. C; Parks, E. K.; Liu, K.; Pobo, L. G; Riley, S. J. *J. Chem. Phys.* **1985**, 82, 3659.

49. Kappes, M. M.; Shär, M.; Radi, P.; Schumacher, E. *J. Chem. Phys.* **1986**, 84, 1863. Peterson, K. I.; Dao, P. D.; Farley, R. W.; Castleman, Jr., A. W. *J. Chem. Phys.* **1984**, 80, 1780. Whetten, R. L.; Zakin, M. R.; Cox, D. M.; Trevor, D. J. Kaldor, A. *J. Chem. Phys.* **1986**, 85, 1697. Rohlfing, E. A.; Cox, D. M.; Kaldor, A. *J. Phys. Chem.* **1985**, 88, 4497.

50. Zheng, L.-S.; Karner, C. M.; Brucat, P. J.; Yang, S. H.; Pettiette, C. L.; Craycraft, M. J.; Smalley, R. E. *J. Chem. Phys.* **1986**, 85, 1681.

51. Herrmann, A.; Hofmann, M; Leutwyler, S.; Schumacher, E.; Woste L. *Chem. Phys. Lett.* **1979**, 62, 216. Delacretaz, G.; grant, E. R.; Whetten, R. L.; Woste, L.; Zwanziger, J. W. *Phys. Rev. Lett.* **1986**, 56, 2598.

52. Rohlfing, E. A.; Valentini, J. *J. Chem. Phys. Lett.* **1986**, 126, 113. Crumley, W. H.; Hayden, J. S.; Gole, J. L. *J. Chem. Phys.* **1986**, 84, 5250.

53. Fu, Z.; Lemire, G. W.; Hamrick, Y. M.; Taylor, S.; Shui, J.-C.; Morse, M. D. *J. Chem. Phys.* **1988**, 88, 3524.

54. Woodward, J. R.; Cobb, S. H.; Gole, J. L. *J. Phys. Chem.* **1988**, 92, 1404.

55. Cheng, P. Y.; Duncan, M. A. *Chem. Phys. Lett.* **1988**, 152, 341.

56. Advances in Metal and Semiconductor Clusters, Volumn 1, ages 1-36, 1993, Jai Press Inc.; Jarrold, M. F.; Creegan, K. M. *Chem. Phys. Lett.* **1990**, 166, 116;

57. Mamyrin, B. A.; Karataev, V. I.; Schmikk, D. V.; Zagulin, V. A. *Soc. Phys. JETP* **1973**, 37, 45.

58. *Advanced in Metal and Semiconductor Clusters*, Volume 1, Pages 37-82, JAI Press Inc.

59. W. Weltner, Jr., *Magnetic Atoms and Molecules* (Van Nostrand Reinhold, 1983)

60. L. B. Knight, Jr., R. J. Van Zee, and W. Weltner, Jr., Chem. Phys. Lett. 94, 296 (1983).

61. M. J. Pellin and D. M. Gruen, *J. Chem. Phys.* **79**, 5887 (1983)
62. M. D. Morse, G. P. Hansen, P. R. R. Langridge-Smith, Lan-Sun Zheng, M. E. Geusic, D. L. Michalopoulos and R. E. Smalley, *J. Chem. Phys.* **80**, 5400 (1984)

63. D. M. Kolb, H. H. Rotermund, W. Schrittenlancher and W. Schroeder, *J. Chem. Phys.* **80**, 695 (1984).

64. R. J. Van Zee and W. Weltner, Jr. *High Temp. Sci.* **17**, 181 (1984).

65. J. A. Howard, R. Sutcliffe and B. Mile, *J. Phys Chem.* **88**, 2183 (1984).

66. L. B. Knight, Jr., R. W. Woodward, R. J. Van Xee and W. Weltner, Jr., *J. Chem. Phys.* **79** 5820 (1983)

67. H. Lischka, R. Shepard, F. B. Brown and I. Shavitt, Int. *J. Quantum Chem. Symp.* **15**, 91 (1981); P. E. M. Siegbahn, *J. Chem. Phys.* **72**, 1647 (1980); B. Liu and M. Yoshimine, *J. Chem. Phys.* **74**, 612 (1981); P. Saxe, D. Fox, H. F. Schaefer III and N. C. Handy, *J. Chem. Phys.* **77**, 554 (1982).

68. P. E. M. Siegbahn, A. Heiberg, B. O. Roos and B. Levy, *Physica Scripta*, **21**, 323 (1980); B. O. Roos, P. R. Taylor, P. E. M. Siegbahn, heiberg and B. O. Roos, *J. Chem. Phys.* **74**, 2381, (1981).

69. *Recent Developments and Applications of Multiconfiguration Hartree-Fock Methods*, NRCC Proceedings No. 10, M. Dupuis, eitor, NRCC. 1981.

70. Dingguo Dai, K. Balasubramanian, *J. Chem. Phys.* **98**, 7098 (1993).

71. S. P. Walch, C. E. Bauschlicher, *Chem. Phys. Lett.* **94**, 290 (1983).

72. L. B. Knight, R. J. Van Zee and W. Weltner, *Chem. Phys. Lett.* **94**, 296 (1983).

73. S. P. Walch, C. E. Bauschlicher, "*Theoretical Studies of Transition Metal Dimers.*" Comparison of Ab Initio Quantum Chemistry with Experiment for Small Molecules, D. Reidel Publishing Company, 1984.

74. See: http://www.cem.msu.edu/~reedp/columbus.html

75. This online software details see url: http://www.lle.rochester.edu/support/documentation/dalton/Master.html

Chapter 2

1. *Advances in Metal and Semiconductor Clusters*, edited by M. A. Duncan, Vol. 3, 1995, JAI Press Inc.

2. Moskovits, M.: *Metal clusters,* Chap. 7. New York: Wiley 1986.

3. G. A. Ozin, *Faraday Symp. Chem. Soc.* **14**, 7 (1980)

4. D. M. Kolb, in *Matrix Isolation Spectroscopy,* edited by A. J. Barnes *et al.* (Reidel, New York, 1981), Chap. 18.

5. D. M. Lindsay, F. Meyer, and W. Harbich, *Atoms, Molecules and Clusters* **12**, 15-18 (1989).

6. W. Harbich, S. Fedrigo, and F. Meyer; D. M. Lindsay, J. Lingnieres and J. C. Rivoal, D. Kreisle, *J. Chem. Phys.* **93**, 12 (1990)

7. Besocke, K., Berger, S., Hofer, W. O., Littmark, U.: *Radiat. Eff.* **66**, 35 (1982)

8. Z. Hu, B. Shen, Q. Zhou, S. Deosaran, J. R. Lombardi, D. M. Lindsay, *J. Chem. Phys.* **95**, 2206 (1991)

9. W. Harbich, S. Fedrigo, J. Buttet, D. M. Lindsay, *Mat. Res. Soc. Symp. Proc.* Vol. 206, 1991.

10. Eric Whittle, David A. Dows, and George C. Pimentel. *Matrix Isolation Method for the Experimental Study of Unstable Species* (1954)

11. Beat Meyer, *Low Temperature Spectroscopy* (American Elsevier Publishing Company, Inc, New York, 1976)

12. This expression may be derived from results given in: Steinfeld, J.I.: *molecules and radiation.* Cambridge MA, London: MIT press 1978.

Chapter 3

1. C. V. Raman and K. S. Krishnan, *Nature*, **121**, 501, 1928.

2. A. Smekal, *Naturswiss.*, **11**, 873, 1923.

3. G. Landsberg and L. Mandelstam, *Naturwiss.*, **16**, 557, 772, 1928.

4. J. Cabannes, *Compt. Rend.*, **186**, 1201, 1928.

5. *Molecular Spectra and Molecular Structure*, Vol II: *Infrared and Raman Spectra of Polyatomic Molecules.* Gerhard Herzberg, F. R. S. C., Chapter III.2, p258. Van Nostrand Teinhold Company.

6. Zhengdong Hu, Bo Shen, Qinwei Zhou, S. Deosaran, J. R. Lombardi and D. M. Lindsay, *J. Chem. Phys.* **95**, 2206, 1991.

7. Pellin, M. J.; Foosnaes, T.; Gruen, D. M. *J. Chem. Phys.*, **1981**, 17, 5547.

8. Pellin, J.; Foosnaes, T.; Gruen, D. M. in *Metal Bonding and Interactions in High-Temperature Systems*; Gold, J. L., Stwalley, W. C., Eds.; *ACS Symposium Series 179*; American Chemical Society: Washington, DC, 1982; p 219.

9. Beat Meyer, Low Temperature Spectroscopy, Elsevier, New York, 1971.

Chapter 4

4.1 Luminescence Spectra of Mass-selected Pt_2 in Argon

1. Jansson, K.; Scullman, R. *J. Mol. Spectrosc.* **1976**, 61, 299.

2. Ho, Joe; Polak, M. L.; Ervin, K. M.; Lineberger, W. C. *J. Chem. Phys.* **1993**, 99, 8542.

3. Taylor S.; Lemire, G.; Hamrick. Y. M.; Fu, Z; Morse, M. *J. Chem. Phys.* **1988**, 89, 5517.

4. Balasubramanian, K. *J. Chem. Phys.* **1987**, 87, 6573.

5. Dong, Jian-Guo; Hu, Zhengdong; Craig, Robert; Lombardi, John R.; Lindsay, D. M. *J. Chem. Phys.* **1994**, 101, 9280.

6. Wang, Huaiming; Haouari, Hanae; Craig, Robert; Lombardi, John R.; Lindsay, D. M. *J. Chem. Phys.* **1996**, 104, 3420.

7. Hu, Z.; Dong, Jian-Guo; Lombardi, John R.; Lindsay, D. M. *J. Chem. Phys.* **1994**, 101, 95.

8. Wang, Huaiming; Haouari, Hanae; Craig, Robert; Liu, Yifei; Lombardi, John R.; Lindsay, D. M. *J. Chem. Phys.* **1997**, 106, 2101.

9. Wang, Huaiming; Liu, Yifei; Haouari, Hanae; Craig, Robert; Lombardi, John R.; Lindsay, D. M. J. Chem. Phys. **1997**, 106, 6534.

10. Hu, Z.; Shen, B.; Lombardi, J. R.; Lindsay, D. M. *J. Chem. Phys.* **1992**, 96, 8757.

11. The 0-0 through 0-2 transitions show a weak, but relatively sharp feature (most evident for 0-2, see Figure 1) displaced to the red of the principal band by a constant 11 ± 2 cm^{-1}, plus a broader (and still weaker) emission displaced (also to the red) by 34 ± 4 cm^{-1}. These features are not consistent (as predicted by the Table 1 data) with either sequence structure or matrix site effects (which should be displaced proportional to v''). Likely assignments are a librational mode and a phonon side band (see also ref 9) for the 11 and 34 cm^{-1} features, respectively.

12. System II of the gas-phase spectrum (ref 3) may, in fact, be a vibrational hot band: M. Morse, private communication.

13. Pinegar, J. C.; Karlsson, L.; Langenberg, J. D.; Costell

14.Ho, Q. D.; Morse. M. D. *Dispersed Fluorescence Spectroscopy of Jet-Cooled AgAu and Pt_2.* To be published in *J. Chem. Phys.*

4.2 Absorption, resonance Raman, and Raman excitation spectra of hafnium trimers

1. Z. Hu, J.-G. Dong, J. R. Lombardi, and D. M. Lindsay, *J. Phys. Chem.* **97**, 9263(1993)

2. Z. Hu, B. Shen, J. R. lombardi, and D. M. Lindsay, *J. Chem. Phys.* **96**, 8757(1992)

3. H. Haouari, H. Wang, R. Craig, J. R. Lombardi, and D. M. Lindsay, *J. Chem. Phys.* **103**, 9527(1995)

4. Z. Hu, B. Shen, J. R. Lombardi, and D. M. Lindsay, *J. Chem. Phys.* **96**, 8757(1992); Z. Hu, B. Shen, Q. Zhou, S. Deosaran, J. R. Lombardi, and D. M. Lindsay, *Proc. SPIE* **1599**, 65(1991)

5. H. Wang, R. Craig, H. Haouari, Y. Liu, J. R. Lombardi, and D. M. Lindsay, *J. Chem. Phys.* **105**, 5355(1996)

6. G. A. Ozin and D. F. McIntosh, *J. Phys. Chem.* **90**, 5756(1986)

7. H. Wang, R. Craig, H. Haouari, J.-G. Dong, Z. Hu, A. Vivoni, J. R. Lombardi, and D. M. Lindsay, *J. Chem. Phys.* **103**, 3289(1995)

8. H. Haouari, H. Wang, R. Craig, J. R. Lombardi, and D. M. Lindsay, *J. Chem. Phys.* **103**, 9527(1995)

9. G. Herzberg, *Electronic Spectra of Polyatomic Molecules* (Van Nostrand, New York, 1996)

10.E. Rohlfing and J. Valentini, *Chem. Phys. Lett.* **126**, 113(1986)

4.3 Spectroscopy of Yttrium Dimers in Argon Matrices

1. Morse, M. D. *Chem. Rev.* **86**, 1049 (1986).

2. Hu, Z.; Zhou, Q.; Lombardi, J. R.; Lindsay, D. M. *In Spectroscopy of Mass-selected Zirconium Dimers in Argon, in Physics and Chemistry of Finite Systems: from clusters to Crystals, edited by P. Jena, S. N. Kahana, and B. K. Rao (Kluwer Academic, Dordrecht, 1992).*

3. Hu, Z.; Shen, B.; Deosaran, S.; Lombardi, J. R.; Lindsay, D. M.; Harbich, W. *Proc. SPIE* **1599**, 65 (1991).

4. Efremov, Y. M.; Samoilova, A. N.; Kozhukhovsky, V. B.; Gurvich, L. V. *J. Mol. Spectrosc.* **73**, 430 (1978).

5. Wang, H.; Liu, Y.; Haouari, H.; Craig, R.; Lombardi, J. R.; Lindsay, D. M. *J. Chem. Phys*, **106**, 6534, (1997).

6. Wang, H.; Haouari, H.; Craig, R.; Liu, Y; Lombardi, J. R.; Lindsay, D. M. *J.Chem. Phys*, **106**, 2101 (1997).

7. Ho, J.; Ervin, K. M.; Polak, K. L.; Gilles, M. K.; .Lineberger, W. C. *J. Chem. Phys*, **95**, 4845, (1991).

8. Huber, K. P.; Herzberg, G. *Constants of Diatomic Molecules* (Van Norstrand, New York, 1979).

9. Hu, Z.; Shen, B.; Deosaran, S.; Lombardi, J. R.; Lindsay, D. M.; Harbich, W. *J. Chem. Phys*, **95**, 2206 (1991).

10. Gee, A. R.; O'Shea, D. C.; Cummins, H. Z., *Solid State Commun.* **4**, 43 (1965).

11. Herzberg, G. *Molecular Spectra and Molecular Structure, I. Spectra of Diatomic Molecules*, D.Van Nostrand Company, Inc. New York, (1950).

12. Verhaegan, G.; Somoes, S.; Drowart, J. *J. Chem. Phys.* **40**, 239 (1964).

13. Casey, S. M.; Leopold, D. G. *J. Phys. Chem*, **97**, 816 (1993).

14. Walch, S. P.; Bauschlicher, C. W., Jr. In *Comparison of ab Initio Quantum Chemistry with Experiment;* R. J. Bartlett., Ed.; D. Reidel: Dordrecht, p39 (1985).

15. Dai, D. G.; Balasubramanian, K. *J. Chem. Phys.*, **98**, 7098 (1993).

16. Knight, L. B., Jr.; Woodward, R. W.; Van Zee, R. J.; Weltner, W., Jr. *J. Chem. Phys.* **79**, 5820 (1983).

17. Badger, R. M. *J. Chem. Phys.* **2**, 128(1934); **3**, 710(1935)

18. Weisshaar, J. C. *J. Chem. Phys.* **90**(3), 1429(1989)

19. Hopkins, J. B.; Langridge-Smith, P. R. R; Morse, M. D.; Smalley, R. E. *J. Chem. Phys.* ,**78** 1627 (1983)

20. Simard, B.; Hackett, P. A. *Chem. Phys. Lett.* **186** (4,5) (1991)

21. Bordas, C.; Broyer, M.; Chevaleyre, J.; Dugourd, Ph. *Chem. Phys. Lett.* **197**(6),562 (1992)

4.4 Absorption, Resonance Raman and Raman Excitation Spectra of Lanthanum Dimers in Argon Matrices

1. Huaiming Wang, Hanae Haouari, Robert Craig, John R. Lombardi, and D. M. Lindsay, *J. Chem. Phys.*, **104**, 3420 (1996).

2. Huaiming Wang, Yifei Liu, Robert Craig, Hanae Haouari, John R. Lombardi, and D. M. Lindsay, *J. Chem. Phys.*, **106**, 2101 (1997).

3. Huaiming Wang, Yifei Liu, Robert Craig, Hanae Haouari, John R. Lombardi, and D. M. Lindsay, *J. Chem. Phys.*, **106**, 6534 (1997).

4. Fang Li, Yifei Liu, X. Chen, X. Shen. John R. Lombardi, and D. M. Lindsay, manuscript of "Raman sepctra of Yttrium dimers in argon matrices", to be submitted.

5. Michael D. Morse, *Chem. Rev.*, 1986, Vol. **86**, 1078.

6. Verhaegen, G., Smoes, S., Drowart, J., J.Chem. Phys. **40**, 239 (1964).

7. Knight, L.B., Jr, Woodward, R. W., Van Zee, R. J., Weltner, W., Jr., *J. Chem. Phys.*, **79**, 5820 (1983).

8. Micheal Dolg, Hermann Stoll and Heinzwerner Preuss, *J. Mol. Struct. (Theochem)* **277** (1992) 239-249.

9. Z. Hu, B. Shen, J. R. Lombardi, and D. M. Lindsay, *J. Chem. Phys.* **96**, 8757 (1992)

10. Z. Hu, B. Shen, Q. Zhou, S. Deosaran, D.M. Lindsay, and J. R. Lombardi, SPIE Vol. 1599, *Recent Advances in the Use of Light in Physics, Chemistry, Engineering and Medicine*, **65** (1991).

11. Moskovits, M; DiLella, D. P.; Limm, W. *J. Chem. Phys.* 1984, 80, 626.

12. Fang Li, Yifei Liu, X. Chen, X. Shen. John R. Lombardi, and D. M. Lindsay, manuscript of "Raman sepctra of Yttrium dimers in argon matrices", to be submitted.

13. S. P. Walch, C. W. Bauschlicher, "Theoretical studies of transition metal dimers", D. Reidel Publishing Company, 1984.

Chapter 5

1. R. J. Van Zee, S. Li, And W. Weltner, Jr. *J. Chem. Phys.* **100**, 4010, (1994).

2. Knight, L. B., Jr.; Woodward, R. W.; Van Zee, R. J.; Weltner, W., Jr. *J. Chem. Phys.* **79**, 5820 (1983).

3. Dai, D. G.; Balasubramanian, K. *J. Chem. Phys.* **98**, 7098 (1993).